Investigación sobre la Flexibilidad de la Demanda en Redes Eléctricas Inteligentes: Control Directo de Cargas

---

Research on Demand-Side Flexibility in Smart Grids: Direct Load Control

Ph.D. Dissertation

By

Joaquín Garrido-Zafra

Supervisor

Antonio Moreno-Muñoz

Co-supervisor

Aurora Gil-de-Castro

Programa de Doctorado en Computación Avanzada, Energía y Plasmas

Departamento de Ingeniería Electrónica y de Computadores

Universidad de Córdoba

Córdoba, Spain

June 2022

TITULO: *Research on Demand-Side Flexibility in Smart Grids: Direct Load Control*

AUTOR: *Joaquín Garrido Zafra*

Campus de Rabanales
Ctra. Nacional IV, Km. 396 A
14071 Córdoba

https://www.uco.es/ucopress/index.php/es/
ucopress@uco.es

TÍTULO DE LA TESIS: Investigación sobre la Flexibilidad de la Demanda en Redes Eléctricas Inteligentes: Control Directo de Cargas

DOCTORANDO: Joaquín Garrido Zafra

INFORME RAZONADO DE LOS DIRECTORES DE LA TESIS

(se hará mención a la evolución y desarrollo de la tesis, así como a trabajos y publicaciones derivados de la misma)

El doctorando Joaquín Garrido Zafra ha progresado de manera significativa como investigador desde que comenzara su tesis doctoral en enero 2019. Durante estos años el doctorando ha realizado todas las actividades obligatorias y opcionales, trabajando de forma constante y sin pausa, siguiendo el plan de investigación establecido. Lo que me ha resultado reseñable es su capacidad para trabajar con una mínima supervisión. Nos ha impresionado mucho su entusiasmo y sus conocimientos de ingeniería, así como su afán por trabajar en un entorno de tiempo real. Además, ha participado activamente en diversos proyectos de investigación financiados en concurrencia competitiva, de los cuáles ha ido obteniendo numerosas publicaciones y que presenta en su documento de tesis.

Durante este periodo de tesis doctoral, el doctorando ha realizado una amplia labor analítica, experimental y de consulta y seguimiento de normativa hasta desarrollar el prototipo, con pruebas en laboratorio usando equipos que ha tenido que programar y controlar para simular diferentes escenarios de funcionamiento, con la programación de microcontroladores, integración con sensores de medida, comunicaciones, prototipado, calibración, así como numerosos ensayos en los que ha comprobado su correcto funcionamiento realizando medidas con una amplia diversidad de cargas eléctricas.

En definitiva, esta tesis supone un hito importante tanto para esta universidad como para el área en que se enmarca ya que ha contribuido al conocimiento general de este ámbito de las redes eléctricas inteligentes y la gestión activa de la demanda.

Como principales frutos del trabajo realizado se han derivado los tres siguientes artículos publicados en revistas incluidas en los tres primeros cuartiles de la relación de revistas del ámbito de la especialidad y referenciadas en la última relación publicada por el Journal Citation Reports (SCI y/o SSCI):

- **J. Garrido-Zafra**, A. Moreno-Munoz, A. Gil-de-Castro, E.J. Palacios-Garcia, C.D. Moreno-Moreno, and T. Morales-Leal. (2019). A novel direct load control testbed for smart appliances. *Energies*, *12*(17), 3336. doi: 10.3390/en12173336.
  JCR: 2,702 (2019). 63/112 (Q3) - Energy & Fuels.

- **J. Garrido-Zafra**, A. Moreno-Munoz, A. R. Gil-de-Castro, F. J. Bellido-Outeirino, R. Medina-Gracia and E. Gutiérrez-Ballesteros, "Load Scheduling Strategy to Improve Power Quality in Electric-Boosted Glass Furnaces," in IEEE Transactions on Industry Applications, vol. 57, no. 1, pp. 953-963, Jan.-Feb. 2021, doi: 10.1109/TIA.2020.3029758.
  JCR: 3,654 (2020). 78/273(Q2) - Engineering, Electrical & Electronic; 22/90(Q1) - Engineering, multidisciplinary.

- **J. Garrido-Zafra**, A. R. Gil-de-Castro, R. Savariego-Fernandez, M. Linan-Reyes, F. Garcia-Torres, and A. Moreno-Munoz, "IoT Cloud-Based Power Quality Extended Functionality for Grid-Interactive Appliance Controllers," in IEEE Transactions on Industry Applications, vol. 58, no. 3, pp. 3909-3921, May-June 2022, doi: 10.1109/TIA.2022.3160410.
  JCR: 3,654 (2020). 78/273(Q2) - Engineering, Electrical & Electronic; 22/90(Q1) - Engineering, multidisciplinary.

Por todo ello, se autoriza la presentación de la tesis doctoral.

Córdoba, 15 de junio de 2022
Firma de los directores

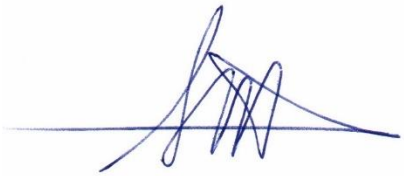

Fdo.: Antonio Moreno Muñoz

Fdo.: Aurora R. Gil de Castro

TESIS POR COMPENDIO DE PUBLICACIONES

La presente tesis doctoral cumple con los requisitos establecidos en la normativa del programa de doctorado en Computación Avanzada, Energía y Plasmas de la Universidad de Córdoba para su presentación como compendio de publicaciones. Este compendio está formado por **3 artículos** publicados en revistas incluidas en los tres primeros cuartiles de la última relación publicada por el Journal Citation Report (JCR). Además, el doctorando aparece como primer autor de las publicaciones habiendo aceptado los coautores su presentación en esta tesis doctoral.

- **J. Garrido-Zafra**, A. Moreno-Munoz, A. Gil-de-Castro, E.J. Palacios-Garcia, C.D. Moreno-Moreno, and T. Morales-Leal. (2019). A novel direct load control testbed for smart appliances. *Energies*, *12*(17), 3336. doi: 10.3390/en12173336.
  JCR: 2,702 (2019). 63/112 (Q3) - Energy & Fuels.

- **J. Garrido-Zafra**, A. Moreno-Munoz, A. R. Gil-de-Castro, F. J. Bellido-Outeirino, R. Medina-Gracia and E. Gutiérrez-Ballesteros, "Load Scheduling Strategy to Improve Power Quality in Electric-Boosted Glass Furnaces," in IEEE Transactions on Industry Applications, vol. 57, no. 1, pp. 953-963, Jan.-Feb. 2021, doi: 10.1109/TIA.2020.3029758.
  JCR: 3,654 (2020). 78/273(Q2) - Engineering, Electrical & Electronic; 22/90(Q1) - Engineering, multidisciplinary.

- **J. Garrido-Zafra**, A. R. Gil-de-Castro, R. Savariego-Fernandez, M. Linan-Reyes, F. Garcia-Torres, and A. Moreno-Munoz, "IoT Cloud-Based Power Quality Extended Functionality for Grid-Interactive Appliance Controllers," in IEEE Transactions on Industry Applications, vol. 58, no. 3, pp. 3909-3921, May-June 2022, doi: 10.1109/TIA.2022.3160410.
  JCR: 3,654 (2020). 78/273(Q2) - Engineering, Electrical & Electronic; 22/90(Q1) - Engineering, multidisciplinary.

Córdoba, 15 de junio de 2022
El doctorando

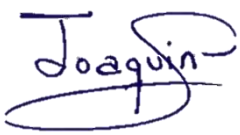

Fdo: Joaquín Garrido Zafra

Tesis doctoral subvencionada parcialmente por el proyecto I+D+I del Programa Estatal de Investigación, Desarrollo e Innovación Orientada a Retos de la Sociedad 2016 (MINECO): *Control y Gestión de Nanorredes Aislables (COMING).*
Referencia: **TEC2016-77632-C3-2-R.**

Además, también está parcialmente subvencionada por los proyectos cofinanciados por el Fondo Europeo de Desarrollo Regional (FEDER) y tramitados por el Centro para el Desarrollo Tecnológico Industrial (CDTI):

Desarrollo de un prototipo para la atenuación de los efectos de las cargas no lineales sobre las redes de alumbrado público (PERTURBIAP)
Referencia: **12018061**
Adecuación de los prototipos desarrollados para la corrección de los efectos ocasionados por las cargas no lineales en las redes de alumbrado público a nivel de prefabricación industrial
Referencia: **12018184**

Y por el proyecto I+D+I cofinanciado por el programa INTERREG SUDOE y el Fondo Europeo de Desarrollo Regional (FEDER): *Integración de microrredes combinadas de refrigeración, calefacción y energía en edificios públicos de energía cero con altos requisitos de calidad y continuidad de la energía (IMPROVEMENT)*
Referencia: **SOE3/P3/E0901**

Agradecimientos

Después de los más de tres años dedicados a este trabajo, es hora de agradecer a todas y cada una de las personas que han hecho posible que esta tesis doctoral llegue a su fin. En primer lugar, a mi director de tesis Antonio Moreno, cuya supervisión ha sido clave, no solo para finalizar el doctorado, sino también para terminar con éxito mis estudios de grado y de máster. Gracias por la orientación durante todo el proceso, la confianza y por hacerme partícipe de tantos logros. Del mismo modo, también me gustaría dar las gracias a mi codirectora Aurora Gil por transmitirme ese rigor científico, por sus constantes revisiones para que esta tesis fuese una realidad y por los ánimos. Además, ambos habéis demostrado una calidad humana encomiable. Una tesis doctoral no solo influye en el plano laboral de una persona, también en su plano personal. Gracias por todo el apoyo.

Por supuesto, también me gustaría agradecer todo el apoyo del resto de compañeros de departamento que un día fueron mis profesores y que día tras día propician un ambiente de trabajo inmejorable. A Josele, con el que entendí lo que era la docencia en esas prácticas de la asignatura de Electrónica de Potencia, y a Juan Luna y José María Flores, con los que aún sigo aprendiendo cada día. A Víctor Pallarés, por transmitirme todo ese conocimiento y su serenidad, que tanto hace falta en la universidad. También a Isabel Moreno y a Kiko Bellido por sus consejos tan valiosos.

A Ricardo y David, con los que compartí horas y horas de laboratorio y muchos cafés malos de máquina. Gracias por crear ese ambiente de trabajo que teníamos en el que nos apoyábamos en los momentos de agobio y celebrábamos las buenas noticias de algún compañero como propias. Muchas gracias también a Rafa Savariego, por su ayuda imprescindible en momentos de estrés y por esos ratos de charla que hemos tenido y seguiremos teniendo. Hoy os puedo llamar amigos, me quedo también con eso.

A mis amigos del pueblo de toda la vida: José Modesto, José Manuel, Raúl y Juan. Gracias por entender mis ausencias y lo que esto significa para mí. Os he robado mucho tiempo que espero poder devolveros algún día.

De mi época de bachillerato, no puedo olvidarme de dos grandes amigos: Alejandro y Antonio. Gracias por todo el apoyo que recibí en forma de ánimos y, sobre todo, de clases particulares de refuerzo para entender lo que tocase ese día, ya podía ser la sintaxis de C, el algebra de Boole o los problemas de hidráulica. También me acompañasteis durante el grado. Echo de menos esos ratos en el piso, esperando en los banquitos del campus y esas horas de clase a las 16:00 de la tarde, por muy sorprendente que pueda parecer esto último. A mi profesor de tecnología industrial, Antonio Moyano. Bien sabías que para mí sería todo un reto superar el bachillerato. Recuerdo el primer suspenso con un tres y los ánimos que me diste, realmente los necesitaba. La fuerza de voluntad está muy bien, pero que un profesor e ingeniero en electrónica confíe en ti es otro nivel. Creo que esto también influyó bastante en la elección de mis estudios. A mi amiga Sonia por todo el apoyo personal. Gracias por estar en esos momentos tan duros y por esas conversaciones que tanto bien me hicieron.

Gracias también a mis chicos de la academia por acogerme como uno más y brindarme esas noches de baile que nunca olvidaré y que me vienen muy bien. Descubrí un mundo

maravilloso del que espero no salir nunca. Aún tengo en mi cabeza ese “1, 2, 3, 5, 6, 7”; nunca veré esa cuenta de la misma forma.

A José Guadalupe, que en poco tiempo se ha convertido en un gran amigo, por saber escuchar y ayudarme a tomar las decisiones correctas.

Por último, quisiera agradecer todo el apoyo recibido por parte de mi familia. A mi tío Antonio, que, a pesar de no haber tenido oportunidad de formarse, día a día devora libros para calmar su curiosidad. Gracias por tu interés y por tus palabras tan necesarias para quitarle hierro al asunto: “¿Que tal van esas investigaciones? ¿Compramos placas solares entonces o no?”. A mi tío Paco, por orientarme en mis primeros pasos allá por 2009 y por empujarme a que descubriera lo maravillosa que es esta rama de la ingeniería, a la que ahora me dedico profesionalmente; ahí empezó todo. A mis tíos, Manolo y Conchi, por señalar siempre el camino correcto y crear las condiciones para que hoy esté donde estoy. A mi tío Juanma, por impregnarme con su filosofía de vida que tanto me ha aportado. Os lo agradeceré toda la vida. A mi madre, que ha vivido todas mis preocupaciones muy de cerca y desde siempre ha estado a mi lado, aun cuando las circunstancias eran claramente hostiles. Eres una guerrera y así lo has dejado patente. A mis niños, Jaime y Jesús, por entender el porqué de mis ausencias. Y, por supuesto, a mi padre, por tus grandes enseñanzas y lecciones que siguen vigentes más que nunca. Te fuiste orgulloso de saber lo que tu hijo mayor había conseguido y lo feliz que estaba por ello. Nunca podré alcanzar a agradeceros todo el esfuerzo que habéis hecho para que llegara este momento, soy lo que soy gracias a vosotros.

Gracias también a Ana, no solo por revisar partes de este documento, sino también por entenderme, apoyarme y hablar mi mismo idioma en lo que a la universidad se refiere, que no es nada desdeñable.

Este trabajo es la culminación de una etapa que comenzó con un niño curioso que jugaba con cables en su casa, siempre preguntaba el porqué de las cosas y que cuando, más tarde, su madre orgullosa decía lo que había estudiado, la gente respondía: no podía haber sido de otra forma. Así pues, también le doy las gracias a ese niño que convirtió sus inquietudes en su afición y más tarde en su profesión, le doy las gracias por haber atravesado este proceso tan duro y por haber sacado fuerzas hasta de la propia salud, porque, sin duda, lo que estaba por venir merecía la pena.

Gracias a todos.

Abstract

In recent decades, the European Union has made decisive efforts to maintain its global leadership in renewable energies to meet climate change targets resulting from international agreements. There is a deliberate intention to reduce the usage of non-renewable energy sources and promote the exploitation of renewable generation at all levels as shown by energy production data within the Eurozone.

The electricity sector illustrates a successful implementation of these energy policies: The electricity coming from combustible fuels was at historical lows in 2018, accounting for 83.6 % of the electricity generated from this source in 2008. By contrast, the pool of renewables reached almost 170 % of the 2008 production. Against this background, power systems worldwide are undergoing deep-seated changes due to the increasing penetration of these variable renewable energy sources and distributed energy resources that are intermittent and stochastic in nature. Under these conditions, achieving a continuous balance between generation and consumption becomes a challenge and may jeopardize the system stability, which points out the need of making the power system flexible enough as a response measure to this trend.

This Ph.D. thesis researches one of the principal mechanisms providing flexibility to the power system: The demand-side management, seen from both the demand response and the energy efficiency perspectives. Power quality issues as a non-negligible part of energy efficiency are also addressed. To do so, several strategies have been deployed at a double level. In the residential sector, a direct load control strategy for smart appliances has been developed under a real-time pricing demand response scheme. This strategy seeks to minimize the daily cost of energy in presence of diverse energy resources and appliances. Furthermore, a spread spectrum technique has also been applied to mitigate the high-frequency distortion derived from the usage of LED technology lighting systems instead of traditional ones when energy efficiency needs to be improved. In the industrial sector, a load scheduling strategy to control the AC-AC power electronic converter in charge of supporting the electric-boosted glass melting furnaces has been developed. The benefit is two-fold: While it contributes to demand flexibility by shaving the peaks found under conventional control schemes, the power quality issues related to the emission of subharmonics are also kept to a minimum.

Concerning the technologies, this Ph.D. thesis provides smart solutions, platforms, and devices to carry out these strategies: From the application of the internet of things paradigm to the development of the required electronics and the implementation of international standards within the energy industry.

Keywords: Demand response, demand-side management, direct load control, internet of things, power quality, power system flexibility, smart grids.

Resumen

En las últimas décadas, la Unión Europea ha realizado esfuerzos decisivos para mantener su liderazgo mundial en energías renovables con el fin de cumplir los objetivos de cambio climático resultantes de los acuerdos internacionales. Muestra una intención deliberada de reducir el uso de fuentes de energía no renovable y promover la explotación de la generación renovable a todos los niveles, como demuestran los datos de producción de energía en la eurozona.

El sector de la electricidad ilustra un caso de éxito de estas políticas energéticas: la electricidad procedente de combustibles fósiles estaba en mínimos históricos en 2018, representando el 83,6 % de la electricidad generada a partir de esta fuente en 2008; en cambio, el grupo de renovables alcanzó casi el 170 % de la producción de 2008. En este contexto, los sistemas eléctricos de todo el mundo están experimentando profundos cambios debido a la creciente penetración de estas fuentes de energía renovable y de recursos energéticos distribuidos que son de naturaleza variable, intermitente y estocástica. En estas condiciones, lograr un equilibrio continuo entre generación y consumo se convierte en un reto y puede poner en peligro la estabilidad del sistema, lo que señala la necesidad de flexibilizar el sistema eléctrico como medida de respuesta a esta tendencia.

Esta tesis doctoral investiga uno de los principales mecanismos que proporcionan flexibilidad al sistema eléctrico: la gestión de la demanda vista tanto desde la perspectiva de la respuesta a la demanda como de la eficiencia energética. También se abordan los problemas de calidad de suministro entendidos como parte no despreciable de la eficiencia energética. Para ello, se han desplegado varias estrategias a un doble nivel. En el sector residencial, se ha desarrollado una estrategia basada en el control directo de cargas para los electrodomésticos inteligentes siguiendo un esquema de respuesta a la demanda con precios en tiempo real. Esta estrategia busca minimizar el coste diario de la energía en presencia de diversos recursos energéticos y electrodomésticos. Además, también se ha aplicado una técnica de espectro ensanchado para mitigar la distorsión de alta frecuencia derivada del uso de sistemas de iluminación con tecnología LED, empleados para la mejora de la eficiencia energética frente a las tecnologías convencionales. En el sector industrial, se ha desarrollado una estrategia de planificación de cargas para controlar el convertidor AC-AC de los hornos de fundición de vidrio con soporte eléctrico. El beneficio es doble: mientras que se contribuye a la flexibilidad de la demanda al eliminar los picos encontrados en los esquemas de control convencionales, también se reducen al mínimo los problemas de calidad de suministro relacionados con la emisión de subarmónicos.

En cuanto a las tecnologías, esta tesis doctoral aporta soluciones, plataformas y dispositivos inteligentes para llevar a cabo estas estrategias: desde la aplicación del paradigma del internet de las cosas hasta el desarrollo de la electrónica necesaria y la implementación de estándares internacionales dentro de la industria energética

Palabras clave: Calidad de suministro, control directo de cargas, flexibilidad del sistema eléctrico, internet de las cosas, redes eléctricas inteligentes, respuesta a la demanda.

Thesis details

Thesis Title:	Research on Demand-Side Flexibility in Smart Grids: Direct Load Control
Título de la Tesis:	Investigación sobre la Flexibilidad de la Demanda en Redes Eléctricas Inteligentes: Control Directo de Cargas
Author:	Joaquín Garrido Zafra
Supervisor:	Prof. Dr. Antonio Moreno-Muñoz
Co-supervisor:	Prof. Dra. Aurora Gil-de-Castro

Publications related to the Ph.D. Thesis

1st authored journal papers

[J1] **J. Garrido-Zafra**, A. Moreno-Munoz, A. Gil-de-Castro, V. Pallares-Lopez, and T. Morales-Leal. (2018). Supraharmonics emission from LED lamps: A reduction proposal based on random pulse-width modulation. Electric Power Systems Research, 164, 11-19. doi: 10.1016/j.epsr.2018.07.032.

[J2] **J. Garrido-Zafra**, A. Moreno-Munoz, A. Gil-de-Castro, E.J. Palacios-Garcia, C.D. Moreno-Moreno, and T. Morales-Leal. (2019). A novel direct load control testbed for smart appliances. *Energies*, *12*(17), 3336. doi: 10.3390/en12173336.

[J3] **J. Garrido-Zafra**, A. Moreno-Munoz, A. R. Gil-de-Castro, F. J. Bellido-Outeirino, R. Medina-Gracia and E. Gutiérrez-Ballesteros, "Load Scheduling Strategy to Improve Power Quality in Electric-Boosted Glass Furnaces," in IEEE Transactions on Industry Applications, vol. 57, no. 1, pp. 953-963, Jan.-Feb. 2021, doi: 10.1109/TIA.2020.3029758.

[J4] **J. Garrido-Zafra**, A. R. Gil-de-Castro, R. Savariego-Fernandez, M. Linan-Reyes, F. Garcia-Torres, and A. Moreno-Munoz, "IoT Cloud-Based Power Quality Extended Functionality for Grid-Interactive Appliance Controllers," in IEEE Transactions on Industry Applications, vol. 58, no. 3, pp. 3909-3921, May-June 2022, doi: 10.1109/TIA.2022.3160410.

Co-authored journal papers

[J6] R. Medina-Gracia, A. d. R. G. de Castro, **J. Garrido-Zafra**, A. Moreno-Munoz and E. Cañete-Carmona, "Power Quality Sensor for Smart Appliance's Self-Diagnosing Functionality," in *IEEE Sensors Journal*, vol. 19, no. 20, pp. 9486-9495, 15 Oct.15, 2019, doi: 10.1109/JSEN.2019.2924574.

[J7] M. Alonso-Rosa, A. Gil-de-Castro, A. Moreno-Munoz, **J. Garrido-Zafra**, E. Gutierrez-Ballesteros, and E. Cañete-Carmona. (2020). An IoT based mobile augmented reality application for energy visualization in buildings environments. *Applied Sciences*, *10*(2), 600. doi: 10.3390/app10020600.

[J8] F. Garcia-Torres, C. Bordons, J. Tobajas, J. J. Márquez, **J. Garrido-Zafra** and A. Moreno-Muñoz, "Optimal Schedule for Networked Microgrids Under Deregulated Power Market Environment Using Model Predictive Control," in IEEE Transactions on Smart Grid, vol. 12, no. 1, pp. 182-191, Jan. 2021, doi: 10.1109/TSG.2020.3018023.

[J9] E. Gutierrez-Ballesteros, A. Gil-de-Castro, S. Rönnberg, and **J. Garrido-Zafra**. (2020). Impact factors in LED lamp measurement reproducibility. *Lighting Research & Technology*. doi: 10.1177/1477153520971250.

[J10] M. Linan-Reyes, **J. Garrido-Zafra**, A. Gil-de-Castro, and A. Moreno-Munoz. (2021). Energy Management Expert Assistant, a New Concept. *Sensors*, *21*(17), 5915. doi: 10.3390/s21175915.

1st authored publications in proceedings with peer-review

[C1] **J. Garrido-Zafra**, A. Moreno-Munoz, A. Gil-de-Castro, F. Bellido-Outeirino, R. Medina-Gracia, and E. G. Ballesteros, "Load Scheduling Approach for Energy Management and Power Quality enhancement in Glass Melting Furnaces," 2019 IEEE International Conference on Environment and Electrical Engineering and 2019 IEEE Industrial and Commercial Power Systems Europe (EEEIC / I&CPS Europe), 2019, pp. 1-6, doi: 10.1109/EEEIC.2019.8783727.

[C2] **J. Garrido-Zafra**, A. Gil-de-Castro, R. Savariego-Fernandez, M. Linan-Reyes, A. Moreno-Munoz, and F. García-Torres, "A Novel Microgrid Responsive Appliance Controller," 2020 IEEE International Conference on Environment and Electrical Engineering and 2020 IEEE Industrial and Commercial Power Systems Europe (EEEIC / I&CPS Europe), 2020, pp. 1-6, doi: 10.1109/EEEIC/ICPSEurope49358.2020.9160723.

Co-authored publications in proceedings with peer-review

[C3] A. Escribano-Escribano, J. M. Flores-Arias, F. J. Bellido-Outeiriño, **J. Garrido-Zafra**, and E. J. P. García, "Feasibility Analysis of several RES installations for a NGO in Ethiopia through a Developed Holistic SW Tool," 2019 IEEE 23rd International Symposium on Consumer Technologies (ISCT), 2019, pp. 173-175, doi: 10.1109/ISCE.2019.8901013.

[C4] J. de Dios Fuentes-García, J. M. Flores-Arias, F. J. Bellido-Outeiriño, F. J. Quiles-Latorre, M. A. Ortiz-López and **J. Garrido-Zafra**, "Monitoring of photovoltaic systems for self-consumption without over-consumption," 2019 IEEE 9th International Conference on Consumer Electronics (ICCE-Berlin), 2019, pp. 239-241, doi: 10.1109/ICCE-Berlin47944.2019.8966189.

[C5] F. J. López-Alcolea, E.J. Molina, J. Vazquez, A. Parreño-Torres, P. Roncero-Sanchez, A. Moreno-Munoz, **J. Garrido-Zafra**, and F. Garcia-Torres, "Detection and Compensation of Current Harmonics in a Microgrid Using an Active Power Filter Supported by an IoT Sensor Network," 2021 IEEE International Conference on Environment and Electrical Engineering and 2021 IEEE Industrial and Commercial Power Systems Europe (EEEIC / I&CPS Europe), 2021, pp. 1-6, doi: 10.1109/EEEIC/ICPSEurope51590.2021.9584592.

[C6] F. Vera-Coca, A. Gil-de-Castro, R. Medina-Gracia, **J. Garrido-Zafra**, R. Savariego-Fernández and A. Moreno-Munoz, "Interactive visualization of IoT power quality data on mobile devices," 2021 IEEE International Conference on Environment and Electrical Engineering and 2021 IEEE Industrial and Commercial Power Systems Europe (EEEIC / I&CPS Europe), 2021, pp. 1-6, doi: 10.1109/EEEIC/ICPSEurope51590.2021.9584771.

The following Ph.D. dissertation is presented as a collection of papers whose main body (Chapters 2-5) includes the first authored journal papers [J1-J4].

Contents

Agradecimientos/Acknowledgements **VII**
Abstract **IX**
Resumen **XI**
Thesis details **XIII**
Contents **XVII**
List of Tables **XXI**
List of Figures **XXIII**
List of acronyms **XXVII**
List of Symbols **XXXI**
1. Introduction **1**
1.1. The energy sector 1
1.2. The power grids 2
1.3. The Smart Grid 4
1.4. Power system flexibility 5
1.4.1. The need for flexibility 5
1.4.2. Sources of flexibility 6
1.4.2.1. Flexible generation 6
1.4.2.2. Flexible transmission and grid interconnection 6
1.4.2.3. Control over VRES 6
1.4.2.4. Energy storage facilities 7
1.4.2.5. Demand-side management 7
1.4.2.6. Other sources of flexibility 9
1.5. Power quality, reliability, and resilience 10
1.5.1. Power quality disturbances 10
1.5.1.1 Transients 13
1.5.1.2 Short-duration RMS variation 13
1.5.1.3 Long-duration RMS variation 14
1.5.1.4 Imbalance 15
1.5.1.5 Waveform distortion 15
1.5.1.6 Voltage fluctuation 17

1.5.1.7 Power frequency variations 17
1.5.2. Economic implications and issues of poor power quality 17
1.6. Internet of Things 20
1.7. Objectives 21
1.8. Methodology 21
1.9. Contributions 22
1.10. Structure of the thesis 23
References 24
2. Supraharmonics emission from LED lamps: A reduction proposal based on random pulse-width modulation 29
2.1. Introduction 30
2.2. Power quality in lighting systems review 31
2.2.1. Current situation of Supraharmonics 32
2.3. Survey of LED drivers topologies 33
2.4. RPWM techniques 35
2.5. Material and methods 36
2.5.1. PRBS generator 38
2.5.2. Look-up tables generator 38
2.5.3. RPPM methods 39
2.6. Results and discussion 40
2.7. Conclusions 42
Acknowledgements 42
References 42
3. A novel direct load control testbed for smart appliances 47
3.1. Introduction 48
3.2. Home energy management systems. State of the art. 49
3.3. Smart appliances overview 50
3.4. Structure of the smart appliance control testbed 51
3.4.1. LabVIEW 52
3.4.2. Linking GAMS and LabVIEW 54
3.4.3. An optimization model for demand side management 54
3.5. Case study 57
3.6. Conclusions and future work 63
Acknowledgements 63
References 63
4. Load scheduling strategy to improve power quality in electric-boosted glass furnaces 67
4.1. Introduction 68

4.2. State of the art review 68
4.3. Materials and methods 70
4.3.1. Laboratory setup 70
4.3.2. Mathematical background 72
4.3.3. Thermal considerations 74
4.3.4. Problem formulation 75
4.4. Results and discussion 76
4.4.1. Case study 1: A large-scale subharmonic minimization 76
4.4.2. Case study 2: A small-scale subharmonic minimization 80
4.4.3. Case study 3: Lab testing 82
4.5. Conclusions 84
Acknowledgements 84
References 85
5. IoT cloud-based power quality extended functionality for grid-interactive appliance controllers 87
5.1. Introduction 88
5.2. Overview 89
5.2.1. IoT communication protocols 89
5.2.2. IoT data protocols 90
5.2.3. OpenADR standard 90
5.3. Grid-interactive appliance controller extended functionality 91
5.4. The internet of things platform developed 94
5.5. Protective functionalities provided by the devices 95
5.5.1. Overconsumption 97
5.5.2. Power system frequency deviation 98
5.5.3. Voltage disturbances 100
5.5.4. Voltage harmonic distortion 103
5.5.5. Current harmonic distortion 104
5.6. Conclusions 105
Acknowledgements 105
References 106
6. Conclusions 111
7. Future works 113

List of Tables

Table 1. 1.	Principal PQ disturbances as classified by IEC.	11
Table 1. 2.	Categories and typical characteristics of power system electromagnetic phenomena (IEEE std 1159-2019).	12
Table 1. 3.	Average costs by type of poor PQ event from the survey results.	19
Table 1. 4.	Direct cost per voltage sag.	19
Table 2. 1.	Classification of the different random switching methods.	35
Table 3. 1.	Main parameters of the model.	58
Table 3. 2.	Result summary.	61
Table 4. 1.	Results summary for case study 1.	80
Table 4. 2.	Results summary for case study 2.	81
Table 4. 3.	Results summary for the experimental results.	84
Table 4. 4.	Results validation with case study 2 as reference.	84

List of Figures

Figure 1. 1. a) Evolution of the primary energy production by fuel in EU-27 from 2008 to 2018 and, b) primary energy production in 2018. 1

Figure 1. 2. a) Evolution of the net electricity generation in EU-27 from 2008 to 2018 and, b) net electricity generation in 2018. 3

Figure 1. 3. a) Evolution of the final electricity consumption in EU-27 from 2008 to 2018 and, b) final electricity consumption in 2018. 3

Figure 1. 4. Classification of demand-side management measures..... 7

Figure 1. 5. Demand response programs timescale. 9

Figure 1. 6. Impact of power quality disturbances. 18

Figure 2. 1. Group II. STFT (left) and FFT (right) of the current. 31

Figure 2. 2. Voltage and current waveforms. Figure to the left is a LED lamp equiped with aPFC, and figure to the right without PFC. 32

Figure 2. 3. A three-stage converter LED driver. 34

Figure 2. 4. Characteristics of a randomized switching signal. 35

Figure 2. 5. Test scenario and the equipment used. 37

Figure 2. 6. Block diagram of the FPGA implementation..... 37

Figure 2. 7. Pseudo-random shift registers to generate PRBS. 38

Figure 2. 8. States diagram of the finite state machine that generates each waveform. 39

Figure 2. 9. Discrete carrier waves: a) RPPMa and b) RPPMb..... 40

Figure 2. 10. Frequency spectrum of the experimental input current when: a) conventional PWM, b) RPPMa and c) RPPMb is employed. 41

Figure 3. 1. Smart appliances control testbed overview. 52

Figure 3. 2. LabVIEW graphic user interface. 53

Figure 3. 3. Dynamic-link library flowchart for linking both environments..... 54

Figure 3. 4. Smart home topology employed in the case study. 55

Figure 3. 5. Smart appliances models employed in the optimization: a) Washing machine demand, b) dishwasher demand, and c) tumble drier demand. .. 58

Figure 3. 6. Optimization results using tariff A: a) Power injected by the PV system, smart appliances consumption, non-shiftable consumption, and PV

production, b) Electric water heater performance: Consumption, ambient and water temperature as well as hot water demand, c) energy storage system performance: Power and state of charge, and d) total consumption from the utility and energy prices. 60

Figure 3. 7. Optimization results using tariff DHA: a) Power injected by the PV system, smart appliances consumption, non-shiftable consumption, and PV production, b) Electric water heater performance: Consumption, ambient and water temperature as well as hot water demand, c) ESS performance: Power and state of charge and d) total consumption from the utility and energy prices..... 62

Figure 4. 1. Glass pane melting process. 68

Figure 4. 2. Laboratory setup. 71

Figure 4. 3. Developed prototype. 71

Figure 4. 4. Primitive current waveform. 72

Figure 4. 5. An example of a complex plane for $N = 5$ and $h = 1N$ to show how the resultant component is built. 74

Figure 4. 6. Nominal powers and setpoints dataset to be used in the case studies..... 76

Figure 4. 7. Results for the ICC and accumulator-based methods (case study 1): a) Current spectrum (without the fundamental component), b) percentage of fit for each load in the ICC method and c) aggregated power profile. 77

Figure 4. 8. Results for the proposed MBQP problem in four scenarios of the case study 1: a) Current spectrum (without the fundamental component), b) percentage of fit for each load and d) aggregated power profile. 79

Figure 4. 9. Results for ICC and accumulator-based methods as well as the proposed problem with $\gamma = 50\ \%$ (scenario 2) in case study 2: a) Current spectrum (without the fundamental component), b) percentage of fit for each load and d) aggregated power profile. 81

Figure 4. 10. Experimental current waveform, spectrum, and power profile when applying: a) The ICC, b) Accumulator-based method, and c) the proposed MBQP problem (scenario 2). 83

Figure 5. 1. GIAC overview. 92

Figure 5. 2. RTOS task diagram. 93

Figure 5. 3. Block diagram of the IoT platform with the GIAC and the laboratory equipment. 94

Figure 5. 4. Schematic diagram of the corrective actions for each PQ deviation. 96

Figure 5. 5. Laboratory setup. 97

Figure 5. 6. a) Power profiles employed in the tests as a reference, b) Power consumption when loads 1 and 2 are limited to 1.0 kW and 0.5 kW respectively (Red dashed lines) and c) Power consumption when both loads are limited to 1.0 kW (Red dashed line). 98

Figure 5. 7. a) Power consumption for loads 1 and 2 and measured at the source terminal when both loads are employed to compensate power system frequency deviations (47-52 Hz). b) Power consumption for loads 1 and 2 and measured at the source terminal when both loads are employed to compensate power system frequency deviations (49.5-50.5 Hz). Red dashed lines are the limits at EN 50160. 99

Figure 5. 8. Load voltage and current, as well as device measurements during a test voltage sag. 100

Figure 5. 9. a) Voltage disturbances configured for scenario 1 and limits defined by standards IEEE 1547 and IEC 61727. The shaded part denotes the prohibited region. b) Voltage disturbances identified by the GIAC and power consumption of loads in scenario 1. 102

Figure 5. 10. a) Voltage disturbances configured for scenario 1 and limits defined by standards IEEE 929 and VDE 0126-1-1. The shaded part denotes the prohibited region. b) Voltage disturbances identified by the GIAC and power consumption of loads in scenario 2. 103

Figure 5. 11. Voltage THD profile configured for the test, power consumption for loads 1 and 2, and measured at the source terminal. Red dashed lines are the limits defined in IEEE 519 (12 %), EN 50160 (8 %), and the loads' reconnection criterion (6 %). 104

Figure 5. 12. a) Profiles employed for the 3rd and 4th harmonics and limits defined by the standard IEC 61000-3-2 (red dashed lines), b) Power consumption of load 1 and THD of the current. 105

List of acronyms

AC	Alternating current
ADC	Analog to digital converter
API	Application programming interface
aPFC	Active power factor correction
ASM	Ancillary services market
CAGR	Compound annual growth rate
CAIDI	Customers average interruption duration index
CBP	Capacity bidding programs
CENELEC	Comité Europeo de Normalización Electrotécnica
CIGRE	Consejo internacional de grandes redes eléctricas
CMP	Capacity market programs
CoAP	Constrained application protocol
COP26	26^{th} conference of the parties
CPP	Critical peak pricing
dPF	Displacement power factor
DB	Demand bidding
DC	Direct current
DER	Distributed energy resource
DF	Distortion factor
DG	Distributed generation
DLC	Direct load control
DLL	Dynamic-link library
DoE	Department of Energy
DPMP	Decentralized permissioned marketplace
DR	Demand response
DW	Dishwasher
EDRP	Emergency demand response programs
EMC	Electromagnetic compatibility
EMI	Electromagnetic interference
EMS	Energy management system
ESD	Electrostatic discharge
ESS	Energy storage system
EV	Electric vehicle
EWH	Electric water heater
FFT	Fast Fourier Transform
FPGA	Field programmable gate arrays

GAMS	General algebraic modeling system
GDX	GAMS data exchange
GEB	Grid-interactive buildings
GIAC	Grid-interactive appliance controller
GSM	Global system for mobile communication
GUI	Graphic user interface
HEMS	Home energy management system
HTTP	Hypertext transfer protocol
HVAC	Heating-ventilation-air conditioning
IC	Integrated circuit
I/C	Interruptible/curtailable
ICC	Integral cycle control
ICT	Information and communication technologies
IEA	International Energy Agency
IEC	International Electrotechnical Commission
IEEE	Institute of Electrical and Electronics Engineers
IoT	Internet of Things
ISR	Interrupt service routine
LED	Light emitting diode
LPWAN	Low-power wide-area network
LSB	Least significant bit
LTE	Long term evolution
M2M	Machine to machine
MBQP	Mixed-binary quadratic problem
MG	Microgrid
MQTT	Message queuing telemetry transport
MILP	Mixed-integer linear programming
NAT	Network address translation
NEMP	Nuclear electromagnetic pulse
NGSI	Next-generation service interface
NILM	Non-intrusive load monitoring
nPFC	Non-power factor correction
OCB	Orion context broker
OpenADR	Open automated demand response
OpenLEADR	Python implementation of OpenADR
PEC	Power electronic converter
PEV	Plug-in electric vehicle
pPFC	Passive power factor correction
PFC	Power factor correction
PQ	Power quality
PRBS	Pseudo random binary signal
pu	Per unit

PV	Photovoltaic
PWM	Pulse width modulation
REST	Representational state transfer
RCFMFD	Random carrier frequency modulation fixed duty
RCFMVD	Random carrier frequency modulation variable duty
REE	Red eléctrica de España (Spanish distribution system operator)
RMS	Root mean square
RPPM	Random pulse position modulation
RPWM	Random pulse width modulation
RTOS	Real-time operating system
RTP	Real time pricing
SA	Smart appliance
SAIDI	System average interruption duration index
SAIFI	System average interruption frequency index
SAREF	Smart appliances reference
SD	Standard deviation
SEPIC	Single-ended primary-inductor converter
SG	Smart grid
SGL	Single-precision floating-point
SoAP	Simple object access protocol
SoC	System on Chip
SOC	State of charge
SPI	Serial peripheral interface
SQL	Structured query language
SST	Spread spectrum techniques
STFT	Short-time Fourier transform
TCL	Thermostatically controlled loads
TD	Tumble dryer
THD	Total Harmonic Distortion
TOE	Tons of oil equivalent
TOU	Time of use
TPF	Total power factor
TSC	Total subharmonic content
TV	Television
UART	Universal asynchronous receiver transmitter
UDP	User datagram protocol
UMTS	Universal mobile telecommunication system
VEN	Virtual end node
VI	Virtual instrument
VoLL	Value of lost load
VPP	Virtual power plants
VTN	Virtual top node
WM	Washing machine
WPAN	Wireless personal area network

WSDL	Web service description language
XML	Extensible markup language
XMPP	Extensible messaging and presence protocol

List of Symbols

A	Amplitude of the carrier waveform
α	Tilt angle of the PV system
α_i	Duration of the on-state within the i-th period
α_j	Number of active cycles to be distributed in N
b_h^j	Fourier coefficient for the sine
C	Look-up table values of the carrier waveform
C'	Opposite values to those stored in the look-up table
C_{ess}	Capacity of the energy storage system
C_p	Specific heat of the water
C_{wh}	Capacity of the electric water heater tank
γ	Fraction of cycles that are distributed according to the regular distribution
$\Gamma_j(k_j, t)$	Matrix of shifted consumptions
dP_{ess}^{max}	Maximum ratio of change of $P_{ess}(t)$
D_i	Duty cycle of the i-th period
$D_{wh}(t)$	Hot water consumption at time slot t
δ_i	Logical variable that indicates the state of the main switch at each position i
δ_i^j	Logical variable that indicates the state of the main switch for each load j at each position i
δ_{RPPMa}	Amplitude Resolution of the RPPMa carrier waveform
δ_{RPPMa}	Amplitude Resolution of the RPPMb carrier waveform
ε_i	Delay time of the on-pulse within the i-th period
f_{max}	Maximum value of the frequency
f_{min}	Minimum value of the frequency
f_s	Frequency of the while loop that generates each carrier sample
f_{sw}	Frequency of the carrier waveforms
g_{wh}	Loss factor of the electric water heater
h	Harmonic index
η_{pv}	Efficiency of the PV system
θ_k^j	Position of the cycle k to be allocated for the load j
i	Index that refers to the position of a given cycle within a modulation period T_p

$i_j(t)$	Current waveform of the load j
$i_p(t)$	Current waveform with the minimum energy that can be supplied to a load j using the integral cycle control
I_1	RMS value of the fundamental current component
I_h	RMS value of the current component h
I_{h-max}	Maximum value of I_h
I_h^p	Horizontal component of I_h
I_h^q	Vertical component of I_h
J_{Sub}	Cost function of the MBQP
j	Index that refers to each smart appliance or load
k_j	Index associated with each shifted consumption that may be generated for each smart appliance j
L	Number of loads involved in the scheduling process using the ICC
λ	Latitude of the PV system
N	Number of samples of the carrier waveform or number of cycles in ICC
N_j	Number of smart appliances
N_k^j	Number of possible consumption profiles
$P_{ess}(t)$	Power exchanged with the energy storage system at time slot t
P_{ess}^{max}	Maximum power exchanged with the energy storage system
$P_g(t)$	Power consumption from the grid at time slot t
P_g^{max}	Maximum power imported from the grid
P_j	Nominal power of the load j
P_j^{sp}	Power setpoint for each load j
P_{max}	Maximum power consumption for a given load
$P_{ns}(t)$	Non-shiftable power at time slot t
$P_{pv}(t)$	Power provided by the PV system at time slot t
P_{pv}^{pk}	Installed power of the PV system
$Pr(t)$	Price of the energy at time slot t
$P_{sa}(t)$	Power consumption of the common use smart appliances at time slot t
P_{nwh}	Nominal power of the electric water heater
ρ	Water density
$SOC(t)$	Current state of charge of the energy storage system at time slot t
SOC_{max}	Maximum state of charge
SOC_{min}	Minimum state of charge
$T_{amb}(t)$	Average ambient temperature at time slot t
T_c	Period of the mains supply voltage
T_i	Duration of the i-th period
T_{inlet}	Average temperature of the inlet water
T_p	Modulation period considered for ICC
$T_{wh}(t)$	Average temperature of the water stored inside the electric water heater tank at time slot t
T_{wh}^{max}	Maximum temperature of the water inside the electric water heater tank

T_{wh}^{min}	Minimum temperature of the water inside the electric water heater tank
THD_i	THD of the current
THD_{max}	Maximum value of the THD
THD_{min}	Minimum value of the THD
φ_h	Phase angle of the component I_h
ϕ	Longitude of the PV system
V	RMS value of the mains voltage
$x_j(k_j)$	Binary variable that represents the state of each consumption profile
$x_{wh}(t)$	Binary variable that indicates the state of the electric water heater at time slot t

Chapter 1

Introduction

1.1. The energy sector

In recent decades, the European Union (EU) has focused on remaining a global reference in the field of renewable energies to meet climate change targets. In this regard, the commitments resulting from the last 26th conference of the parties (COP26) based on the Paris Agreement [1] to hold the increase in the global average temperature below 1.5 ºC above pre-industrial levels, are a clear example of this policy. To this end, the countries involved, together with the EU, agreed upon several secondary objectives such as increasing the ability to adapt to the adverse impacts of climate change, curbing greenhouse gas emissions, and providing the necessary funding to support these measures. These actions reinforce the ambition for Europe to remain a world power also in terms of the energy transition.

This evolution is also reflected in the historical primary energy production data collected by the statistical office of the EU, Eurostat [2]. Figure 1. 1 depicts the relative evolution (concerning levels of 2008) of the primary energy production by fuel within the EU-27 during the period 2008-2018 and a detailed distribution of primary energy sources in 2018 as a pie chart, trends are quite illustrative. The production of primary energy within the EU was 634.8 million tons of oil equivalent (toe) in 2018, 1.1 % lower than in 2017: Renewable energies and biofuels (34.2 %), nuclear (30.8 %), solid fossil fuels (18.3 %), natural gas (9.3 %), oil and petroleum products (3.9 %), non-renewable wastes (2.1 %), as well as oil shale, oil sands, and peat products (1.4 %).

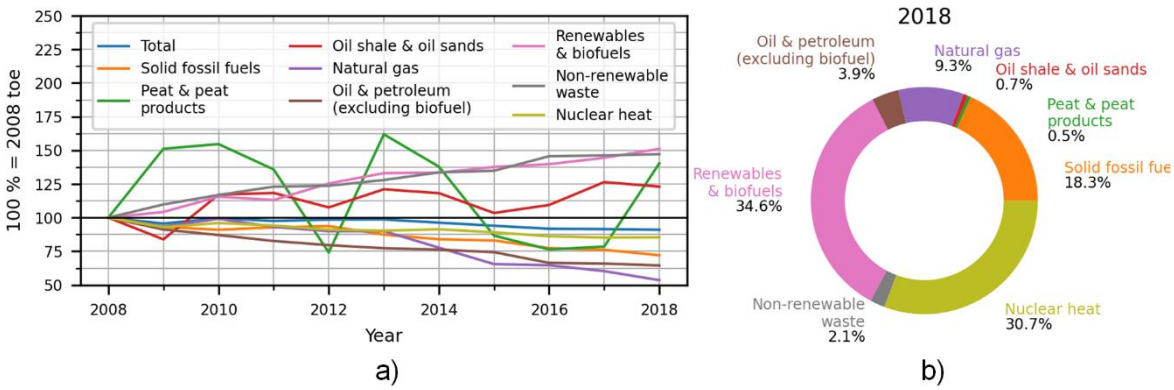

Figure 1. 1. a) Evolution of the primary energy production by fuel in EU-27 from 2008 to 2018, and b) primary energy production in 2018.

In general terms, the trend in primary energy production has been downward in recent years, with a relatively strong fall in 2009, agreeing with the global financial and economic crisis. This fall is mainly due to the descending trends of solid fossil fuels, natural gas, and oil petroleum products, with 11.8, 5.3, and 2.1 % of reduction respectively in the period 2017-2018. However, this decline did not exclusively take place in the last year, the trend of these energy sources is predominantly negative since 1990 but with minor increases. In fact, the primary energy produced by solid fossil fuels, natural gas, and oil petroleum products was 28.0, 46.4, and 35.5 % lower than in 2008. By contrast, the highest growth was reported by renewable energies and biofuels, as well as non-renewable wastes, with 2.8 and 1.5 % of variation respectively in 2017. The energy production from renewable sources has increased significantly in recent decades [3] and accounted for the highest share in primary energy production since 2015. Nuclear energy remains practically unchanged from the previous year (0.1 % increase) but accounted for 85.4 % of the nuclear energy produced in 2008. Oil shale and oil sand as well as peat products have had a more unstable trend over this decade. In particular, the first ones, with maximums of 162.0 % (2013) and minimums of 74.14 % (2012) compared to 2008. Although both energy sources have experienced an increase compared to 2008 (23.1 and 40.4 % respectively), only peat products grew by 78.7 % for 2017 in contrast to oil shale and oil sand (-2.64 %).

1.2. The power grids

Power systems around the world are undergoing significant changes in response to several key drivers: The increasing availability of low-cost variable renewable energy sources (VRES), the deployment of distributed energy resources (DER), advances in digitalization, and growing opportunities for electrification [4], since electricity is playing an ever-more central role in the lives of citizens and expected to be the energy source on which people rely for almost all their everyday needs such as mobility, cooking, lighting, heating, or cooling.

In terms of electricity generation, Figure 1. 2 illustrates the evolution of the net production in the decade 2008-2018 relative to 2008 levels within the EU-27, as well as the breakdown of the different energy sources at the end of this period using a pie chart. The EU-27 reached 2802 TWh in 2018, 0.45 % lower than in 2017 and 1.3 % lower than in 2008 (the highest generation on record). Nearly a half of the generation (45.5 %) was covered by combustible fuels such as natural gas, coal, and oil, and almost a quarter (25.8 %) came from nuclear power plants. Concerning renewable energy sources (RES), the highest share of net electricity generation in 2018 was from hydropower plants (13 %), followed by wind turbines (11.3 %) and solar power (4.1 %). Furthermore, geothermal, and other sources accounted for 0.22 and 0.18 % respectively. Net electricity generation has been growing since there has been recorded data although, with the arrival of the global economic and financial crisis in 2008-2009, this upward trend changed, and net electricity generation fell to 2003 levels. In subsequent years, the net electricity generation has been stable, but still lower than in 2008 (1.45 % lower in 2018). The electricity coming from combustible fuels is at historical lows. It has followed a general downward trend since 2008, accounting for the 83.6 % of the electricity generated from this source in 2008, which means a 16.4 % of reduction. The electricity from nuclear power plants shows a similar behavior and has never returned to 2008 levels (86.2 % in 2018). The production of solar plants and wind turbines has reported the highest growth: From 0.26 and 3.92 % of the total production in 2008 to 4.1 and 11.3 % respectively in 2018. However, the electricity produced by hydropower plants has remained stable in this period. Furthermore, the group of hydropower, wind and solar plants reached in 2018 almost 170 % of the 2008 production, and the electricity generated by wind turbines has approached levels like those of the hydropower plants. Geothermal and

other electricity sources also illustrate a significant growth; however, they are still a minority in the total breakdown. In summary, the relative weight of the RES in the EU's electricity has undergone strong growth in parallel with a large decrease in the significance of combustible fuels as well as a moderate decline in the amount of nuclear energy utilization. Concretely, the RES of electricity have increased their importance by almost 12 percentage points in the period 2008 to 2018. By contrast, both the electricity coming from combustible fuels and nuclear power plants registered a reduction of 8.1 and 3.8 percentage points over the same period.

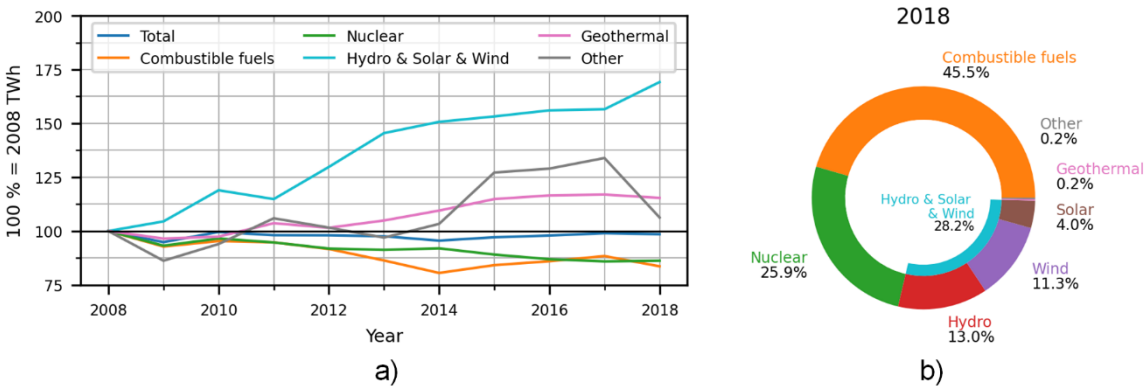

Figure 1. 2. a) Evolution of the net electricity generation in EU-27 from 2008 to 2018, and b) net electricity generation in 2018.

Finally, Figure 1. 3 shows the evolution of the final energy consumption by sector in EU-27 over the previously considered period as well as a detailed breakdown of the different sectors in 2018. The electricity available for final consumption within the EU-27 reached 2590 TWh in 2018, practically the same as in 2017. The distribution of electricity consumption among the different sectors in 2018 is depicted by the pie chart and has evolved roughly constant throughout the decade of study as can be seen from the figure: Industry (36.5 %), transport (2.3 %), services (28.6 %), household (27.3 %), others (5.3 %). In fact, the final consumption, and the consumption of the different sectors account for 98.7, 94.2, 104.0, 103.1, 101.6, and 91.54 respectively from the 2008 levels. The highest variation occurred in electricity consumption of the industrial sector, as well as in the "others" category.

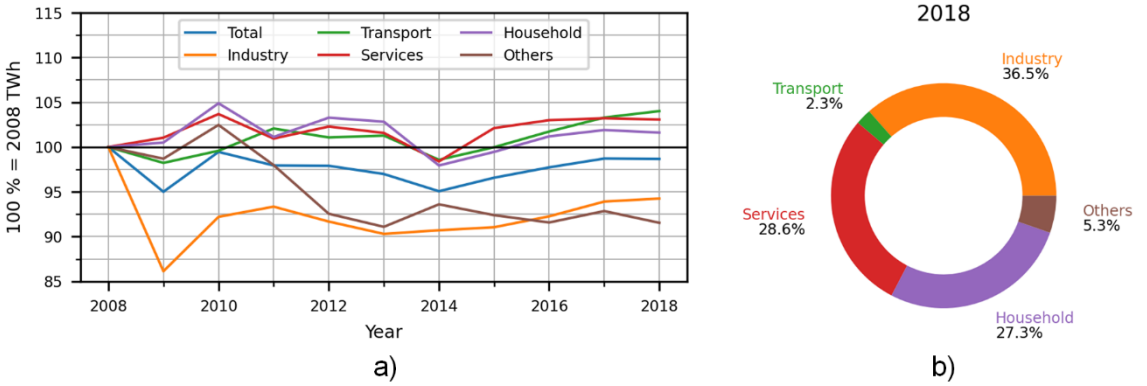

Figure 1. 3. a) Evolution of the final electricity consumption in EU-27 from 2008 to 2018, and b) final electricity consumption in 2018.

Moreover, it should be noted the generalized fall in 2009 due to the global economic and financial crisis. The final electricity consumption decreased moderately by 5.0 % concerning the levels of 2008 as well as the electricity demanded by almost all sectors: Industry (-13.9 %), transport (-1.8 %), services (1.05 %), household (0.5 %), others (-1.3 %), leading to the conclusion that this fall was mainly due to the industrial sector.

1.3. The Smart Grid

The classical power system was originally built to deliver the electrical energy generated by central power plants to the relatively nearby end-users safely and reliably. For this purpose, the voltage level is increased up to 60-750 kV at the source to be transmitted over high-voltage transmission lines and then is gradually reduced to be delivered to consumers in a two-stage distribution process: First, from substations to transformation centers at medium voltage (5-20 kV) and finally from this point to the end-users at low-voltage (230-400 V) [5][6]. Broadly speaking, the structure of the conventional grid can be summarized as follows: Power stations that generate the electrical power, high-voltage transmission lines that transport the power from suppliers to a cluster of consumers as well as medium and low-voltage distribution lines that interconnect individual consumers. Notice that the energy flow is thus unidirectional from power plants to end-users.

This architecture has remained practically unaltered since its conception as it has been highly effective for decades in covering the initially stated needs of providing electrical energy to end-users reliably and safety. However, this vision of the power system is being forced to face new conditions and more demanding requirements in both the industrial and residential sectors because of the current digital revolution as has already been mentioned at the beginning of the previous section. Some of them are detailed below [7]:

- **The increased energy demand** owing to population growth and the proliferation of new technologies such as the electric vehicle (EV).

- **The need to increase the production and carriage capacity** in the current power plants as well as the reduction of the transmission and distribution energy losses and illegal usage.

- **The challenge of reducing the operating costs**, while improving the management of the existing transmission and distribution infrastructures.

- **The rapid growth of distributed generation (DG)** due to grid-connected DER and VRES in presence of conventional power plants. These resources are mainly solar photovoltaic (PV) panels and wind turbines.

- **The need to replace equipment and deploy new technologies** over existing infrastructure. In most cases, the power devices employed in the transmission and distribution systems are transformers, power switches, power breakers, utility meters, and relays, and these components have their potential problems due to the old technology in use. Moreover, the feedback or the capacity of collecting information and measurements during these stages is still quite limited today.

Against this background, the power grid has evolved and must continue doing so to overcome such barriers. This new paradigm of the power system has been called Smart Grid (SG). Although there is no standard definition of the SG yet, the European Technology

Platform (ETP) for SG provides the following definition in its documentation for the strategic deployment of the European electricity networks of the future [8]: “A Smart Grid is an electricity network that can intelligently integrate the actions of all users connected to it - generator, consumers and those that do both – in order to efficiently deliver sustainable, economic and secure electricity supplies”. Notice that now end-users take an active role and can act as energy producers and consumers, becoming what is known as prosumers [9]. The SG could be seen as a digital upgrade of both transmission and distribution grids, in which the idea of a one-way flow of energy and information from suppliers to end-users turns into a complex scheme of a bidirectional flow. Moreover, aspects such as scalability, maintainability, security, and interoperability between devices are central to the SG concept [10]. To this end, the SG must be undoubtedly linked to several concepts such as the Information and communication technologies (ICT) to ensure the exhaustive coordination of stakeholders, the use of RES, and the decentralization of them through the DG, the deployment of smart meters or the advanced metering infrastructure (AMI) towards the monitoring of the consumption and the creation of statistics, and the demand-side management (DSM) to achieve a better balance between generation and consumption as will be discussed later [11].

1.4. Power system flexibility

The concept of power system flexibility has been introduced recently by academics and international organizations. Although a global definition has not been reached yet, as a general rule, flexibility describes the capacity of the power grid to respond to changes in demand or supply while preserving the stability of the system. Thus, from a technical viewpoint, flexibility is essential to address the generation-demand imbalances, however, other aspects need to be considered. A more complete definition is provided by the International Energy Agency (IEA): “Flexibility is the ability of a power system to reliably and cost-effectively manage the variability and uncertainty of demand and supply across all relevant timescales”. Notice how flexibility extends to other dimensions such as time, management, uncertainty, and cost [12]. These points are further detailed below:

- **Time**: Indicates how fast the system can be restored to a given state when it suffers a deviation. Control actions are often classified into short-term, mid-term, and long-term measures.

- **Management measures** or control procedures are performed by the power system operator to deal with unexpected events. These corrective actions depend directly on the time interval available to be applied.

- **Uncertainty** or absence of information about future evolution. The more uncertainty characterizes the system, the more flexibility is required for its proper operation.

- **Cost**: Although the power system scheduler should always offer flexibility, this concept implies an extra charge. Accordingly, a level of commitment must be found between the amount of flexibility and its associated cost.

1.4.1. The need for flexibility

All power systems have a certain degree of flexibility aiming to continuously balance the generation and consumption and ensure system stability. Concretely, this flexibility is employed to maintain the foremost power grid parameters (i.e., voltage and frequency)

within the safe range reported by international standards. although variability and uncertainty have always been considered in power systems, these inherent flexibility mechanisms have demonstrated to be insufficient to perform a successful system regulation when dealing with the presence of large quantities of grid-connected VRES, as is being experienced in recent years since VRES are now cheaper to acquire for electricity generation due to the government funding and the absence of fuel costs. Mainly, these VRES refers to solar, wind, or hydro resources. In this regard, achieving an acceptable balance between generation and demand turns out to be a major challenge due to the intermittent and stochastic dynamic that characterizes these energy sources. Therefore, given these reasons, making the power planning and operation more flexible has become a global priority to achieve the power system transformation in response to these novel trends. Moreover, the current context brought by the covid-19 pandemic has revealed that a flexible and well-functioning power system is crucial to maintaining the operation of critical infrastructures such as those in the healthcare sector [13].

1.4.2. Sources of flexibility

Regulators and system operators recognize that flexibility in all power systems must be addressed by ensuring the following elements [14-17]:

1.4.2.1. Flexible generation

Flexibility is often offered by power plants with fast start-up and shut-down operation and high-power ramp capabilities. Moreover, one of the main features of these flexible sources is an efficient operation at a lower minimum level in periods with high penetration of VRES or even the ability to perform deep turndowns. In this regard, it is crucial to ensure a minimum marginal cost so that these power plants can compete in the market as a source of flexibility. Some of these plants include hydro plants, conventional gas-fired, coal-fired, and fuel-fired power plants, as well as dispatchable renewable power plants (i.e., biomass, geothermal plants, etc). Currently, conventional power plants are the predominant source of flexibility in modern power systems. DG can also perform a fast response to power mismatches to provide local flexibility by modulating their production.

1.4.2.2. Flexible transmission and grid interconnection

Transmission networks are responsible for this kind of flexibility. Among other features, transmission networks must restrict their bottlenecks and have enough capacity to take advantage of a wide range of resources that help to achieve the generation-demand balance. These resources include the use of smart network technologies that better optimize the energy transmission and the interconnection between neighboring power systems. Furthermore, grid interconnection opens the door for electricity trade which could be highly advantageous for power systems extended over multiple time zones. Consequently, their peak-load intervals take place at different times, and their RES with a strong dependency on the time, such as the photovoltaic plants, also reach their maximum production at different times. Therefore, a coordinated strategy can contribute to smoothing out peak demand periods and make use of the energy surpluses.

1.4.2.3. Control over VRES

Uncertainty and variability are part of the VRES's nature and often limit the amount of flexibility that can be provided or sometimes even contribute to the opposite. Therefore, greater control over the generation of these resources can help alleviate the situation. A

scenario with congestion of the transmission lines or when the produced power exceeds the required system demand may be the best example to understand this issue. In such a case, flexibility can be offered via the renewable generation curtailment although this action is the least preferred choice, as it can lead to a suboptimal operation from both viewpoints: Owner's revenues and loss of renewable energy.

1.4.2.4. Energy storage facilities

The spread of storage systems throughout the power grid is undoubtedly another source of flexibility and is especially relevant when considering a context with high penetration of generation coming from VRES. These storage infrastructures can help the power system to absorb the energy surpluses or inject the required energy to solve a momentary mismatch between supply and demand. Currently, pumped hydro energy storage accounts for the highest amount of total storage capacity worldwide. Nevertheless, other technologies such as batteries, ultracapacitors, flywheels, and compressed air are also becoming popular.

1.4.2.5. Demand-side management

DSM is a portfolio of measures to improve the energy system on the side of consumption and evolved during the 1970s because of economic, political, social, technological, and resource supply factors [18]. The US Department of Energy (DoE) provides the following definition of DSM [19]: "DSM is the planning, implementation and monitoring activities of electric utilities that are designed to encourage consumers to modify their level and pattern of electricity usage". DSM includes both energy efficiency (EE) and demand response (DR) measures as can be depicted in Figure 1. 4. These measures range from improving the EE by using less energy while providing the same or even better level of service to the consumers to the implementation of DR techniques such as the use of smart energy tariffs with incentives for certain consumption patterns or sophisticated real-time control of DER. More specifically, EE includes both the use of high-efficiency equipment and energy conservation strategies while DR is divided into explicit and implicit measures.

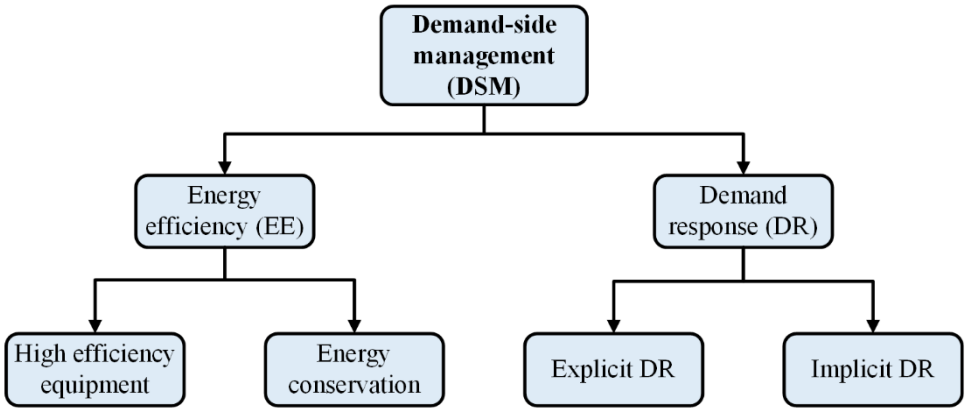

Figure 1. 4. Classification of demand-side management measures.

Regarding the concept of DR, the US DoE also defines it as [20] "Changes in electric usage by end-use customers from their normal consumption patterns in response to changes in the price of electricity over time, or to incentive payments designed to induce lower electricity use at the time of high wholesale market prices or when system reliability is jeopardized". DR has already proven to be a resource that the grid operator can use to provide system reliability, stability, and security services. As shown in Figure 1. 4, DR services are normally classified into two groups attending to the mechanism used to promote the

response: Explicit and implicit DR. Explicit DR is a committed and dispatchable DR action traded on the energy market and is usually provided by an independent aggregator, virtual power plants (VPP) or a supplier. In this case, consumers receive an incentive to change their consumption in certain scenarios such as the grid congestion or balance problems among others. This is referred to as incentive-driven DR. The following programs can be found within this category:

- **Demand bidding/buyback programs (DB)**: The utility pays an incentive to reduce electric load when notified of a DR event day. Customers submit load reduction bids for an event, which can be called on a day-ahead or day-of basis. For any event, the customer may elect to submit or not submit a bid. Incentive payments are valued and coordinated with the day-ahead energy market.

- **Direct Load Control (DLC)**: Allows the aggregator control over certain equipment, e.g. switching-off noncritical loads or modifying devices' setpoint to reduce net electrical load. In general, DLC rates are based on system reliability and can therefore be applied within minutes without waiting for a customer response.

- **Emergency demand response programs (ERDP)**: Customers receive incentive payments for load reductions when needed to ensure reliability. Program events are often declared between 30 min and 2 hours after power delivery.

- **Interruptible/curtailable (I/C)**: Customers receive a discounted rate for agreeing to reduce the load on request.

- **Ancillary services market programs (ASM)**: Customers receive payments from a grid operator for committing to restrict load when needed to support the operation of the electric grid (i.e., auxiliary services). A customer load commitment is required ahead of time. If their bids are accepted, they must often be ready to provide load reduction within one hour of being notified.

- **Capacity market programs (CMP)**: CMP involves load reduction commitments months in advance. Customers offer load curtailments as system capacity to replace conventional generation or delivery resources. Customers typically receive day-of notice of events (less than two hours) and face penalties for failure to curtail when called upon to do so. Incentives usually consist of up-front reservation payments.

Concerning implicit DR, some of the most common DR products are summarized below. Under this scheme, consumers agree to be exposed to hourly or shorter-term tariffs in which the price of the electricity varies depending on production costs. Therefore, consumers adapt their consumption (through automation or personal choice) to save on the electricity bill. Implicit DR is also known as priced-based DR.

- **Time-of-use (TOU)**: A rate with different unit prices for usage during different blocks of time, for a 24-hour day. Daily pricing blocks include an on-peak, partial-peak, and off-peak price for non-holiday weekdays, being the on-peak price the highest, and the off-peak price the lowest. These tariffs include diurnal and seasonal variations in electricity cost but are fixed several months before. It can be integrated within the operations planning stage.

- **Real-Time Pricing (RTP)**: A retail rate in which the price fluctuates hourly reflecting changes in the wholesale price of electricity. These are typically known to customers on a day-ahead or hour-ahead basis.

- **Critical Peak Pricing (CPP)**: Hybrid of the TOU and RTP. The basic rate structure is TOU. However, the normal peak price is replaced with a much higher CPP event price under specified trigger conditions (e.g., when system reliability is compromised, or supply prices are very high). It is called on the day of economic dispatch.

Finally, Figure 1. 5 summarizes the load commitment timescales over which these DR schemes operate.

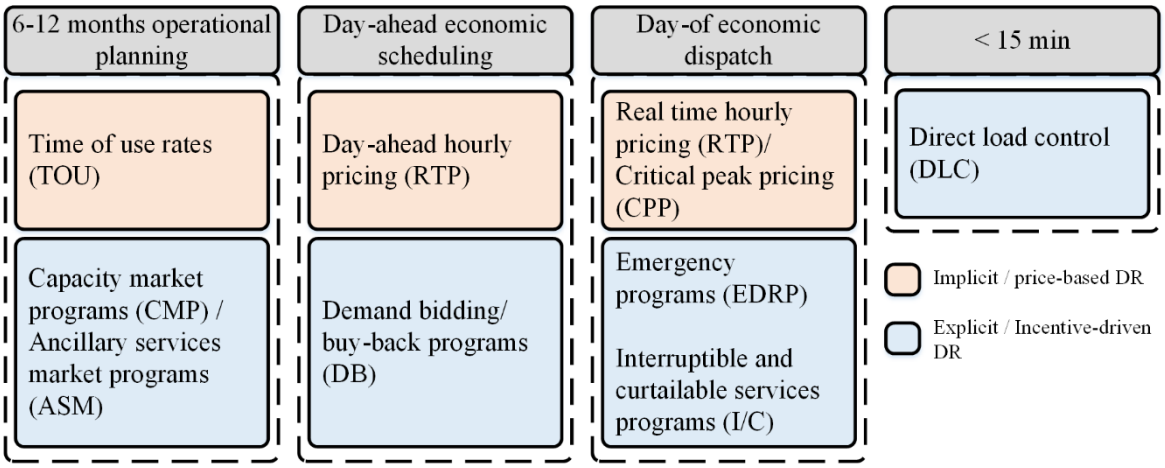

Figure 1. 5. Demand response programs timescale.

1.4.2.6. Other sources of flexibility

Other flexibility resources include ancillary services. The power grid requires ancillary services to ensure reliability and support its main function of delivering electrical energy to consumers. These services are power generator control capacity services employed by system operators as a flexibility mechanism to preserve the instantaneous and continuous balance between generation and consumption. Although most balance requirements are being covered by regulation, spinning, and non-spinning reserve ancillary services, new ancillary services such as load following, frequency response reserve or inertia response are also proliferating.

Moreover, on a smaller scale, the utilization of EV and multi-mode operation of combined cycle units have also been revealed as another source of flexibility by providing a particular case of energy storage system or recovering exhaust heat from thermal units to drive a steam turbine and generate more electricity, respectively.

Finally, this thesis seeks to improve the power system flexibility as will be discussed later in each chapter. To do so, it mainly makes use of DSM in both dimensions DR and EE besides control over VRES and energy storage facilities.

1.5. Power quality, reliability, and resilience

The main goal of modern power systems is to deliver the required electrical energy to its customers as economically as possible with an acceptable level of reliability. Nowadays, the working and social habits of modern society have led end-users to expect the supply to be continuously available on demand. However, it is not possible to achieve a risk-free power system. In this context, engineers and power system managers try to maintain reliability as high as possible within their socio-economic constraints [21].

In most countries, the electricity sector is currently a deregulated and competitive environment where accurate information on system performance must be provided to ensure adequate service to customer needs. To this end, a series of indices have been proposed under the concept of reliability. In the electric power industry, reliability reflects the ability to supply electricity in the amount demanded by users. Specifically, reliability has to do with total electrical interruptions (outages), that is, the complete loss of voltage. These reliability indices include measurements such as the number of interruptions and how long they last, the customers affected, and the power interrupted. There are a wide variety of indices to measure reliability, but the most common is the system average interruption duration index (SAIDI), system average interruption frequency index (SAIFI), and customers average interruption duration index (CAIDI) as defined in IEEE Standard 1366 [22]. SAIDI and SAIFI values include sustained interruptions, which are defined as outages that last at least 5 minutes (although this is not uniform and may vary).

Another concept related to reliability is that of power quality (PQ), although they are two different issues. While the simplest idea of reliability is whether the power is available as it is needed, PQ can be defined as the degree to which current and voltage maintain their waveforms adjusted to a perfect sine wave with constant amplitude and frequency at a given point of the power system. An additional requirement of the current quality is that it must be in phase with the voltage waveform. Therefore, PQ is the combination of voltage and current quality [23]. As will be detailed further in the following section, a wide variety of electromagnetic disturbances are collected under this term and all of them can affect a critical installation to the extent that it depends on the sensitivity of each and particular load.

Finally, the concept of resilience is currently attracting a lot of interest. The topic has become one of the most studied issues in the energy industry since Hurricane Katrina dramatically exposed the vulnerability of the power grid in Louisiana in 2005. The frequency of extreme weather events such as hurricanes, tsunamis, ice storms, and other natural disasters as well as man-made cyber and physical attacks have increased in recent years and affect an increasing number of human and environmental victims worldwide [24]. This term comes from the Latin root "resilire", which means “the ability to spring back or rebound”. If disruptive events can occur regularly, for a system, resilience would be the ability to anticipate, compensate, adapt, and recover from a potentially damaging event [25].

1.5.1. Power quality disturbances

In recent years, the increasing number of electronic equipment connected to the power grid that can generate electromagnetic disturbances or be affected by them has caused the community to become interested in the measurement and classification of these disturbances as a first step to subsequently decide on the appropriate strategy to address their mitigation. In this regard, prestigious international organizations such as the International Electrotechnical Commission (IEC) and the Institute of Electrical and Electronics Engineers (IEEE) have made decisive efforts by providing relevant standards and regulations related to PQ issues from several viewpoints. Although this section is mainly focused on standards that address the classification of the principal electromagnetic phenomena causing PQ

disturbances within the power system, many others intended for specifying measurement techniques or limits for these disturbances are also included to bring a more detailed insight and introduce the required background for the understanding of the remaining chapters. Accordingly, the IEEE std 1159 "*Recommended practice for monitoring electric power quality*" [26] and IEC 61000-2-5 "*Electromagnetic compatibility (EMC) - Part 2-5: Environment – Description and classification of electromagnetic environments*" [27] have been considered as the reference in this section. These standards offer classifications with different approaches and terminology (e.g., the term sag is used in the PQ community as a synonym of the IEC term dip) as illustrated in Table 1. 1 and Table 1. 2.

Table 1. 1. Principal PQ disturbances as classified by IEC.

Categories	**PQ disturbances**
Conduced low-frequency phenomena	Harmonics of the fundamental power frequency
	Voltage amplitude and frequency changes (e.g., Dips, interruptions, imbalances, power frequency variations)
	Common-mode voltages
	Signaling voltages in power supply networks (Power line carrier)
	Islanding supply networks
	Induced low-frequency voltages
	DC voltage in AC networks
Radiated low-frequency phenomena	Magnetic and electric fields
Conduced high-frequency phenomena	Induced continuous-wave voltages or currents
	Unidirectional transients
	Oscillatory transients
Radiated high-frequency phenomena	Continuous oscillatory disturbances
	Modulated disturbances
	Pulsed disturbances
Electrostatic discharge phenomena (ESD)	ESD currents
	Fields produced by ESD currents
Nuclear electromagnetic pulse (NEMP)	-

Table 1. 2. Categories and typical characteristics of power system electromagnetic phenomena (IEEE std 1159-2019).

Categories			**Typical spectral content**	**Typical duration**	**Typical voltage magnitude**
Transients					
	Impulsive				
		Nanoseconds	5 ns rise	< 50 ns	
		Microseconds	1 μ rise	50 ns – 1 ms	
		Milliseconds	0.1 ms rise	> 1 ms	
	Oscillatory				
		Low frequency	< 5kHz	0.3 – 50 ms	0 – 4 pu (a)
		Medium frequency	5 –500 kHz	20 μs	0 – 8 pu
		High frequency	0.5 – 5 MHz	5 μs	0 – 4 pu
Short-duration RMS variations					
	Instantaneous				
		Sag		0.5 – 30 cycles	0.1 – 0.9 pu
		Swell		0.5 – 30 cycles	1.1 – 1.8 pu
	Momentary				
		Interruption		0.5 cycles – 3 s	< 0.1 pu
		Sag		30 cycles – 3 s	0.1 – 0.9 pu
		Swell		30 cycles – 3 s	1.1 – 1.4 pu
	Temporary				
		Interruption		3s – 1 min	< 0.1 pu
		Sag		3s – 1 min	0.1 – 0.9 pu
		Swell		3s – 1 min	1.1 – 1.4 pu
Long-duration RMS variations					
	Sustained interruptions			> 1min	0 pu
	Undervoltages			> 1min	0.8 – 0.9 pu
	Overvoltages			> 1min	1.1 – 1.2 pu
	Current overload			> 1min	
Imbalance					
	Voltage			Steady state	0.5 – 2 %
	Current			Steady state	1 – 30 %
Waveform distortion					
	DC offset			Steady state	0 – 0.1 %
	Harmonics		0 – 9 kHz	Steady state	0 – 20 %
	Interharmonics		0 – 9 kHz	Steady state	0 – 2 %
	Notching			Steady state	
	Noise		Broadband	Steady state	0 – 1 %
Voltage fluctuations			< 25 Hz	Intermittent	0.1 – 7 % 0.2 – 2 P_{st} (b)
Power frequency variations				< 10 s	± 0.1 Hz

[a] Per unit (pu)
[b] Flicker severity index as defined in IEC 61000-4-15:2010 and IEEE Std 1453.

As can be derived from these classifications, the IEEE adopts a quantitative approach as opposed to the qualitative one assumed by the IEC. Therefore, the IEEE Std 1159 is more specific in terms of delimitation of different electromagnetic phenomena, as it provides clear

numerical limits or ranges (e.g., specific magnitudes, frequency ranges, or time durations) against labels such as “low-frequency” and “high-frequency” given by the IEC for the particular case of this PQ parameter. At the same time, the IEC classification also employs the categories “conduced” and “radiated” to describe the nature of electromagnetic phenomena. Given all these reasons, the main body of this section follows the structure proposed by the IEEE. Electromagnetic phenomena and their characteristics are discussed in the following lines.

1.4.3.1 Transients

Transients give the name to a phenomenon that is undesirable and momentary in nature and can be classified into two categories: Impulsive and oscillatory transients depending on the waveshape of a current or voltage transient. IEEE Std C62.41.1-2002 [28] deals with defining standard impulsive and oscillatory transient test waves to test electrical equipment.

- **Impulsive transients**: Impulsive transients are sudden, nonpower frequency change from the nominal condition voltage, current, or both, that is unidirectional in polarity. The most common cause of impulsive transients is lightning and are often damped quickly by impedance circuit elements due to the high frequencies involved. There can be a significant difference in the transient characteristics from one location to another within the power system. Impulsive transients are often characterized by their peak value, rise, and decay, or duration times.

- **Oscillatory transients**: Oscillatory transients are sudden, nonpower frequency change in the steady-state condition of voltage, current, or both, that includes both positive and negative polarity values. An oscillatory transient consists of a voltage or current whose instantaneous value changes polarity rapidly and often decays within a fundamental-frequency cycle. The subclasses are high, medium, and low frequency and have been chosen to correspond with typical types of oscillatory transients within the power system. High-frequency oscillatory transients (> 500 kHz) are normally provoked by switching events or can be the response of one point of the system to an impulsive transient. When the frequency of the primary frequency component of an oscillatory transient is within the range of 5 – 500 kHz, the category used is medium frequency. Back-to-back capacitor energization can give rise to this electromagnetic phenomenon. Finally, low-frequency oscillatory transients (< 5 kHz and duration between 0.3 and 50 milliseconds) are normally found in sub-transmission and distribution lines and can be the result of many types of events (e.g., capacitor, ferro resonance, or transformers energization).

1.4.3.2 Short-duration RMS variation

These PQ disturbances are related to or usually provoked by fault conditions, power supply of large loads with high initial currents, or intermittent loss of connection in power conductors. It consists of a variation of the root mean square (RMS) value of the voltage or current from the nominal during a time greater than 0.5 cycles of the power frequency but less than or equal to 1 minute. When the affected variable is voltage, it can be further described using a modifier indicating the magnitude of the voltage variation (e.g., sag, swell, interruption) and possibly a modifier indicating the duration of the variation (e.g., instantaneous, momentary, temporary). These modifiers regarding the voltage are detailed as follows:

- **Instantaneous**: A type of short-duration RMS voltage variation with a duration between 0.5 cycles and 30 cycles of the power frequency.

- **Momentary**: A type of short-duration RMS voltage variation with a duration between 0.5 cycles of the power frequency and 3 seconds.

- **Temporary**: A type of short-duration RMS voltage variation with a duration between 3 seconds and 1 minute.

- **Interruption**: It is considered a complete loss of voltage and refers to an RMS voltage variation in which the RMS of the voltage on one or more phases falls below 0.1 pu for a time period of less than 1 minute. Power systems faults, equipment failures or control malfunctions can result in an interruption.

- **Sag**: A type of short-duration RMS voltage variation where the RMS of the voltage on one or more phases is within the range 0.1 – 0.9 pu. Voltage sags are often related to system faults but are also provoked by large load changes when the power consumption increases.

- **Swell**: A type of short-duration RMS voltage variation where the RMS of the voltage on one or more phase wires is above 1.1 pu from durations from 0.5 cycles to 1 minute. Typical magnitudes are between 1.1 and 1.2 pu. Voltage swells are much less frequent than voltage sags and can be caused by switching off a large load, switching on a large capacitor bank or when a single line-to-ground fault occurs, resulting in a temporary voltage rise on the unfaulted phases.

Several standards or recommended practices guidelines commonly used to describe the interconnection between generators or DERs and the utility such as IEEE Std 1547 [29], IEC 61727 [30], IEEE Std 929 [31], and VDE 0126-1-1 [32] provide limits in terms of magnitude-duration curves for these types of voltage variation as will be further discussed in the following chapters.

1.4.3.3 Long-duration RMS variation

These PQ disturbances represent a variation of the voltage or current RMS value from the nominal for a time period greater than 1 minute. The causes are usually the load variations on the system and system switching operations rather than system faults. Similar to the short-duration RMS variation, it can be further described using a modifier indicating the magnitude of the voltage variation. In this sense, three subcategories are possible: Overvoltage, undervoltage, and sustained interruption.

- **Overvoltage**: An overvoltage involves an RMS increase in the voltage greater than 1.1 pu for a period of time exceeding 1 minute. Typical values in power systems are within the range 1.1 – 1.2 pu. Overvoltages can also be the consequence of switching off a large load or of a variation in the reactive power of the system when a large capacitor bank is connected. A wrong connection of the transformer taps can also provoke a system overvoltage.

- **Undervoltage**: A system undervoltage occurs when the RMS value of either voltage or current falls below 0.9 pu with the same time condition as system overvoltages.

Concerning the causes, undervoltages are produced by the opposite events to overvoltages. Overloaded circuits can also produce system undervoltages.

- **Sustained interruptions**: A sustained interruption is defined as the decrease of the voltage to less than 10 % of nominal for a period of time exceeding 1 minute. Voltage interruptions longer than 1 minute are often permanent in nature and require manual intervention for restoration.

1.4.3.4 Imbalance

In a three-phase system, imbalance (or unbalance) is defined as the ratio of the magnitude of the negative sequence component to the magnitude of the positive sequence component, expressed as a percentage. This definition can be applied for either voltage or current. The voltage imbalance is often around 5 % in normal three-phase power systems. Current imbalance can be significantly higher when single-phase loads are present in the system.

1.4.3.5 Waveform distortion

Waveform distortion involves a steady-state deviation from the theoretical power frequency sinusoid principally characterized by the spectral content of the deviation. There are five primary types of waveform distortion under this category:

- **DC offset**: The existence of direct current (DC) voltages or currents in an alternating current (AC) power system can be the result of geomagnetic disturbances or due to the consequence of half-wave rectification that many devices include in their electronics. The presence of DC components in AC networks can lead to an increase in transformer saturation, among other adverse effects.

- **Harmonics**: Sinusoidal voltages or currents having frequencies that are integer multiple of the frequency at which the supply system is designed to operate (termed the *fundamental frequency*; usually 50 or 60 Hz) are called harmonics. Harmonics contribute to the waveform distortion in combination with the fundamental voltage or current and their presence is mainly due to the nonlinear nature of devices and loads connected to the power system. Electronic-based equipment (e.g., Pulse-width modulation converters, switching power supplies, or rectifiers) is often responsible for this harmonic distortion that is currently a growing concern for many power system stakeholders. IEC 61000-4-7 [33] defines a harmonics measurement technique and IEC 61000-3-2 [34] establishes limits for individual harmonics. Moreover, in order to characterize the harmonic distortion in a single quantity, various indices such as the total harmonic distortion (THD) or total demand distortion (TDD) have been proposed in IEC 61000-4-7 and IEEE Std 519 [35]. These standards and some others also provide limits for these indices in both the current (IEEE Std 519) and the voltage (IEEE Std 519 and EN 50160 [36]) magnitudes. Most standards agree on establishing ranges within the frequency spectrum since the frequency components behave quite differently depending on the frequency range to which they belong. The low-frequency range often referred as frequency harmonic range or simply harmonics covers from DC to 3 kHz (IEEE Std 519) or 9 kHz (IEC 61000) for both the current and the voltage signals while higher frequencies, particularly the range 2 – 150 kHz, are still under discussion. In fact, the concern about conduced emissions that were originally focused on the range 450 kHz – 30 MHz was extended down to 2 kHz later. This frequency range (2 – 150 kHz)

known as supraharmonics in the literature is giving rise to much research at different locations, but the knowledge is currently limited [37]. In this regard, the growing number of supraharmonics-related issues reported by researchers urges working groups to consider supraharmonics as a PQ problem. There are considerable on-going activities within IEC (both SC 77A and SC 205A), CENELEC, and IEEE to develop standards covering this frequency range. By now, there are several methods for supraharmonics measurement and acquisition proposed by IEC SC 77 and included as informative annexes in IEC 61000-4-30 [38] and IEC 61000-4-7: Annex C of IEC 61000-4-30 for voltage measurements and annex B of IEC 61000-4-7 for voltage and current measurements in the ranges 2 – 150 kHz and 2 – 9 kHz respectively.

- **Interharmonics**: These are voltages or currents in whose spectral content there are frequency components that are not integer multiple of the fundamental frequency. Interharmonics can be found at certain frequencies or as a wideband spectrum at any point of the network. The principal origins of this waveform distortion are pulse-width modulated converters, cycloconverters, static frequency converters, integral cycle control (ICC) and induction furnaces as well as arcing devices, especially those whose control is not synchronized with the power system frequency. Power line carrier signals can also be considered interharmonics. Although the effects of interharmonics are not well known yet, they have been shown to cause flicker or low-frequency torsional oscillations in motors, among others. IEC 61000-4-7 also defined the measurement technique for interharmonics. Finally, it is noteworthy to mention a particular case of interharmonics called subharmonics. These components belong to a special class of interharmonics where frequency components in voltage or current waveforms have a harmonic order lower than one [39].

- **Notching**: Notching is a periodic voltage disturbance characterized by a high-frequency spectral content and is caused when the current commutates from one phase to another (momentary short circuit between two phases) during the normal operation of power electronics converters. The severity of the phenomenon at any point of the power system is given by the source inductance and the isolating inductance between the converter, the magnitude of the current, and the point being monitored. This PQ disturbance can sometimes provoke frequency or timing errors on power electronics circuits that use zero crossings for synchronization purposes since the voltage notch can produce additional zero crossings (e.g., Thyristor-based converters). Notching is further described in IEEE std 519. A variant termed “voltage notching ringing” can also appear when a system resonance results in a ringing response at each of the commutation notches. In such a case, the disturbance can be mitigated by using harmonic filters or capacitor banks to change the system resonance conditions.

- **Noise**: Noise consists of any undesirable disturbance with broadband spectral content (typically below 200 kHz), either voltage or current, that cannot be classified as harmonic distortion or transient. In power systems, noise can be caused by power electronics devices, control circuits, loads with solid-state rectifiers, and arcing equipment. The magnitude of the noise does not normally exceed 1 % of the voltage magnitude and can usually be mitigated by using isolation transformers, line conditioners, filters, or proper grounding circuits.

1.4.3.6 Voltage fluctuation

Voltage fluctuations involve systematic variations of the voltage envelope or a series of random voltage changes, the magnitude of which are typically within the range 0.95 – 1.05 pu. Voltage fluctuations can be caused by equipment that exhibits a rapid variation of the load current magnitude or reactive power. For further details, IEC 61000-3-3 [40] defines several voltage fluctuations and IEEE std 1453 [41] incorporates the IEC methodology for these measurements.

When voltage fluctuations occur in lighting systems, humans can perceive the changes in the lamp illumination intensity, and the phenomenon is referred to as flicker. However, both terms must not be confused. Voltage fluctuations cause flickers. Therefore, voltage fluctuation describes the electromagnetic disturbance, while flicker describes the impact of this on the lighting intensity.

1.4.3.7 Power frequency variations

Power frequency variations reflect the deviation of the power system's fundamental frequency from its specified nominal value (e.g., 50, 60 Hz). The steady-state power system frequency is directly influenced by the rotational speed of the generators in the power system. The frequency depends on the balance between the capacity of the available generation and the consumption at any given instant. Therefore, small mismatches between these variables will cause small instantaneous frequency deviations and the magnitude and duration of these PQ disturbances will depend on the load characteristics and the dynamics of the generation system's response to load changes. Power frequency deviations are often caused by faults in the bulk power transmission system, a large block of loads being disconnected, or a large source of generation changing to islanded mode.

It should be noted that large frequency variations are rare on modern interconnected power systems; However, weak systems such as islanded microgrids are more likely to report these disturbances due to their relatively low inertia and capacity.

Concerning the limits to identify these variations, the standard EN 50160 establishes the thresholds for both interconnected and islanded power systems with 50 Hz nominal frequency. The average value of the frequency measured every 10 seconds must be within the range 49.5 – 50.5 Hz and 47 – 52 Hz during the 99.5 % of the year and 100 % of the time respectively for interconnected power systems. These ranges are more relaxed for islanded power systems: 49 – 51 Hz and 42.5 – 57.5 Hz for 95 % of the week and 100 % of the time.

Finally, it is noteworthy to mention that this Ph.D. thesis pays particular attention to long and short-duration RMS variations, waveform distortion (harmonics and interharmonics), and power frequency variations, as discussed throughout the chapters.

1.5.2. Economic implications and issues of poor power quality

While it is easy to understand how unreliability can affect all customers, the effects of poor PQ, on the other hand, are more difficult to recognize. Pure waveform deviations can create everything from a barely noticeable annoyance for the residential customer to a major disruption to the processes of industrial or commercial customers. As operations based on electronic technology become more common, high PQ requirements become more important, particularly for mission-critical facilities.

The power system reliability literature regarding the economic consequences of an energy supply outage and how they are calculated today represents a mature discipline [42]. The renowned survey [43] found that by 2015 the power outages had cost the US economy some $59 billion, an increase of more than 68% since its previous study in 2004. Commercial and industrial businesses account for more than 97% of these costs. Particularly, and

according to MeriTalk [44], 40% of global health organizations experience an unplanned outage in the year. The average cost is $ 432,000 per incident, where diagnostic imaging systems are among the main affected. To get a closer look the recently published paper [45] presents the direct economic impact of power outages in inpatient and outpatient health care facilities across the United States and the District of Columbia. A combination of traditional metrics has been adopted, including the calculation of the Value of Lost Load (VoLL), achieving the appropriate granularity.

Outages due to catastrophic events are not usually included in reported index numbers. These include ice storms, hurricanes, earthquakes, and floods. Many analysts agree that the per-customer economic costs of these long, severe, and extended outages are far greater than the above and that those larger costs have not yet been well reported or well estimated [46].

On the other hand, there are fewer surveys on the cost of poor energy quality, and not entirely comprehensive. The largest survey was carried out in the EU across sixteen industry sectors [47] and found that the total cost of losses related to poor PQ exceeds €150 billion, where the industry representing over 90%. The survey also identified that voltage dips and interruptions were liable for around 55% of losses and mainly affected electronic equipment, which is now so widespread in the industrial and service sectors. The detailed impact of PQ disturbances facing countries is classified in the following Figure 1. 6. It also shows that the amount of voltage sags detected is about twice as high as long interruptions.

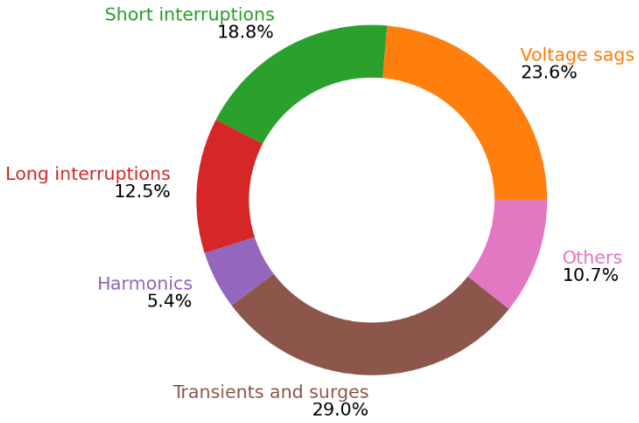

Figure 1. 6. Impact of power quality disturbances.

In the industrial sector, the most important losses occur in manufacturers with continuous processes. In contrast, the average number of disturbances is lower in the service sector. These costs are probably underestimated since it is often difficult to distinguish the root cause of the electrical problems that arise in the office environment. In addition, the survey did not include data centers, which may be the most critical infrastructure in this sector. It should be noted that the highest losses occur in hospitals, which, due to their idiosyncrasy, have a slightly higher PQ cost than others within the service sector. The companies in this study invest € 297.5 million annually in mitigation solutions for various PQ issues. The results of the survey are synthesized in Table 1. 3.

Table 1. 3. Average costs by type of poor PQ event from the survey results.

PQ event	Average cost (€)
Surge or transient	12000-18000
Long interruption	90000
Short interruption (service sector)	18000-36000
Short interruption (Industry)	7000-14000
Voltage sag	2000-4000

Another well-known study [48] based on information provided by 985 United States companies, concluded that for PQ disturbances other than sags, the cost per year to the US digital economy and industrial companies is $6.7 billion. Overall, the data suggest that while the US economy (across all business sectors) is losing between $104 billion and $164 billion per year due to outages, PQ disturbances alone account for $15-24 billion per year.

A very recent paper includes the latest information on the impact of PQ issues in the UK [49]. This study explores the various challenges and gaps in British electricity distribution. No specific comprehensive and large-scale studies have been carried out in the world in recent years. This doctoral thesis [50] presents an extensive summary of all the surveys carried out worldwide from the end of the 20th century to the decade 2010 and their main conclusions. In next table is presented the summary of the direct cost per event. Reported damages due to long interruptions are also included only as a reference. The results of these surveys can still be extrapolated to most current cases.

Table 1. 4. Direct cost per voltage sag.

Section	Division	Activities	financial loss	Currency
Manufacturing	General	Large industrial and commercial (US)	7694	US$
	Paper and paper products	Paper manufacturing (US)	30000	US$
	Chemical and Chemical products	Chemical industry (US)	50000	US$
	Non-metallic mineral products	Glass industry (EU)	250000	€
	Non-metallic mineral products	Glass plant (US)	200000	US$
	Basic metals	Steel works (EU)	350000	€
	Basic metals	Steel works (UK)	250000	US$
	Computer, electronic and optical products	Semiconductor (US, EU and Far East)	2500000	US$
	Computer, electronic and optical products	Semiconductor (EU)	3800000	€
	Machinery and equipment	Equipment manufacturing (US)	100000	US$
	Motor vehicles, trailers	Automobile industry (US)	75000	US$
Information and communication	Telecommunications	Telecommunications (EU)	30000	€
	Information service activities	US computer center (US)	600000	US$
	Information service activities	Computer center (EU)	750000	€
Financial and insurance activities	Activities auxiliary to financial services and insurance activities	Credit card processing (US)	250000	US$

1.6. Internet of Things

The concept Internet of Things (IoT) was originally introduced in 1999 by the pioneer of British technology, Kevin Ashton [51]. Everyday objects become smarter by including internet connectivity and ubiquitous sensors and given the progress of the fourth industrial revolution (or industry 4.0), these objects will end up connected sooner or later. Although the digital transformation of an industrial system is already a major achievement, the IoT will bring about a revolution in society. Undoubtedly, the idea of industry 4.0 involves embracing the IoT paradigm [52] which means that the network is extended to the real world covering all kinds of daily objects. The main areas of IoT investments (industries and use cases) include manufacturing operations, transportation, SG, smart buildings, and, increasingly, consumer IoT, smart home automation, and retail. The unprecedented boom of IoT has been fueled by several market enablers:

- **Decrease sensors and electronic components costs**. In the last 15 years, the average cost has decreased by more than 40%.

- **Increase of Edge Computing**. Centralized computing represents a limitation for IoT since it increases the amount of data transferred and the related costs. Edge computing allows processing exactly where and when it is required.

- **Global hyper-connectivity** allows processing in near real-time the information collected by the myriad of deployed IoT sensors.

The underlying aim is not just to create data, but also to extract valuable insights from the data generated by these devices. In this regard, communication technologies play a central role and should enable a dynamic and secure deployment of IoT so that this large amount of generated data can be properly managed. While challenging, the next generation of 5G and new IoT connectivity will speed up the ability to collect data and upload it to the cloud, which means massive exploitation of these technologies [53]. At the end of 2018, there were an estimated 22 billion connected IoT devices in use around the world and, this number will rise to 38.6 billion by 2025. Moreover, forecasts suggest that by 2030 around 50 billion of these devices will be in use worldwide, creating a web of interconnected devices [54].

IoT paves the way not only for the transformation of products, which can be customized in quasi-real-time but also for service models. From an industrial point of view, the adoption of IoT and interconnected services should be based on the following basic design principles [55]:

- **Interoperability**: All material and human resources within industry 4.0 should offer the ability to be interconnected using IoT and its applications.

- **Virtualization**: Buildings or industrial facilities should have a virtual copy representing all the information collected by sensors or systems as well as simulation models.

- **Decentralization**: Objects located at the industrial facilities should have autonomous decision-making capabilities.

- **Real-time capabilities** through data acquisition, analysis, and decision-making by incorporating the required artificial intelligence.

- **Service-oriented** by offering an extensive portfolio of services to enable the interaction and creation of new applications and, therefore, a higher value-added process.

- **Modularity**: Systems should be as flexible and scalable as possible within the smart industry.

The implementation of these basic principles makes tailor-made manufacturing production possible, as well as automatic diagnosis, adjustment, and optimization of the process, and what is more, this is also essential to support workers in their activities and improve their working conditions [56].

1.7. Objectives

The basic aim of this Ph.D. thesis is the research the main mechanisms to promote the demand flexibility within the SG by providing smart solutions, platforms and devices that operate in coordination with each other under energy optimization criteria as well as PQ and reliability. Several secondary objectives are proposed to achieve this purpose:

1. To study the energy nature of the power electronics converters (PEC) in terms of energy consumption and PQ, with special emphasis on non-conventional waveform distortion phenomena such as subharmonics and supraharmonics.

2. To develop and apply techniques or criteria based on the main findings of the previous study to ensure an optimal PQ as well as analyze and validate their effectiveness.

3. To develop a platform including the appropriate tools for energy management and DLC.

4. To investigate the potential of thermostatically controlled loads (TCL) in terms of demand flexibility

5. To develop an IoT device for DLC, test its functionality and validate its behavior in a real scenario.

6. To deploy an IoT platform for data storage and communications between these nodes.

1.8. Methodology

Given all the abovementioned objectives, the methodology employed in this Ph.D. dissertation to accomplish them is given in this section in terms of activities. Each activity indicates the objective(s) to which it is related.

1. Analysis of the state-of-art PQ of the main PEC. This activity is intended to achieve objectives 1 and 2.

2. Analysis of the state-of-art in energy optimization problems as well as the modeling of DER and TCL. This activity is intended to achieve objectives 3 and 4.

3. Formulation of the energy optimization problem to be included in the platform considering the behavior of the TCL. This activity is intended to achieve objectives 3 and 4.

4. Design and implementation of the required electronics and firmware to enable data acquisition and processing. This activity is intended to achieve objective 5.

5. Design and implementation of the required electronics and firmware to enable the control and communication layer of the IoT device. This activity is intended to achieve objective 5.

6. Planning and definition of real scenarios for advanced applications of IoT devices. This activity is intended to achieve objective 5.

7. Design of the test conditions to evaluate the performance of the system under certain events such as PQ disturbances or faults. This activity is intended to achieve objective 5.

8. Analysis of the state-of-art communication technologies and protocols, as well as data storage and cloud computing systems that could be employed in residential and industrial environments. This activity is intended to achieve objective 6.

9. Analysis and discussion of the improvements brought about by the adopted solutions and techniques. This activity is intended to achieve objectives 2, 4, 5, and 6.

10. Identification of possible improvements and future works. This activity is intended to achieve objectives 2, 3, 5, and 6.

1.9. Contributions

The main contributions of this Ph.D. thesis are detailed below:

- Implementation and validation of the spread spectrum techniques (SST) as an effective solution to mitigate supraharmonic components of the current in a power factor correction (PFC) boost converter prototype for lighting systems. Concretely, a couple of random pulse-position modulations was employed. (Chapter 2)

- Development of a research test bench flexible enough to incorporate different tools of different origins such as weather forecasting application programming interfaces (API), DR providers from the utility, and mathematical optimization features based on the LabVIEW systems design platform and development environment for a visual programming language (Chapter 3).

- Development of an EMS that makes use of a mixed-integer linear programming (MILP) problem for the management of residential loads and flexibility resources,

such as solar PV generation and battery storage system, under the criterion of minimizing the day ahead cost of electricity (Chapter 3).

- Formulation of a load scheduling strategy in terms of an optimization problem to control the AC-AC PEC responsible for supporting the electric-boosted glass melting furnaces. The benefit is two-fold: On one hand, this strategy contributes to demand flexibility by reducing certain demand peaks found under conventional control schemes. As a result, the associated financial penalties are significantly reduced. On the other hand, this strategy also minimizes the waveform distortion due to subharmonics (Chapter 4).

- Integration of the optimal accumulator-based scheme for AC cycle distribution within the modulation period in the previous strategy, so that the temperature ripple of each electrode can be modulated by a selected percentage (Chapter 4).

- Deployment of a novel infrastructure to automate the response of energy resources to certain DR signals or PQ events while providing a standard solution and a dedicated platform (Chapter 5).

- Development of a novel grid-interactive appliance controller (GIAC) based on the combination of the IoT PQ sensor and the implementation of the standard OpenADR. In particular, the main contribution has been the functionality extension regarding similar devices in the literature: Integration of IoT connectivity, enlargement of the monitored PQ parameters, concerning the main international standards, and standardization of the communication required to perform the DR actions among other features (Chapter 5).

1.10.Structure of the thesis

This section presents the organization of the document. As was mentioned above, this thesis is presented as a collection of papers, therefore, the main body is composed of several articles which have been previously published or accepted for publication in JCR-indexed international journals. The following lines provide a brief description of each chapter with the objectives addressed:

- **Chapter 2** contains the paper published in Elsevier's *Electric Power System Research* Journal (Q2). This article provides a survey of the main PEC topologies typically employed in lighting applications according to the power delivered and points out the PQ problem related to high-frequency emissions in LED drivers. In this regard, a couple of techniques to reduce the presence of supraharmonics in the current spectrum using the SST are implemented. Concretely, the random pulse-position modulation is applied in a PFC boost converter using a LED lamp as a load, and the results are compared to the conventional PWM to be validated. The digital implementation of the control is also detailed. Objectives 1 and 2 are closely related to this publication.

- **Chapter 3** includes the article published in MDPI's *Energies* Journal (Q3). This publication addresses the development of a DLC testbench for smart appliances (SA)

providing a brief state-of-the-art review of home energy management systems (HEMS) and SA to put this research in context. More in-depth, this paper describes the integration of the required tools to make such a testbench possible and formulates the MILP problem employed by the platform to perform the SA scheduling process and decide the energy resources behavior. The electric water heater (EWH) is included as a TCL contributing to the demand flexibility. Finally, two case studies are presented. Objectives 3 and 4 are closely related to this publication.

- **Chapter 4** presents the paper published in IEEE Transactions on Industry Applications (Q1) in 2020. This paper studies the consumption and frequency emissions (subharmonics) present in AC-AC PEC controlled by the integral cycle control (ICC) in electric-boosted glass melting furnaces. Furthermore, a load scheduling strategy for the energy management of these converters involved in this energy-intensive industry is developed. The strategy aims to minimize the energy of subharmonic components and is formulated as a mixed-binary quadratic programming (MBQP) problem with constraints related to thermal behavior. Finally, several case studies are presented, and the strategy is validated by comparing the theoretical results with the actual performance of a small laboratory-scale prototype. Objectives 1, 2, and 4 are closely related to this publication.

- **Chapter 5** contains the paper published in IEEE Transactions on Industry Applications (Q1) in 2022. It provides a brief review of the main IoT protocols and addresses both the development of the IoT sensor/actuator for DLC, referred to as grid-interactive appliance controller (GIAC), and the deployment of the IoT platform to enable the communications, collection and store the data. Moreover, the integration of the standard OpenADR to simplify and automate the DR events is detailed. Finally, several case studies including the most common PQ disturbances according to the standards are reported to validate both the grid-interactive appliance controller and the IoT platform developed. Objectives 3, 5, and 6 are closely related to this publication.

- **Chapter 6** puts forward the main conclusions of the Ph.D. thesis.

- **Chapter 7** outlines the future works that can be realized within the framework created by this Ph.D. thesis.

References

[1] United Nations. Framework Convention on Climate Change, 21st Conference of the Parties, Paris. (2015). *Adoption of the Paris Agreement*. Available: https://unfccc.int/sites/default/files/english_paris_agreement.pdf

[2] Eurostat (European Commission), *Energy, transport and environment statistics: 2020 edition*, Luxembourg: Publications Office, 2020, doi: 10.2785/522192.

[3] International Energy Agency, *Renewables 2021: Analysis and forecast to 2026*, 2021. Available: www.iea.org/t&c/

[4] International Energy Agency, *Status of Power System Transformation 2019: Power system flexibility*, Paris, France: OECD Publishing, 2019, doi: 10.1787/7c49400a-en.

[5] ENTSO-E, *Interconnected Networks of ENTSO-E 2019*, 2019. Available: https://eepublicdownloads.entsoe.eu/clean-documents/Publications/maps/2019/Map_ENTSO-E-4.000.000.pdf

[6] Redeia, *Mapa de situación geográfica*, 2018. Available: www.ree.es

[7] I. Colak, "Introduction to smart grid," *2016 International Smart Grid Workshop and Certificate Program (ISGWCP)*, 2016, pp. 1-5, doi: 10.1109/ISGWCP.2016.7548265.

[8] European Technology Platform SmartGrids Strategic Deployment Document for Europe's Electricity Networks of the Future, 2012. Accessed: 13-06-2022. [online]. Available: https://www.edsoforsmartgrids.eu/policy/eu-steering-initiatives/smart-grids-european-technology-platform/.

[9] C. Dai, K. Cheng, Y. Lei, and Y. Yang, "Research hotspots and evolution of energy prosumer: A literature review and bibliometric analysis," *Mathematical Problems in Engineering*, vol. 2020, Oct., 2020, Art. No. 5703101, doi: 10.1155/2020/5703101.

[10] I. Colak, R. Bayindir, and S. Sagiroglu, "The effects of the smart grid system on the national grids," in *8th International Conference on Smart Grid (icSmartGrid)*, 2020, pp. 122-126, doi: 10.1109/icSmartGrid49881.2020.9144891.

[11] C. Cecati, G. Mokryani, A. Piccolo and P. Siano, "An overview on the smart grid concept," *IECON 2010 - 36th Annual Conference on IEEE Industrial Electronics Society*, 2010, pp. 3322-3327, doi: 10.1109/IECON.2010.5675310.

[12] A. Akrami, M. Doostizadeh and F. Aminifar, "Power system flexibility: an overview of emergence to evolution," *Journal of Modern Power Systems and Clean Energy*, vol. 7, no. 5, pp. 987-1007, Sept. 2019, doi: 10.1007/s40565-019-0527-4.

[13] R. J. Heffron, M. F. Körner, M. Schöpf, J. Wagner and M. Weibelzahl, "The role of flexibility in the light of the COVID-19 pandemic and beyond: Contributing to a sustainable and resilient energy future in Europe," *Renewable and Sustainable Energy Reviews*, vol. 140, Apr., 2021, Art. no. 110743, doi: 10.1016/j.rser.2021.110743.

[14] B. Mohandes, M. S. El Moursi, N. Hatziargyriou, and S. El Khatib, "A review of power system flexibility with high penetration of renewables," *IEEE Transactions on Power Systems*, vol. 34, no. 4, pp. 3140-3155, Jan., 2019, doi: 10.1109/TPWRS.2019.2897727.

[15] O. M. Babatunde, J. L. Munda, and Y. Hamam, "Power system flexibility: A review," *Energy Reports*, vol. 6, suppl. 2, pp. 101-106, Feb., 2020, doi: 10.1016/j.egyr.2019.11.048.

[16] J. Cochran, M. Miller *et al.*, "Flexibility in 21st century power systems" (No. NREL/TP-6A20-61721). National Renewable Energy Lab. (NREL), Golden, CO (United States). Doi: 10.2172/1130630

[17] A. Nikoobakht, J. Aghaei, T. Niknam, H. Farahmand, and M. Korpås, "Electric vehicle mobility and optimal grid reconfiguration as flexibility tools in wind integrated power systems," *International Journal of Electrical Power & Energy Systems*, vol. 110, pp. 83-94, Sept., 2019, doi: 10.1016/j.ijepes.2019.03.005.

[18] C. W. Gellings, "Evolving practice of demand-side management," *Journal of Modern Power Systems and Clean Energy*, vol. 5, no. 1, pp. 1-9, Jan., 2017, doi: 10.1007/s40565-016-0252-1.

[19] Energy Information Administration, *U.S. Electric Utility Demand-Side Management 2000*. US Dept. Energy, Washington, DC, USA, Tech. Rep., 2002. Available: https://www.eia.gov/electricity/data/eia861/dsm/058900.pdf

[20] U.S Department of Energy, *Benefits of demand response in electricity markets and recommendations for achieving them: A report to the United States Congress pursuant to section 1252 of the energy policy act of 2005*. US Dept. Energy, Washington, DC, USA, Tech. Rep., 2006. Available: https://www.energy.gov/oe/downloads/benefits-demand-response-electricity-markets-and-recommendations-achieving-them-report

[21] R. Billinton and R. N. Allan, "Reliability of electric power systems: An overview," in *Handbook of Reliability Engineering*, H. Pham, London: Springer, 2003, pp. 511-528, doi: 10.1007/1-85233-841-5_28.

[22] M. H. J. Bollen, " What is power quality?," *Electric power systems research*, vol. 66, no. 1, pp. 5-14, Jul., 2003, doi: 10.1016/S0378-7796(03)00067-1.

[23] "IEEE Guide for Electric Power Distribution Reliability Indices," in *IEEE Std 1366-2012 (Revision of IEEE Std 1366-2003)*, pp.1-43, May 2012, doi: 10.1109/IEEESTD.2012.6209381.

[24] N. Bhusal, M. Abdelmalak, M. Kamruzzaman and M. Benidris, "Power System Resilience: Current Practices, Challenges, and Future Directions," in *IEEE Access*, vol. 8, pp. 18064-18086, 2020, doi: 10.1109/ACCESS.2020.2968586.

[25] A. Gholami, T. Shekari, M. H. Amirioun, F. Aminifar, M. H. Amini and A. Sargolzaei, "Toward a Consensus on the Definition and Taxonomy of Power System Resilience," in *IEEE Access*, vol. 6, pp. 32035-32053, 2018, doi: 10.1109/ACCESS.2018.2845378.

[26] "IEEE Recommended Practice for Monitoring Electric Power Quality," in IEEE Std 1159-2019 (Revision of IEEE Std 1159-2009), pp.1-98, Aug. 2019, doi: 10.1109/IEEESTD.2019.8796486.

[27] *Electromagnetic Compatibility (EMC)—Part 2-5: Environment—Classification of electromagnetic environments*, IEC 61000-2-5:2017.

[28] "IEEE Guide on the Surge Environment in Low-Voltage (1000 V and less) AC Power Circuits," in *IEEE Std C62.41.1-2002*, pp. 1-173, Apr. 2003, doi: 10.1109/IEEESTD.2003.94253.

[29] "IEEE Standard for Interconnection and Interoperability of Distributed Energy Resources with Associated Electric Power Systems Interfaces," in *IEEE Std 1547-2018 (Revision of IEEE Std 1547-2003)*, pp. 1-138, Apr. 2018, doi: 10.1109/IEEESTD.2018.8332112.

[30] Photovoltaic (PV) systems - Characteristics of the utility interface. IEC 61727:2004. Available: https://webstore.iec.ch/publication/5736 (accessed Nov. 16, 2021).

[31] "IEEE Recommended Practice for Utility Interface of Photovoltaic (PV) Systems," in *IEEE Std 929-2000*, pp. i-, 2000, doi: 10.1109/IEEESTD.2000.91304.

[32] *Automatic disconnection device between a generator and the public low-voltage grid*. DIN VDE V 0126-1-1:2013-08. Available: https://www.vde-verlag.de/standards/0100178/din-vde-v-0126-1-1-vde-v-0126-1-1-2013-08.html (accessed May. 29, 2022)

[33] *Electromagnetic compatibility (EMC) Part 4-7: Testing and measurement techniques — General guide on harmonics and interharmonics measurements and instrumentation, for power supply systems and equipment connected thereto*. IEC 61000-4-7:2002 +AMD1:2008.

[34] *Electromagnetic compatibility (EMC) Part 3-2: Limits- Limits for harmonics current emissions (equipment input current ≤ 16 A per phase).* IEC 61000-3-2:2014.

[35] "IEEE Recommended Practice and Requirements for Harmonic Control in Electric Power Systems," in *IEEE Std 519-2014 (Revision of IEEE Std 519-1992)*, pp. 1-29, Jun., 2014, doi: 10.1109/IEEESTD.2014.6826459.

[36] *Voltage characteristics of electricity supplied by public electricity networks*. EN 50160:2011/A2:2020. Available: https://www.en-standard.eu/une-en-50160-2011-a2-2020-voltage-characteristics-of-electricity-supplied-by-public-electricity-networks/ (accessed May. 31, 2022).

[37] S. Rönnberg, M. Bollen, H. Amaris, G. Chang, I. Gu, L. Kocewiak, J. Meyer, M. Olofsson, P. Ribeiro, and J. Desmet, "On waveform distortion in the frequency range of 2 kHz challenges," *Electr. Power Syst. Res.*, vol. 150, pp. 1- 10, doi: 10.1016/j.epsr.2017.04.032.

[38] *Electromagnetic compatibility (EMC) Part 4-30: Testing and measurement techniques- Power quality measurements methods*. IEC 61000-3-30:2015.

[39] "IEC 60050 - International Electrotechnical Vocabulary - Details for IEV number 103-07-29: "sub-harmonic component"" [Online]. Available: http://www.electropedia.org/iev/iev.nsf/display?openform&ievref=103-07-29. [Accessed: 08-Jun-2022].

[40] Electromagnetic compatibility (EMC) Part 3-3: Limits- Limitation of voltage changes, voltage fluctuations and flicker in public low-voltage supply systems, for equipment with rated current <= 16 A per phase and not subject to conditional connection. IEC 61000-3-3:2013/AMD1:2017.

[41] "IEEE Recommended Practice for the Analysis of Fluctuating Installations on Power Systems," in *IEEE Std 1453-2015 (Revision of IEEE Std 1453-2011)*, pp.1-74, 30 Oct. 2015, doi: 10.1109/IEEESTD.2015.7317469.

[42] P. Larsen, A. H. Sanstad, K. Hamachi LaCommare, and J. H. Eto, *Frontiers in the Economics of Widespread, Long-Duration Power Interruptions: Proceedings from an Expert Workshop*. Berkeley, USA: Lawrence Berkeley National Lab. (LBNL), 2019. Available: https://eta-publications.lbl.gov/sites/default/files/long_duration_interruptions_workshop_proceedings.pdf

[43] J. Eto, *Cost of Power Interruptions to Electricity Consumers in the United States – Revised Update*. Berkeley, USA: Lawrence Berkeley National Lab. (LBNL), 2017. Available: https://emp.lbl.gov/publications/cost-power-interruptions-electricity

[44] "ITaas + Trust". Available: https://www.meritalk.com/study/rx-itaastrust/

[45] G. Mendes, A. Loew and S. Honkapuro, "Regional Analysis of the Economic Impact of Electricity Outages in US Healthcare Facilities," *2019 IEEE Power & Energy Society General Meeting (PESGM)*, 2019, pp. 1-5, doi: 10.1109/PESGM40551.2019.8973689.

[46] A. Silverstein, R. Gramlich, and M. Goggin, M. *A customer-focused framework for electric system resilience*. Washington DC: Grid Strategies LLC, 2018. Available: https://www.preventionweb.net/publication/customer-focused-framework-electric-system-

resilience#:~:text=In%20a%20customer%2Dcentric%20framework,power%20generation%20and%20fuel%20supply.

[47] R. Targosz and J. Manson, "Pan-European power quality survey," *2007 9th International Conference on Electrical Power Quality and Utilisation*, 2007, pp. 1-6, doi: 10.1109/EPQU.2007.4424203.

[48] A. Sharma, B. S. Rajpurohit, and S. N. Singh, "A review on economics of power quality: Impact, assessment and mitigation," *Renewable and Sustainable Energy Reviews*, vol. 88, pp. 363-372, May 2018, doi: 10.1016/j.rser.2018.02.011.

[49] S. C. Vegunta, C. F. A. Watts, S. Z. Djokic, J. V. Milanović, and M. J. Higginson, "Review of GB electricity distribution system's electricity security of supply, reliability and power quality in meeting UK industrial strategy requirements," *IET Generation, Transmission & Distribution*, vol. 13, no. 16, pp. 3513-3523, Jul. 2019, doi: 10.1049/iet-gtd.2019.0052.

[50] J. Y. Chan, and J. Milanovic, "Framework for assessment of economic feasibility of voltage sag mitigation solutions", Doctoral dissertation, School of Electrical and electronic engineering, University of Manchester, 2010. Available: https://www.research.manchester.ac.uk/portal/files/54595942/FULL_TEXT.PDF

[51] K. Ashton, "That 'internet of things' thing," *RFID journal*, vol. 22, no. 7, pp. 97-114, 2009, doi: 10.4236/jssm.2015.84056.

[52] F. Shrouf, J. Ordieres and G. Miragliotta, "Smart factories in Industry 4.0: A review of the concept and of energy management approached in production based on the Internet of Things paradigm," *2014 IEEE International Conference on Industrial Engineering and Engineering Management*, 2014, pp. 697-701, doi: 10.1109/IEEM.2014.7058728.

[53] S. Li, L. Da Xu, and S. Zhao, "5G internet of things: A survey," *Journal of Industrial Information Integration*, vol. 10, Jun. 2018, doi: 10.1016/j.jii.2018.01.005.

[54] J. Findstack, "The ultimate list of Internet of Things Statistics for 2022". [Online]. Available: https://findstack.com/internet-of-things-statistics/ (accessed Feb. 1, 2022).

[55] Y. Guan *et al*., "An open virtual neighbourhood network to connect IoT infrastructures and smart objects — Vicinity: IoT enables interoperability as a service," *2017 Global Internet of Things Summit (GIoTS)*, 2017, pp. 1-6, doi: 10.1109/GIOTS.2017.8016233.

[56] S. Jeschke, C. Brecher, T. Meisen, D. Özdemir, and T. Eschert, "Industrial internet of things and cyber manufacturing systems," in *Industrial Internet of Things*, D. Rawat, Cham: Springer, 2017, pp. 3-19, doi: 10.1007/978-3-319-42559-7_1.

Chapter 2

Supraharmonics emission from LED lamps: A reduction proposal based on random pulse-width modulation

Joaquin Garrido-Zafra[1], Antonio Moreno-Muñoz[1], Aurora Gil-de-Castro[1], Víctor Pallares-Lopez[1], and Tomas Morales-Leal[2]

[1]Departamento de Ingeniería Electrónica y de computadores, Escuela politécnica superior, Universidad de Córdoba, Córdoba, Spain

[2]Departamento de Ingeniería Eléctrica y Automática, Escuela politécnica superior, Universidad de Córdoba, Córdoba, Spain

Abstract

There is an outstanding concern from the international standard-setting community about harmonics distortion in the frequency range 2–150 kHz, referred to as supraharmonics. Power electronics has established as a ubiquitous technology, which plays a linchpin role in almost any electrical systems. The classical deterministic pulse-width modulation strategy, entailing at reducing low-frequency harmonics emission (< 2 kHz) in power converters, in a sense, bring them to move at the switching frequency and its multiple, in the kilohertz range. The amplitude of spectral components is the main concern when studying electromagnetic interference from active power factor correction stages, included in state-of-the-art LED drivers. Supraharmonics are nowadays the origin of numerous problems in electrical networks. The standardization bodies are presently updating the compatibility limits in the frequency range from 2 to 150 kHz. Supraharmonics behave differently from (lower frequency) harmonics, as reported in the literature. Fortunately, as will be demonstrated in this paper, it is possible to undertake this issue, from the very beginning, by leveraging technologies like random pulse-width modulation. An experimental system based on digitally controlled LED driver has been set up to evaluate the different methods. The algorithms have been implemented on a compactRIO controller incorporating an FPGA and a realtime processor.

2.1. Introduction

Worldwide energy consumption has risen 30% in the last 25 years. Increasing energy costs have become a significant concern and are expected to continue to increase in the foreseeable future. Businesses, institutions, and consumers will be searching for more efficient products and solutions. Residential and commercial building electricity consumption accounts for almost 60% of total IEA (International Energy Agency) electricity demand. In Europe, transport and industry are major energy consumers, but buildings account for around 41% of all energy consumption. The Public Lighting Systems in our cities is a basic and vital service for city councils and other public administration. On the one hand, citizens demand high-quality service in accordance with our high development society. On the other hand, a lighting installation is an important energy consumption source. Concretely, lighting is responsible for approximately 15% of the global electricity consumption and about 5% of greenhouse gas emissions [1].

In the quest for sustainability, the light-emitting diode or LED light has entailed an energy revolution, involving energy savings of up to 80% compared to incandescent lamps [2]. The transition to LED light is transforming the lighting industry, which has seen a faster than expected drop-off in the price of this disruptive technology. LED lighting not only delivers high efficiency but a high level of brightness, long lifespan and high reliability. Consequently, LED lamps are used in most applications, both indoors and outdoors. Market forecasts estimate extraordinary and continuous growth of LED market throughout the present decade, with LED becoming the dominant lighting technology in terms of the aggregate number of installed units, with a share reaching almost 70% of the global lighting market in 2020 [3].

Since LED lighting represents an energy-efficient technology, the issue of total power factor (TPF) is unavoidable. But the market expects not only for the higher TPF but also for a better performance from the electromagnetic compatibility (EMC) point of view. With the general adoption of self-commutated power electronic converters (PEC) in these electronic devices, generation of harmonics has been shifted from the hertz to the kilohertz frequency band. These high-frequency components, the so-called ‘supraharmonic’ (frequency range: 2–150 kHz), are characteristic in the pulse-width modulation (PWM) operation of PEC employed in the LED driver. The amplitude of spectral components, caused by fixed frequency PWM, is the main issue when facing electromagnetic interference (EMI).

Supraharmonic behaves differently from (lower frequency) harmonics and interharmonics. An increase in the number of malfunctions and non-intentional equipment behavior due to the presence of Supraharmonics has been reported during the last years, for example, with power line communication, brown goods, biomedical devices, smart meter, ground leakage current switches, and overload of electrolytic capacitors [4]. EMC standards had almost forgotten this frequency range until recently, resulting in lack of requirements [5]. However, standards’ revisions with new compatibility levels for supraharmonic disturbances are on their way [6].

There are different filtering devices for reduction of these undesirable interferences. There are different filtering devices for reduction of these undesirable interferences. Recently novel passive mitigation technologies like a variable capacitance filter have been proposed [7]. Nevertheless, more circuit board space is needed for them, and obviously cost increases, so avoiding the harmful emission is preferable. As will be illustrated in this paper, among the methodologies to deal with this problem, the random PWM (RPWM) represents an outstanding option. Particularly a new improvement in the Random Pulse Position Modulation (RPPM) will be presented with excellent performance.

The organization of the rest of the paper is as follows. Section 2 is devoted to power quality, mainly in the supraharmonic topic. Section 3 presents a survey of LED drivers. Section 4 addresses the RPWM techniques while Section 5 is devoted to results. And finally, Section 6 contains the conclusions.

2.2. Power quality in lighting systems review

There is growing concern about the quality of electricity. One of the main reasons is because new generation of loads are more sensitive to variations in energy quality than in the past [8]. Power quality is not a new term, however still nowadays there are attempts to deal with it. It is an umbrella concept considering many types of power system disturbances. It indistinctly refers to both current and voltage. While the quality of the current usually characterizes the emission of equipment and installations, the quality of the voltage describes how equipment connected to a certain point in the distribution grid is affected by other equipment emissions. Customer equipment affects the voltage quality, and the latter also affects customers, therefore, to find the responsible in a power quality concern is difficult. Both definitions have in common that they are related to the non-sinusoidal waveform of the voltage or current, leading to a distortion. Therefore, this waveform distortion is defined as a steady-state deviation from an ideal sine wave of power frequency principally characterized by the spectral content of the deviation.

With the introduction of LED lamps in the market, numerous papers have been written about power quality, considering the possible increase in the voltage distortion in distribution networks due to the widespread use of that technology. The harmonic generation from LED lamps has been deeply studied at a lab level [9,10], and also over real measurements [11,12]. However, there are still not so many papers on studying the supraharmonic emission of LED lamps [13,14].

It has been shown in [4–6] that LED lamps currently on the market show a large variety of supraharmonic emission. There is no emission limit in that range that applies to LED lamps, so every manufacturer uses their own driver topology. Therefore, it is not possible to use standard supraharmonic models for LED lamps, as nowadays each device appears to be unique. Even worst, in this frequency range, a small change in any electrical component between drivers has a big influence on it.

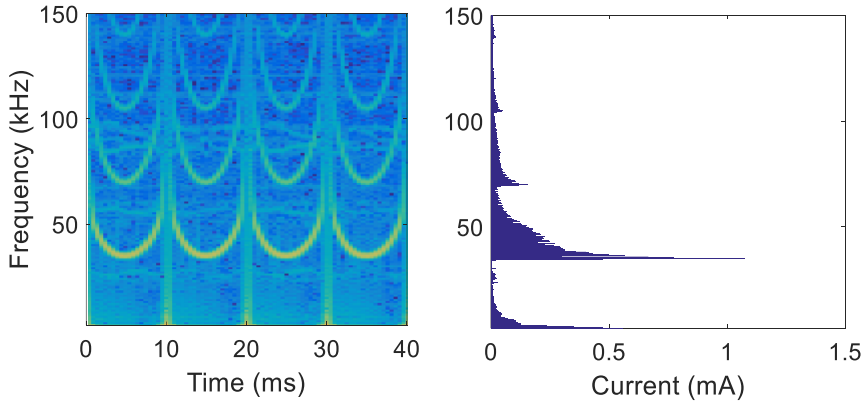

Figure 2. 1. Group II. STFT (left) and FFT (right) of the current.

In [15] according to measurements over 73 LED lamps for indoor lighting, overall, three groups can be observed according to the high frequency emission. From those groups, group II is formed by lamps with a high frequency spectrum mainly characterized by the switching frequency of the driver and its harmonics. Figure 2. 1 shows the current short-time

Fourier transform (STFT) and the fast Fourier transform (FFT) of a LED lamp from group II. Broadband components are seen from 35 to 55 kHz, as well as recurrent oscillations are seen below 9 kHz. This paper is proposing a new technique to mitigate the switching component of lamps from group II.

The index that characterizes the distortion in the low frequency is the Total Harmonic Distortion (THD), representing the relative signal energy present at nonfundamental frequencies, as defined in IEC 61000-4-7 [16]. In the supraharmonic range, only the 200 Hz grouping method is recommended at IEC 61000-4-7, but no indices are standardized. However, several indices have been proposed to characterize the emission within this range based in time-domain analysis and in the frequency-domain [17].

The displacement power factor (dPF) is the cosine of the angle difference between the fundamental components of the voltage and current (at 50/60 Hz). The TPF, however, includes the harmonic part of the active and apparent power, as appears defined in IEEE 1459-2000 [18]. The TPF is the product of the distortion factor (DF), own to the harmonic's presence, and the dPF, where the latter considers only the fundamental of the current and distortion factors in the harmonics.

As nonlinear loads, LED lamps produce highly distorted currents. Depending on the technology used in the rectification stage, the current waveform of the LED driver will be distorted. The different rectifier topologies can be divided into non-power factor correction (nPFC), passive power factor correction (pPFC), and active power factor correction (aPFC). The nPFC topologies emit the highest harmonic currents with (Total Harmonic Distortion of the current) THD_i values usually significantly higher than 100% and the current fundamental has a capacitive characteristic with TPF lower than 0.7 (Figure 2. 2).

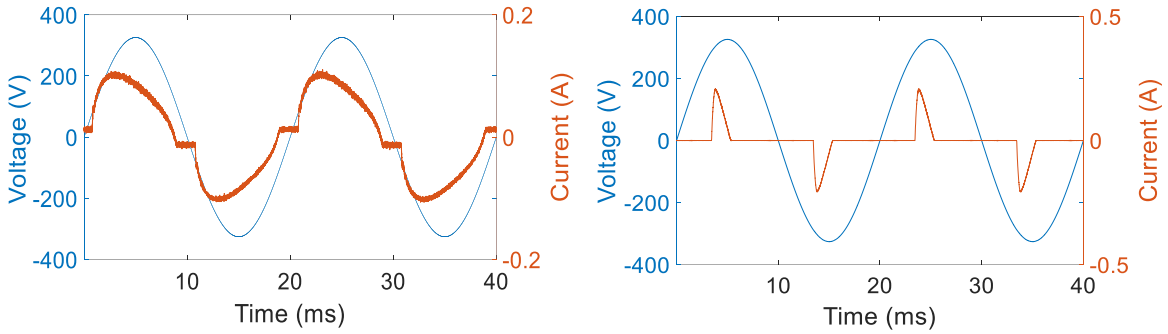

Figure 2. 2. Voltage and current waveforms. Figure to the left is a LED lamp equiped with aPFC, and figure to the right without PFC.

Topologies based on pPFC have mostly a moderate low frequency current distortion (30–90%) and a power factor higher than 0.7. The aPFC is usually based on higher switching frequency devices. This results in an almost sinusoidal current with THDi usually below 10% and TPF close to one, however they emit supraharmonic, that are injected into the grid.

2.2.1. Current situation of Supraharmonics

Concerns about conducted emissions were originally in the range of 450 kHz–30 MHz. With enough foresight, that range was extended down to 150 kHz, and afterward further to 2 kHz. PQ harmonics traditionally range from frequencies just above DC to 3 kHz (in IEEE-519) or 9 kHz (in IEC). There are considerable on-going activities within IEC (both SC 77A and SC 205A), CENELEC and IEEE to develop standards, e.g., compatibility levels, limits and adequate test methods, covering this frequency range in voltage. However, setting current

limits on the total installation (as in IEEE Std. 519) and setting current limits on individual devices (as in IEC 61000-3-2) would be very difficult, as emission in the supraharmonic range behaves differently to that at low frequency. An updated summary of standardization in this supraharmonic range is done in [6].

In recent years, researchers have endeavored to explain the origin and mechanism of interaction within this frequency range. Supraharmonics are composed of various frequency components that can be grouped into three categories (considering one cycle of power system frequency) [19]: constant, varying (in time and/or frequency) or transient, where the second one is by far most common. The remnants of the switching frequency of the active converter (usually at tens of kHz), are visible in most of low-voltage end-user equipment such as fluorescent light [19] and LED lamps [20, 21], and overall, at mostly every household appliance [22, 23]. Moreover, they have also been recently reported with the introduction of EV chargers [24], and renewable energies (solar photovoltaic -PV- installations and wind turbines [25]).

The current drawn by each device contains primary and secondary emission [26] within the supraharmonic range. The primary emission is the emission caused by the device itself. The secondary emission is the emission seen by a device coming from nearby devices. This paper is focused in reducing the primary emission of LED lamps. Supraharmonics can highly affect neighboring devices because its propagation is different to that of harmonics. When connecting end user equipment, the resulting harmonic distortion in the low frequency is very much dependent on the cancellation as depends on aggregation and attenuation factors [10-27]. However, the propagation of Supraharmonics is different mainly due to the secondary emission seen by devices. In this frequency range, the emission from devices mainly spreads to neighboring devices and not to the grid [28-30]. Several examples are reported of the spread of supraharmonics to neighboring devices, as in [13] where the interaction through harmonics, interharmonics, supraharmonics, and light flicker, between PV inverters and LED lamps in low-voltage installations are investigated through different approaches, also in [21] where the same LED lamps were connected at different points, and the secondary emission of the different locations were seen at the terminal of those LED lamps. Moreover, in [31] the current to an electric vehicle is measured for different connection of other devices (LED lamp, microwave oven, TV) showing the presence of primary and secondary emission. That paper shows that the presence of neighboring device can have a strong influence on the emission.

There are reported cases of interference with different types of lamps under certain conditions, especially in the frequency range above 2 kHz [4,32,33] where power line communication is the most common source of high disturbance levels. There are other reported cases of Supraharmonics in [34], where the problem with the light is that its control functions (dimming, corridor and attendance control) are not always working properly. The lamps remain in low dimming mode and light intensity cannot be increased. Also, in [30] is reported malfunctions or impairments of household devices due to supraharmonics, as well as a reduction in lifetime of the devices. Another aspect that is recently studied is the flicker impact in LED lamps due to the high frequency emission [35].

2.3. Survey of LED drivers topologies

High-brightness LED lamps are driven by different PEC. Commercial LED driver options range from merely a filtered rectifier, to advanced multi-stage PEC. Between both sides lies different topologies, that can be classified as follows:

The simplest and cheapest approach is to employ a passive LED driver. Without active regulation, this passive driver must adopt some passive current-limiting element, such a

resistor, between the AC line and the selected LED device [36]. Alternatively, a linear regulation can be included, thereby the current supplied to the LED matrix will be constant and independent from the input voltage. Therefore, this circuit cannot provide a satisfactory TPF.

One stage drivers (low-power design, <20 W) include applications such as bulbs and down lights. The simplest one is the non-isolated PWM buck PEC stage for the LED current control, following the rectifier. pPFC stage can be implemented by including the "three diodes valley fill topology" circuit [37]. When the output voltage is higher than the input one, the boost PEC must be employed. If the output voltage can be higher or lower than the input voltage, the appropriated topologies are the buck-boost, SEPIC or Cuk [38]. Both stages have independent controlled switches and its command circuits, which increases the driver components number. These schemes are not suitable for power over 20 W because of inherently poor PF and EMC issues. Additionally, some high inrush currents may appear and may be needed to deal with them. Finally, these are not recommended for 100–240 VAC (universal input) voltage.

The single-stage flyback converter (mid-power designs, 20–50 W) are a slightly more complicated galvanic isolated PEC. This is employed when there is a regulation requirement or application design specification. This driver can deliver at the same time an optimal TPF value and a regulation of the output current, within wide load range; hence, it has drawn more and more attention in recent years [39]. The biggest drawback is distortion of the AC line input current, mainly the supraharmonic emission.

Multistage converter (see Figure 2. 3) appears as a solution (high-power designs, 50–400 W) to lower the output current ripple without including a large filter capacitor [38,40]. In some LED street lighting applications, the solution is to add an additional second stage. This alternative increases the cost in 15–20% but provides the advantages of an excellent TPF value within wide load range, controllability, and reliability, at the expense of losing 2–3% in its efficiency. The harmonic emission of the above classified solutions has been studied in [41].

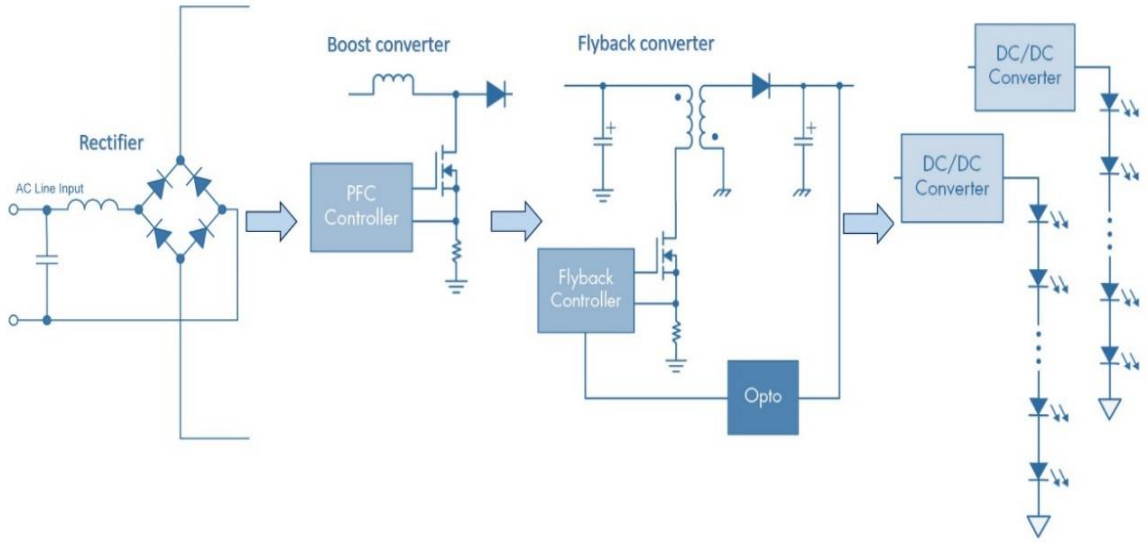

Figure 2. 3. A three-stage converter LED driver.

2.4. RPWM techniques

The conventional (PWM) and alternative techniques (hysteresis control) aimed to reduce emissions below 2 kHz. However, this leads to emission at the PWM switching frequency and its multiples (10 kHz–30 MHz). Therefore, self-switching converters are an important source of supraharmonics. Although there are many mitigation techniques, such as EMI filtering and shielding, and they really are a solution, the emission is anyhow present; so, a method of avoiding somehow their presence itself would be desirable.

Spread spectrum techniques (SST) simply mean distributing the energy of a given signal across a wide frequency band, thereby reducing peak energy. These usually involve the introduction of a random (or at least pseudo-random) quantity. If the switching algorithm is non-deterministic, then its frequency spectrum will be continuous due to the nonperiodicity of the signal. As a result, the average spectral power density of broadband emission can be drastically limited. This method could be used to overcome the interference caused by supraharmonics in a conventional PWM self-commutated PEC stage. In addition, low frequency emission is minimal.

The main characteristics of the different switching strategies are summarized in Table 2. 1 [42], with the aid of Figure 2. 4 where T_i is the duration of the ith cycle; α_i is the duration of the on-state within this cycle and ε_i is the delay time of this on-pulse from the beginning of the switching cycle; the duty cycle D_i is equal to α_i/T_i.

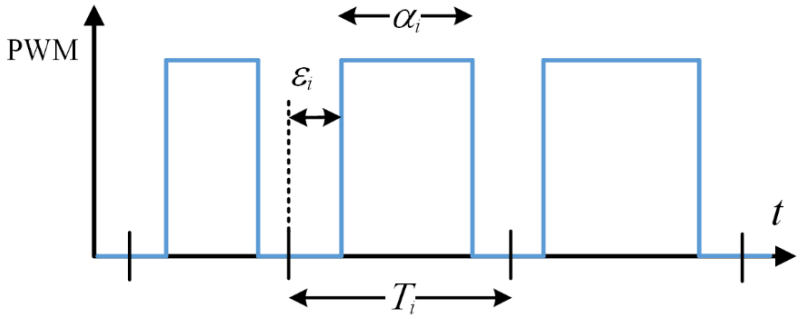

Figure 2. 4. Characteristics of a randomized switching signal.

Table 2. 1. Classification of the different random switching methods.

Modulation	$\boldsymbol{T_i}$	$\boldsymbol{\alpha_i}$	$\boldsymbol{\varepsilon_i}$	$\boldsymbol{D_i = \alpha_i/T_i}$
PWM	Fixed	Fixed	Zero	Fixed
Random pulse-position modulation (RPPM)	Fixed	Fixed	Random	Fixed
Random PWM (RPWM)	Fixed	Random	Zero	Random
Random carrier frequency modulation fixed duty (RCFMFD)	Random	Random	Zero	Fixed
Random carrier frequency modulation variable duty (RCFMVD)	Random	Fixed	Zero	Random

Among the different techniques that can be proposed to include randomization, the first approach is to incorporate it into the carrier frequency. This is a very efficient option because it ensures that the switching frequency does not adjust to a constant value, so that the spectral component in the original switching frequency decreases the resulting spectra.

This is achieved by slowly modulating the carrier signal between two limits (±10%) of the fundamental switching frequency, randomly. Table 2. 1 therefore presents two alternatives: random carrier frequency modulation fixed duty (RCFMFD) and random carrier frequency modulation variable duty. So far, RCFMFD is the only random approach available for commercial integrated circuits.

The key element here is the voltage-controlled oscillator, requiring a random voltage input different at each switching period. Analogical implementation of such a function is achieved by specific integrated circuits [43]. However, the random sampling rate imposes a restriction on the minimum sampling period. For PEC operating with digital feedback controller, the length of the code algorithms cannot allow the switching frequency to be high enough to achieve good spectral dispersion.

Table 2. 1 shows the random techniques with constant sampling frequency: RPWM and RPPM. In both cases the fixed frequency operation allows less design complexity, optimal use of processing capability, as well as greater stability. In RPWM the randomness allows the pulse width to be varied, while its average remains equal to the required duty cycle. This algorithm can be processed very quickly, as is required in high- frequency switching. However, the main harmonics of the PWM switching frequency continue to be present in the obtained power spectra. To overcome this situation, in this paper is proposed the RPPM. Unlike before, here what is randomized is the position of the pulse within each switching period, which is done by including a delay time.

2.5. Material and methods

In order to investigate the effectiveness of the different randomness techniques, a single stage LED driver prototype has been built. Concretely each control strategy has been tested in the aPFC boost converter. In this experiment, this converter was used as an 11 W LED driver, operating at constant switching frequency of 25 kHz and a supply voltage of 230 VRMS.

The digital implementation has been done using the National Instruments CompactRIO platform. The CompactRIO technology is very suitable for laboratory tests with fast prototyping working in real-time (Figure 2. 5) LabVIEW software and a CompactRIO embedded (cRIO 9063) controller have been used to develop a FPGA-based prototype. This cRIO 9063 includes a FPGA from the Zynq®-7000 family. This family is based on the Xilinx All Programmable System-on-chip (SoC) architecture. These chips integrate a feature-rich dual-core ARM® Cortex™ and include on-chip memory, external memory interfaces, and a rich set of peripheral connectivity interfaces.

The main advantage of the FPGA Module is the parallel execution of block diagram operations in a FPGA VI. Portions of the block diagram that do not depend on other portions are parallel executed on the FPGA device. Another advantage is that uses LabVIEW Real-Time, which is configurable, and is running at a priority level above time critical or between time critical and timed structures. To the aim of this paper, a FPGA VI has been designed for the FPGA device to work independently of the rest of the system. This will allow IP Blocks to be easily integrated into SoC for designs that require control devices with very small dimensions.

Synchronization and accurate control of the current and voltage control loops are required. This accuracy was achieved with three analogue channels with differential inputs and with simultaneous capture capability. A loop has been included in the FPGA to capture the three channels (supply current, output voltage and rectified voltage) every 10 μs, which is equivalent to a sampling frequency 100 kS/s. The maximum speed for the architecture in the FPGA is 25 ns.

For the current measurements done in this frequency range, a Pearson current probe model 411 was used. This current probe has a transfer of 100 mV/A, the lower 3 dB cut-off at 5 Hz and the high cutoff at 20 MHz makes it suitable for measurements in the 2–150 kHz. The instrument used was a Tektronix MDO3024 oscilloscope and recorder, with 1 MS/s sampling frequency. The 12-bit resolution of the instrument is enough to analyse the data.

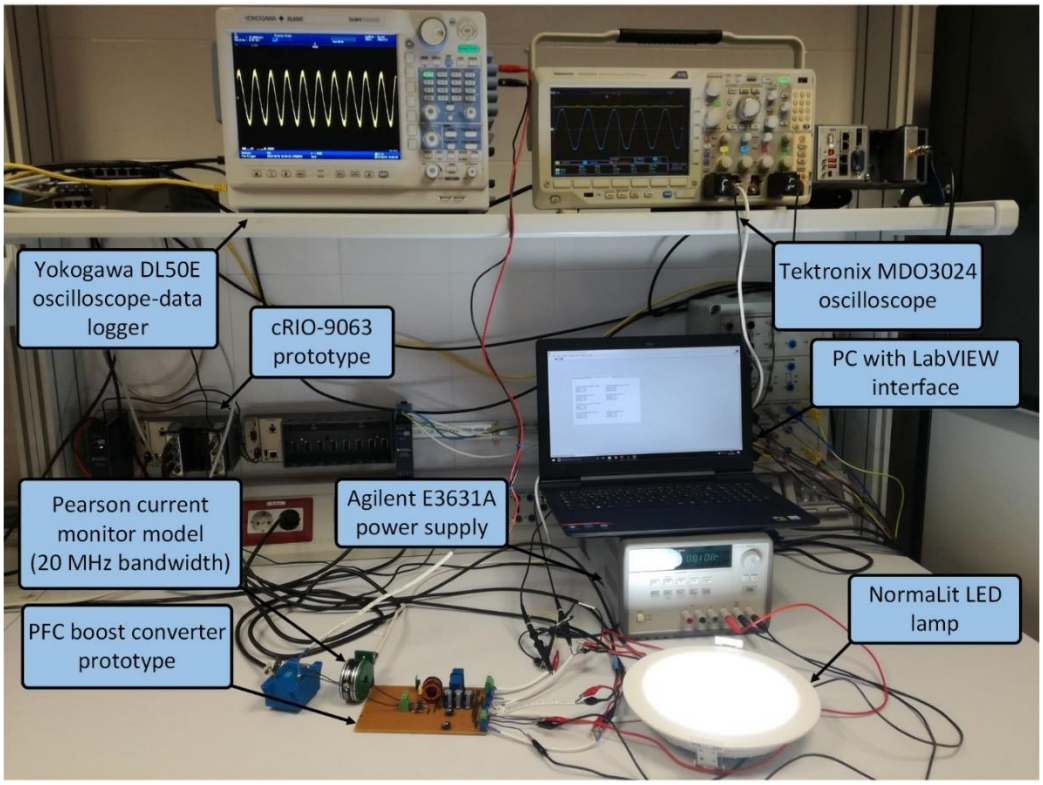

Figure 2. 5. Test scenario and the equipment used.

The PFC consists of a classical multi-loop cascaded control that includes an inner current loop and an outer voltage loop, both based on the well-known proportional-integral (PI) controller. These controllers work with a sampling rate of 100 kS/s and they have been tuned for a phase margin of 35° and 45° respectively. In addition, to avoid disturbing the inductor current, a Hall effect sensor was used instead of a shunt resistor. As shown in Figure 2. 6, the digital implementation is also responsible for generating the pseudorandom binary sequence (PRBS), the carriers' waves of conventional PWM and the random techniques and, finally, the switching signal. Each one of these tasks is performed through different blocks that operate at different clock rates and the communication between them was possible due to the implementation of several shared registers or look-up tables located in the FPGA.

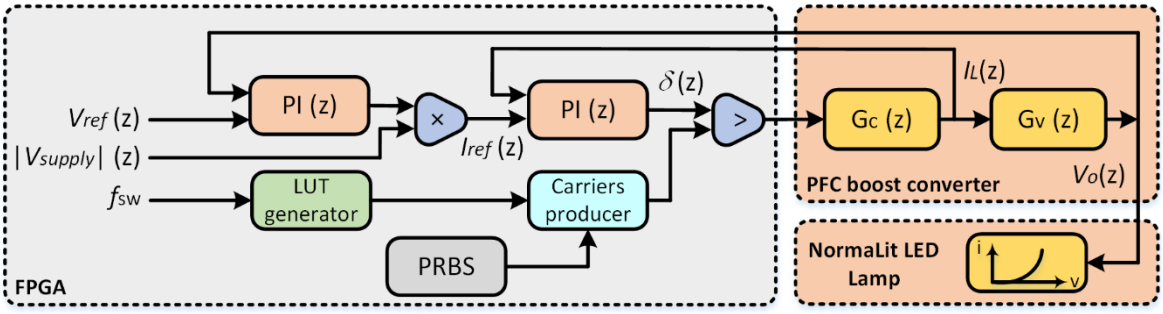

Figure 2. 6. Block diagram of the FPGA implementation.

2.5.1. PRBS generator

To generate a PRBS, 16 bits shift register has been created in which the re-entrant least significant bit is calculated by means of XOR logic gate combinational circuit where the operands are the last value of bits zero, two, eleven and fifteen. For that, it has been used a while loop adding an unsigned integer shift register (see Figure 2. 7). First shift register value has been initialized with the binary pattern "0001011010111001". The initial value must not converge in a lock situation as the register content takes the value "0" otherwise, this wrong behaviour would set the value of PRBS to "0" and the proposed techniques will no longer be random. Another critical parameter is the clock frequency from the PRBS block, which must be at least equal to the switching frequency to generate a new value for each carrier wave period. Experimentally, a considerably higher frequency has been selected, e.g. 400 kHz.

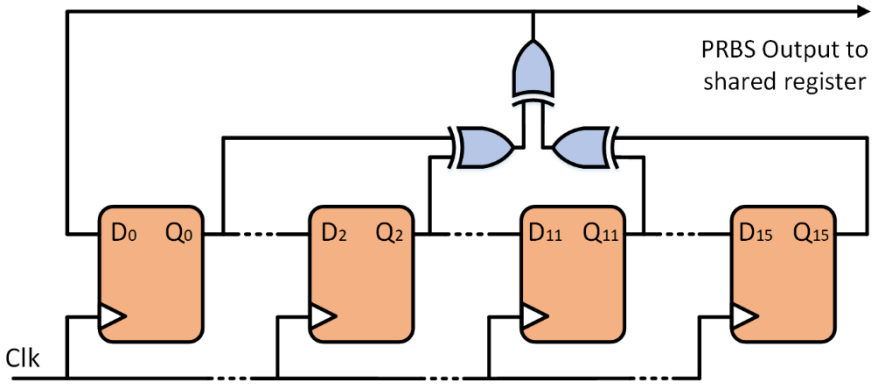

Figure 2. 7. Pseudo-random shift registers to generate PRBS.

The digital implementation of this shift register has been developed using two typical LabVIEW's structures: A while loop and a flat sequence. The latter has three phases or frames to enforce the order of the operations in the sequence. Consequently, there is a high degree of synchronization between each one of the following operations: First, the ticks counter is called to initialize the loop frequency, secondly the re-entrant bit is found and finally, the last frame rotates (with carry) the content of the shift register, where the carry value is the least significant bit (LSB) before calculated. Is also writes a shared register that will be used as source of randomness.

2.5.2. Look-up tables generator

The predefined waveforms of the implemented techniques are stored in a block with a fixed number of floating-point memory locations (SGL type data in LabVIEW). The number of samples is given by (2. 1), where f_{sw} is the frequency of the carrier wave, f_s the frequency of the while loop that generates each carrier sample on the FPGA and the brackets represent the rounding to the nearest even number. Furthermore, for the proposed approach, N must be divisible by 2 just once.

$$N = \left[\frac{f_s}{f_{sw}}\right] \tag{2. 1}$$

In this paper, each carrier wave has been generated at fixed frequency of 4 MHz using 1024 memory position as maximum, therefore the minimum switching frequency is approximately 3.9 kHz. However, the maximum switching frequency depends on the

allowed resolution to which the waveforms are built. The converter can perfectly operate at around 80 kHz, although a common switching frequency for LED driver applications is 25 kHz. With respect to the amplitude resolution, the parameter δ is important to be defined since each sample of this carriers' waves is calculated by adding or subtracting this value from the immediately previous sample. For the proposed techniques described in the following section, this parameter can be determined through the equations (2. 2) and (2. 3) accordingly, where A is the peak amplitude and selected to 100.

$$\delta_{RPPMa} = \frac{2A}{N} \tag{2. 2}$$

$$\delta_{RPPMb} = \frac{4A}{N-2} \tag{2. 3}$$

To build each random carrier wave, a finite state machine has been used (see Figure 2. 8). This algorithm consists of three states: The first one reads the switching frequency selected for the first time, the second state generates or updates the waveforms for each technique and writes them in memory blocks where they will be indexed to produce the carriers' waves, and finally, the last state waits for the switching frequency to change to update these waveforms.

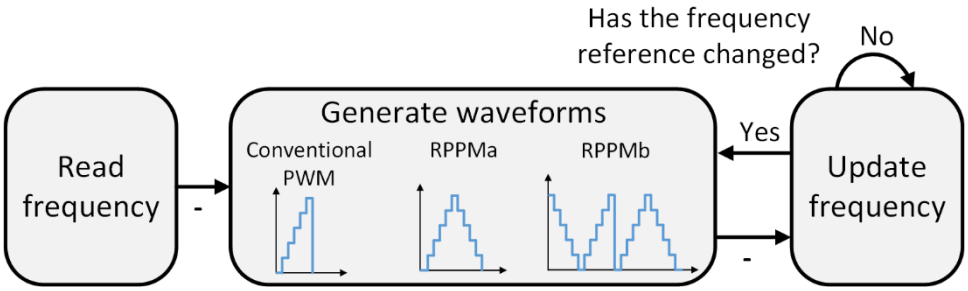

Figure 2. 8. States diagram of the finite state machine that generates each waveform.

2.5.3. RPPM methods

Two strategies have been experimented to achieve RPPM, namely RPPMa, previously employed in inverters with fairly good results [44]; and RPPMb as the novel approach here, respectively. The proposed random carrier for RPPMa, as shown in Figure 2. 9 a), is obtained by randomly combining two triangular carriers, both same fixed frequency, but in opposite phase. The carrier wave has been generated by indexing the above look-up table. It is not necessary to generate two opposite phase triangular carriers and select one of them to form the random waveform. On the contrary, this sequence can be generated through the values of a look-up table, where one of these carriers is stored, and their opposites, which have been calculated through equation (2. 4), where C are the look-up table values. This operation has been performed in LabVIEW with a case structure.

$$C' = A - C \tag{2. 4}$$

The random enables any of the two triangular carriers, which are decided by the "low" or "high" state of the PRBS; finally producing the resultant pseudo-random frequency carrier wave.

Regarding the RPPMb carrier wave, as shown in Figure 2. 9 b), the original period has been divided in two, so the carrier is built with the combination of the two opposite triangular carriers where the order of these ones depends on the state of PRBS. Consequently, each period of this carrier is composed by triangular carriers in opposite phase. To build this carrier, only one period has been stored and the other has been obtained in the same way as the RPPMa carrier.

It is important to emphasize that the average value from the inductor current and output voltage does not change since the volt-second balance of the triggering signal when the converter operates with the proposed techniques has the same value than when the conventional PWM is used. Therefore, there is not any difference between these two techniques as average values is concerned. However, the RPPM can reduce the high frequency dominant harmonics.

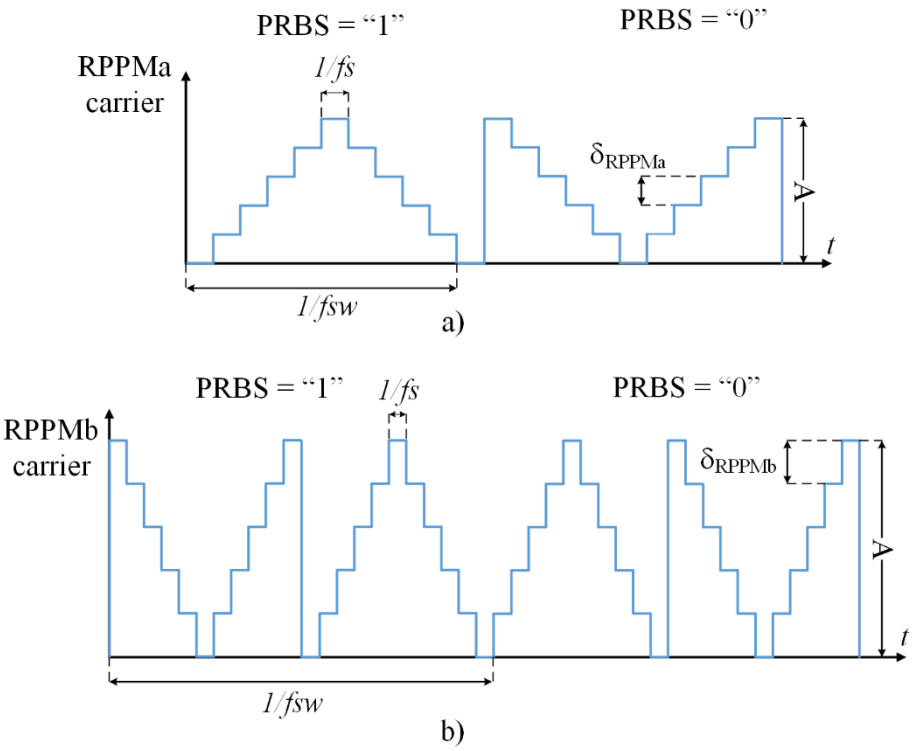

Figure 2. 9. Discrete carrier waves: a) RPPMa and b) RPPMb.

2.6. Results and discussion

In Figure 2. 10, the oscilloscope shows the spectrum of the experimental input current (0 – 125 kHz) for the implemented modulation techniques. Notice that the low-frequency spectrum is characterized by low distortion due to the employed aPFC topology and remains substantially unchanged when the different modulation techniques are applied as expected. However, the interest of this research is focused on the frequency range 2 – 150 kHz, as stated before. In this regard, both RPPMa and RPPMb techniques achieve a better energy distribution across the frequency spectrum than the conventional PWM, as proven the results described below. Furthermore, RPPMb fully mitigates these supraharmonic components and therefore provides better results than RPPMa.

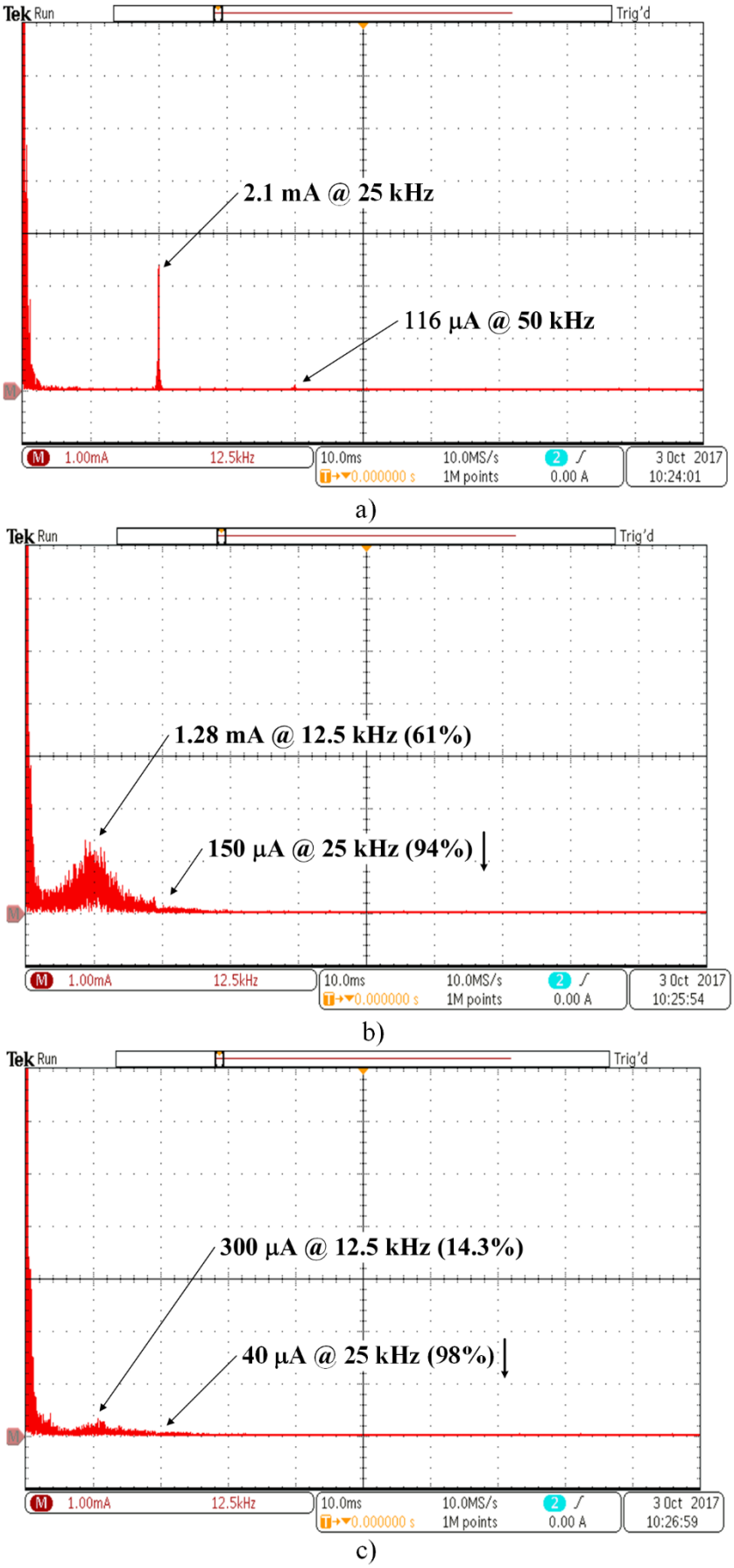

Figure 2. 10. Frequency spectrum of the experimental input current when: a) conventional PWM, b) RPPMa, and c) RPPMb is employed.

As shown in Figure 2. 10 a), when the LED driver operates under conventional PWM technique, two high frequency narrowband components appear: one at switching frequency (25 kHz) with an amplitude of 2.1 mA (0.21% of fundamental component) and the other, at double the switching frequency (50 kHz) with an amplitude of 116 μA.

When implementing the RPPMa technique on the same driver (see Figure 2. 10 b)), the current spectrum shows a broadband component of 1.28 mA at 12.5 kHz due to the spread spectrum method. However, the reduction at switching frequency reaches 94%, which is very significant (150 μA).

As detailed in Figure 2. 10 c), the great advantage from RPPMb technique is that achieves to fully mitigate the component at 25 kHz, also decreasing up to 300 μA (76.5 % of reduction) the broadband component at 12.5 kHz that appears with RPPMa. Thereby, this technique obtains the best result in the supply current spectrum.

2.7. Conclusions

Harmonic emission generated by PEC is one of the key problems when integrating them in the power grid. Traditional grid-commutated PEC caused undesirable high levels of harmonic content (< 2 kHz) and low TPF when connected to the power grid. In self-commutated PEC, through PWM with high switching frequencies (in the kHz range), the desired output voltage can be obtained, reducing or eliminating these discrete low order harmonics. However, this significantly increases harmonic emission spectrum towards higher frequencies (from 2 kHz to 150 kHz). While the low-frequency harmonics are still an important issue, the number of self-commutated PEC with significant Supraharmonics emission increases very fast. Consequently, the present massive integration of energy-efficient devices like LED lighting into the distribution networks provides new challenges to the different stakeholders.

These supraharmonics behave differently from (lower frequency) harmonics and interharmonics. Numerous problems on power systems are presently observed. The work on this frequency range has just started and more research is needed to find suitable ways for quantifying these frequency range emissions. Moreover, the spread of emissions and the impact on other neighbouring devices are another topic of research. CIGRE, IEC and other international working groups are currently reviewing the emission limits in the frequency range 2–150 kHz. The LED manufacturer should consider the EMI/EMC related impact since the early stage of design. Mitigation solutions, such as EMI filters, would not be as necessary if it is possible to reduce the emission itself, from the source, and at a low computational cost, when technologies such as the random switching pattern presented here are properly integrated.

Acknowledgements

This research is supported by the Spanish Ministry of Economy and Competitiveness under Project TEC2016-77632-C3-2-R. Also, the authors would like to thank the support of the University of Cordoba, through the program “II Becas Semillero de Investigación”.

References

[1] Chart LED lights gaining market share globally | The Data Blog. [Online]. Available: https://blogs.worldbank.org/opendata/arabvoices/chart-led-lights-gainingmarket- share-globally. (Accessed 31 March 2018).

[2] How Energy-Efficient Light Bulbs Compare with Traditional Incandescents | Department of Energy. [Online]. Available: https://energy.gov/energysaver/howenergy- efficient-light-bulbs compare-traditional-incandescents. (Accessed 22 October 2017).

[3] J. Baumgartner, T. Wunderlich, F. Jaunich, A. Sato, T. Bundy, G. Grießmann, N. Hanebrink, Lighting the Way: Perspectives on the Global Lighting Market, McKinsey, 2012, https://www.mckinsey.com/~/media/mckinsey/dotcom/client_service/automotive%20and%20assembly/lighting_the_way_perspectives_on_global_lighting_market_2012.ashx.

[4] CENELEC – CLC/TR 50627:2015 – Study Report on Electromagnetic Interference between Electrical Equipment/Systems in the Frequency Range Below 150 kHz, 2015.

[5] M. Bollen, M. Olofsson, A. Larsson, S. Rönnberg and M. Lundmark, "Standards for supraharmonics (2 to 150 kHz)," in IEEE Electromagnetic Compatibility Magazine, vol. 3, no. 1, pp. 114-119, 1st Quarter 2014, doi: 10.1109/MEMC.2014.6798813.

[6] S.K. Rönnberg, M.H. Bollen, H. Amaris, G.W. Chang, I.Y. Gu, Ł.H. Kocewiak, and J. Desmet, On waveform distortion in the frequency range of 2 kHz–150 kHz—review and research challenges, Electr. Power Syst. Res. Vol. 150, pp. 1–10, 2017, doi: 10.1016/j.epsr.2017.04.032.

[7] J. Huang and H. Shi, "Suppression of the Peak Harmonics from Loads by Using a Variable Capacitance Filter in Low-Voltage DC/DC Converters," in IEEE Transactions on Electromagnetic Compatibility, vol. 58, no. 4, pp. 1217-1227, Aug. 2016, doi: 10.1109/TEMC.2016.2552230.

[8] A. Moreno-Muñoz, Power Quality, 1st ed., Springer London, London, 2007, doi: 10.1007/978-1-84628-772-5.

[9] S. Uddin, H. Shareef, and A. Mohamed, Power quality performance of energy-efficient low wattage LED lamps, Measurement vol. 46, no. 10, pp. 3783–3795, 2013, doi: 10.1016/j.measurement.2013.07.022.

[10] P. Verma, N. Patel and N. -K. C. Nair, "CFL to LED Transition: An analysis from harmonics perspective," 2016 IEEE International Conference on Power System Technology (POWERCON), 2016, pp. 1-6, doi: 10.1109/POWERCON.2016.7754034.

[11] S. K. Rönnberg, M. H. J. Bollen and M. Wahlberg, "Harmonic emission before and after changing to LED and CFL — Part I: Laboratory measurements for a domestic customer," Proceedings of 14th International Conference on Harmonics and Quality of Power - ICHQP 2010, 2010, pp. 1-7, doi: 10.1109/ICHQP.2010.5625411.

[12] S. K. Rönnberg, M. Wahlberg and M. H. J. Bollen, "Harmonic emission before and after changing to LED lamps — Field measurements for an urban area," 2012 IEEE 15th International Conference on Harmonics and Quality of Power, 2012, pp. 552-557, doi: 10.1109/ICHQP.2012.6381215.

[13] T. Busatto, F. Abid, A. Larsson, M. H. J. Bollen and G. Singh, "Interaction between grid-connected PV systems and LED lamps: Directions for further research on harmonics and supraharmonics," 2016 17th International Conference on Harmonics and Quality of Power (ICHQP), 2016, pp. 193-197, doi: 10.1109/ICHQP.2016.7783479.

[14] E. O. A. Larsson, M. H. J. Bollen, M. G. Wahlberg, C. M. Lundmark and S. K. Rönnberg, "Measurements of High-Frequency (2–150 kHz) Distortion in Low-Voltage Networks," in

IEEE Transactions on Power Delivery, vol. 25, no. 3, pp. 1749-1757, July 2010, doi: 10.1109/TPWRD.2010.2041371.

[15] A. Gil-De-Castro, R. Medina-Gracia, S. K. Ronnberg, A. M. Blanco and J. Meyer, "Differences in the performance between CFL and LED lamps under different voltage distortions," 2018 18th International Conference on Harmonics and Quality of Power (ICHQP), 2018, pp. 1-6, doi: 10.1109/ICHQP.2018.8378918.

[16] *Electromagnetic compatibility (EMC) Part 4-7: Testing and measurement techniques — General guide on harmonics and interharmonics measurements and instrumentation, for power supply systems and equipment connected thereto*. IEC 61000-4-7:2002 +AMD1:2008.

[17] L. Alfieri, A. Bracale, and A. Larsson. New power quality indices for the assessment of waveform distortions from 0 to 150 kHz in power systems with renewable generation and modern non-linear loads, Energies, no. 10, vol 10, pp. 1633-1677, 2017, doi: 10.3390/en10101633.

[18] "IEEE Standard Definitions for the Measurement of Electric Power Quantities Under Sinusoidal, Nonsinusoidal, Balanced, or Unbalanced Conditions," in IEEE Std 1459-2010 (Revision of IEEE Std 1459-2000) , vol., no., pp.1-50, 19 March 2010, doi: 10.1109/IEEESTD.2010.5439063.

[19] A. Larsson, On High-Frequency Distortion in Low-Voltage Power Systems, University of Technology, Luleå, 2011.

[20] S. K. Rönnberg and M. H. J. Bollen, "Emission from four types of LED lamps at frequencies up to 150 kHz," 2012 IEEE 15th International Conference on Harmonics and Quality of Power, 2012, pp. 451-456, doi: 10.1109/ICHQP.2012.6381216.

[21] A. Gil-de-Castro, A. Larsson, S. Rönnberg, M. Bollen, LED lamps under different EMC environnments, International Conference and Exhibition on Electricity Distribution (CIRED), June, 2015, 2015, pp. 15–18. Available: https://www.diva-portal.org/smash/record.jsf?pid=diva2%3A1013544&dswid=-4025

[22] M. Klatt, J. Meyer, P. Schegner, A. Koch, J. Myrzik, T. Darda, G. Eberl, Emission levels above 2 kHz – Laboratory results and survey measurements in public low voltage grids, IET Conference Proceedings, vol. 1102 pp. 1168-1168, 2013, doi: 10.1049/cp.2013.1102.

[23] A. Grevener, J. Meyer, S. Rönnberg, M. Bollen, J. Myrzik, Survey of supraharmonic emission of household appliances, CIRED Open Access Proc. J. vol. 2017, pp. 870–874, 2017, doi: 10.1049/oap-cired.2017.0458.

[24] S. Schöttke, J. Meyer, P. Schegner and S. Bachmann, "Emission in the frequency range of 2 kHz to 150 kHz caused by electrical vehicle charging," 2014 International Symposium on Electromagnetic Compatibility, 2014, pp. 620-625, doi: 10.1109/EMCEurope.2014.6930980.

[25] S. Rönnberg, M. Bollen, and A. Larsson, Grid impact from PV-installations in northern Scandinavia, IET Conference Proceedings, vol. 1046, pp. 1036-1036, 2013 doi: 10.1049/cp.2013.1046.

[26] M. H. J. Bollen and S. K. Rönnberg, "Primary and secondary harmonics emission; harmonic interaction - a set of definitions," 2016 17th International Conference on Harmonics and Quality of Power (ICHQP), 2016, pp. 703-708, doi: 10.1109/ICHQP.2016.7783333.

[27] A. Gil-De-Castro, M. Bollen, A. Moreno-Muñoz, Street lamps aggregation analysis through IEC 61000-3-6 approach, IET Conf. Publ, 2013, doi: 10.1049/cp.2013.0656.

[28] S. Rönnberg, A. Larsson, M. Bollen, J.L. Schanen, A simple model for interaction between equipment at a frequency of some tens of kHz, International Conference on Electricity Distribution, CIRED, 2011.

[29] S. Rönnberg, M. Bollen, A. Larsson, M. Lundmark, An overview of the origin and propagation of supraharmonics (2–150 kHz), Nordic Conference on Electricity Distribution System Management and Development (2014).

[30] C. Waniek, T. Wohlfahrt, J. M. A. Myrzik, J. Meyer, M. Klatt and P. Schegner, "Supraharmonics: Root causes and interactions between multiple devices and the low voltage grid," 2017 IEEE PES Innovative Smart Grid Technologies Conference Europe (ISGT-Europe), 2017, pp. 1-6, doi: 10.1109/ISGTEurope.2017.8260267.

[31] A. Gil-de-Castro, S. K. Rönnberg and M. H. J. Bollen, "A study about harmonic interaction between devices," 2014 16th International Conference on Harmonics and Quality of Power (ICHQP), 2014, pp. 728-732, doi: 10.1109/ICHQP.2014.6842767.

[32] M. Pikkarainen, S. Vehmasvaara, B. A. Siddiqui, P. Pakonen and P. Verho, "Interference of touch dimmer lamps due to PLC and other high frequency signals," 2012 Electric Power Quality and Supply Reliability, 2012, pp. 1-6, doi: 10.1109/PQ.2012.6256241.

[33] S. K. Ronnberg, M. H. J. Bollen and M. Wahlberg, "Interaction Between Narrowband Power-Line Communication and End-User Equipment," in IEEE Transactions on Power Delivery, vol. 26, no. 3, pp. 2034-2039, July 2011, doi: 10.1109/TPWRD.2011.2130543.

[34] A. Larsson, A. Gil-de-Castro, M. Wahlberg, M. Bollen, Field and laboratory measurements of interference with light equipment due to waveform distortion originating from a large rectifier, International Conference and Exhibition on Electricity Distribution: 15/06/2015–18/06/2015 (2015).

[35] G. Singh, E. R. Collins, S. K. Rönnberg, E. O. A. Larsson and M. H. J. Bollen, "Impact of high frequency conducted voltage disturbances on LED driver circuits," 2017 IEEE Power & Energy Society General Meeting, 2017, pp. 1-5, doi: 10.1109/PESGM.2017.8274378.

[36] S. Li, S. -C. Tan, C. K. Lee, E. Waffenschmidt, S. Y. Hui and C. K. Tse, "A survey, classification, and critical review of light-emitting diode drivers," in IEEE Transactions on Power Electronics, vol. 31, no. 2, pp. 1503-1516, Feb. 2016, doi: 10.1109/TPEL.2015.2417563.

[37] R. Jaschke and K. F. Hoffmann, "Better Line Current by LED Lamps less 25 Watt Equipped With a Six Diode Valley Fill Topology," Proceedings of PCIM Europe 2015; International Exhibition and Conference for Power Electronics, Intelligent Motion, Renewable Energy and Energy Management, 2015, pp. 1-6.

[38] M. Arias, A. Vazquez, J. Sebastián, An overview of the AC–DC and DC–DC converters for LED lighting applications, Autom. J. Control. Meas. Electron. Comput. Commun, vol. 53 (2), pp. 156-172, 2012, doi: 10.7305/automatika.53-2.154.

[39] X. Xie, J. Wang, C. Zhao, Q. Lu and S. Liu, "A Novel Output Current Estimation and Regulation Circuit for Primary Side Controlled High Power Factor Single-Stage Flyback LED Driver," in IEEE Transactions on Power Electronics, vol. 27, no. 11, pp. 4602-4612, Nov. 2012, doi: 10.1109/TPEL.2012.2190523.

[40] T. -J. Liang, W. -J. Tseng, J. -F. Chen and J. -P. Wu, "A Novel Line Frequency Multistage Conduction LED Driver With High Power Factor," in IEEE Transactions on Power Electronics, vol. 30, no. 9, pp. 5103-5115, Sept. 2015, doi: 10.1109/TPEL.2014.2363293.

[41] S. Uddin, H. Sharef, O. Krause, A. Mohamed, M.A. Hannan, N.N. Islam, Impact of large-scale installation of LED lamps in a distribution system, Turk J. Electr. Eng. Comput. Sci, 2015, no. 6, vol. 23, pp. 1769–1780, doi: 10.3906/elk-1404-243.

[42] S. K. Rönnberg, A. G. -d. Castro, M. H. J. Bollen, A. Moreno-Munoz and E. Romero-Cadaval, "Supraharmonics from power electronics converters," 2015 9th International Conference on Compatibility and Power Electronics (CPE), 2015, pp. 539-544, doi: 10.1109/CPE.2015.7231133.

[43] M.-T. Kuo, M.-C. Tsou, Novel frequency swapping technique for conducted electromagnetic interference suppression in power converter applications, Energies, no. 1, vol. 10, pp. 24-47, 2016, doi: 10.3390/en10010024.

[44] S. K. Rönnberg, A. G. Castro, A. Moreno-Munoz, M. H. J. Bollen and J. Garrido, "Solar PV inverter supraharmonics reduction with random PWM," 2017 11th IEEE International Conference on Compatibility, Power Electronics and Power Engineering (CPE-POWERENG), 2017, pp. 644-649, doi: 10.1109/CPE.2017.7915248.

Chapter 3

A novel direct load control testbed for smart appliances

Joaquin Garrido-Zafra[1], Antonio Moreno-Muñoz[1], Aurora Gil-de-Castro[1], Emilio J. Palacios-Garcia[3], Carlos D. Moreno-Moreno[1] and Tomas Morales-Leal[2]

[1]Departamento de Ingeniería Electrónica y de computadores, Escuela politécnica superior, Universidad de Córdoba, Córdoba, Spain

[2]Departamento de Ingeniería Eléctrica y Automática, Escuela politécnica superior, Universidad de Córdoba, Córdoba, Spain

[3]Department of Energy Technology, Aalborg University, Aalborg, Denmark

Abstract

The effort to continuously improve and innovate smart appliances (SA) energy management requires an experimental research and development environment which integrates widely differing tools and resources seamlessly. To this end, this paper proposes a novel Direct Load Control (DLC) testbed, aiming to conveniently support the research community, as well as analyzing and comparing their designs in a laboratory environment. Based on the LabVIEW computing platform, this original testbed enables access to knowledge of major components such as online weather forecasting information, distributed energy resources (e.g. energy storage, solar photovoltaic), dynamic electricity tariff from utilities and demand response (DR) providers together with different mathematical optimization features given by General Algebraic Modeling System (GAMS) This intercommunication is possible thanks to the different applications programming interfaces (API) incorporated into the system and to intermediate agents specially developed for this case. Different basic case studies have been presented to envision the possibilities of this system in the future and more complex scenarios, to actively support the DLC strategies. These measures will offer enough flexibility to minimize the impact on user comfort combined with support for multiple DR programs. Thus, given the successful results, this platform can lead to a solution towards more efficient use of energy in the residential environment.

3.1. Introduction

Much has been written about the new role consumers can play in future smart grid (SG). Driven by the massive integration of renewable energy resources, the SG is evolving swiftly, causing changes in how electricity is produced, managed, marketed, and consumed. If for a while, the SG paradigm meant merely accepting a bi-directional flow of electricity and information, it must continue to evolve to adapt to the current demands of the digital consumer. In the years to come, the computational exploitation of the enormous amounts of information provided by the Internet of Things (IoT) sensors, incorporated at all layers of the SG, will become the main engine of its evolution towards the digital energy network, focused on customer service. This is what has been called "data-driven energy" [1]. A large amount of energy data will support collective decision making, opening the way to more responsive utilities and more engaged consumers. This will undoubtedly impact the evolution of household appliances. In fact, SAs are already showing their potential for data-driven energy [2].

The growing use of energy by domestic appliances shows no signs of slowing, reaching 2900 TWh in 2017. The use of electricity by these loads continues to grow by almost 2% per year, a steady trend since 2010 [3]. Although the electricity demand for major appliances has slightly decreased since 2007, mainly due to improvements in their energy efficiency, the rapid proliferation of small appliances and brown goods has absorbed these savings. The energy consumption due to these small loads has grown twice as fast as that of large appliances in the last decade. In addition, only one-third of domestic appliances consumption is under regulatory protection, particularly in emerging markets. This may become even more relevant in the near future as the demand for electricity in buildings increases due to the impact of the charging infrastructure for electric vehicles. While it is true that there is a need to increase the rigor of existing policies by extending regulatory coverage to a broader range of devices, on the other hand, user awareness may be the key factor. However, to achieve this, consumers should be rewarded to some extent when changing their behavior. The availability of information and communication technologies (ICT) on SG can be decisive in meeting this commitment through the widespread adoption of DR strategies.

In other areas, such as power electronics, it is common to find a complete chain of modeling, development, testing, optimization, virtual validation, and rapid prototyping commercial tools that integrate seamlessly into a convenient testing and development environment such as these tools of Typhoon (Typhon, Somerville, USA) [4] and dSPACE (dSPACE, Paderborn, Germany) [5]. It is possible to find testbed proposals for different applications in SG, like our previous one [6]. In the newly released paper [7], a distributed framework for real-time management and co-simulation of DR in SG is presented. This solution provides a near real-time co-simulation platform to validate new DR-policies exploiting IoT approach performing software-in-the-loop. In the recent papers, authors propose an interesting testbed for distributed DR based on a microgrid (MG) modeled on the PSIM software (Powersim, Rockville, USA) to provide frequency regulation [8] and control over other grid parameters in general [9]. In the model, the nodes of virtual IoT devices are created according to the collective characteristics of their real twins, connected to the system. Network conditions can be reproduced when testing new DR algorithms to provide, e.g. frequency regulation reserve services.

Similarly, in order to support the field of DLC research in this emerging application area of SA, it is necessary to provide new testbeds for lab experimentation. Therefore, the main contribution of this work is the development of a research test bench flexible enough to incorporate different tools of different origins such as weather forecasting APIs, DR

providers from the utility and mathematical optimization features built on the basis of the LabVIEW systems (2015, National Instruments, Austin, USA) design platform and development environment for a visual programming language. It can benefit from user-friendly and intuitive software as well as hardware such as powerful real-time processors, user-programmable field-programmable gate array (FPGA), and full I/O interfaces. However, although it also offers libraries of dedicated functions, it has been necessary to specifically develop a sophisticated software (that did not exist) that supports the seamless link between the tools, since their individual parts are precisely aligned with each other. In this sense, the proposed testbed is a novelty since most of the papers available in the literature are focused on the development of complex mathematical models without considering the integration of these tools that are so important to implement a realistic platform and thus emulate scenarios and test cases as real as possible. Furthermore, this work is a step forward from previous research, as it includes several tools that have never been integrated before.

The organization of the paper as follows. Section 2, and 3 presents the background of the research. Then, Section 4 describes the experimental platform and also examines the control and optimization strategies, considering practical limitations and safety constraints in detail. In Section 5, the case study is discussed. Finally, the conclusions and future work are reported in Section 6.

3.2. Home energy management systems. State of the art.

The combination of the SG paradigm with IoT technologies and the will of consumers to actively participate in their energy control has enhanced the home energy management system (HEMS) concept. These are systems capable of monitoring home consumption at different levels and implementing automation or control mechanisms.

They have evolved at an unstoppable pace in the last years. By 2013, most systems only offered home monitoring, either local or remote and rarely some manual control over switches or dimmable loads [10]. Currently, on the contrary, a wide variety of control systems are available ranging from the simple automatic scheduling of applications to the optimization of energy resources, through advanced algorithms that consider the state of numerous external variables such as energy prices or weather conditions. What is more, they are even able to learn from users thanks to the incorporation of artificial intelligence [11].

Because of this evolution and the large range of devices and algorithms that are being integrated into the HEMS, the number of works in the literature is extensive and unapproachable for a paper whose purpose is not that. However, for example, the authors in [12] define a classification according to the level of complexity of these systems. This will help to situate the present work and the challenges addressed. The levels from the lowest to the highest complexity are Monitoring, Logging, Alarm, Energy Management, and DR.

Nowadays, the first three levels can be regarded as a prerequisite. Every HEMS must carry out home monitoring at different aggregation levels. The basic level is the total household consumption, generally measured by technologies such as Smart Meters, widely deployed across Europe [13]. Nevertheless, the energy footprint of individual elements can be recorded by means of load submetering or non-intrusive load monitoring (NILM) algorithms, which use machine learning to distinguish individual appliances from the total consumption [14].

The capture of measures can be performed with different granularity and be stored in different supports. In this way, all or part of the data is stored in the cloud, from where it is possible to obtain descriptors or apply machine learning algorithms. This also allows for the possibility of generating alarms at different levels, so fast events that require immediate attention can be generated and then processed in the so-called Edge, while more complex

alarm mechanisms can be implemented in higher layers after preprocessing and analysis of historical data.

The aforementioned elements are essential for the creation of reliable controls at the next levels named: energy management and DR. The first focuses on the control of a combination of distributed resources to guarantee a continuous power supply, whereas the second goes a step further and manages the individual consumer appliances.

Among the recent publications, the most used optimization techniques are mixed-integer linear-programming [15], and variation of those [16], as well as population-based algorithms [17]. It is also common to find works that propose multi-objective algorithms to reach a trade-off between the energy savings that can be achieved and the benefits from possible incentives [18].

Nevertheless, as is evident from the most recent publications, the use of Internet technologies as a solution to optimization problems is becoming more and more common [19], as they tackle issues such as the diversity of household appliances, the simultaneous pursuit of several objectives in parallel, and the uncertainty in predicting conditions such as occupancy levels, energy consumption or weather conditions [20].

3.3. Smart appliances overview

What is a SA? There is more than one definition, but popularly a SA is recognized because it has some degree of embedded processing and wireless connectivity. Sometimes called a Net appliance, an Internet appliance or an information appliance, it can be as simple as an application that warns you whenever your refrigerator has a door opened, or as complex as remotely controlling your oven from your smartphone or via a voice assistant. However, in the framework of the SG, the term “smart” focuses on those systems (with communications-enabled) which are able to modulate their electricity consumption in response to external signals such as price information [21], local measurements [22] or direct control commands [23]. In other words, those appliances that can support grid flexibility because they have been configured to respond to DR requests.

In a recent survey [24], 28% of people find SA very attractive, but people are more reluctant to buy them because of price concerns, so 49% of people say this is a barrier to buying. Other barriers include dynamic pricing, lack of interoperability and legal framework as reported by the European parliament [25] and the world economic forum [26]. First, the lack of a dynamic pricing model to the clear majority of customers is an obstacle. Users will not be willing to change their habits if they cannot perceive that this intelligent functionality can bring them substantial financial savings. Second, the high purchase premiums and long replacement cycles of these devices are prolonging their mass adoption. Thirdly, to enable the communication between SAs that use different protocols and standards, and to ensure interoperability, the communication interface must be supported by a data model that conforms to a harmonized reference ontology. A semantic platform called OpenFridge has recently been proposed in [27] that has been deployed and evaluated with real-life users distributed globally. But the candidate for such a reference ontology will almost certainly be the Smart Appliances REFerence ontology (SAREF) [28]. SAREF4ENER [29] is the SAREF extension to be able to fully support DR for the energy domain.

Finally, the lack of a clear legal structure around customer data limits growth in this area. This could include the appliance energy use pattern meaning when, how much and how is energy being consumed. These data could even be monetized. For example, appliance manufacturers might be willing to pay an energy supplier a fee for these data, as they can be of great value in terms of customer service, product support, as well as maintenance. In the case of aggregation [30], how this data could be shared among customers to allow, e.g. for

their energy efficiency comparison. An aggregator can operate on behalf of a group of consumers, having access to data and possible remote adjustment over consumers' appliances. If the security of connected devices used in aggregation is not safeguarded, consumers could be exposed to several risks like data theft or request of appliance ransomware. Security flaws and data privacy issues are main concerns of the users, and only a few regions have well-defined rules about who can access, own, and share utility customer data.

However, the prospects for SA are bright. The global market for SA is projected to reach $38.35 billion by 2020, with a compound annual growth rate (CAGR) of 16.6% over the projected period 2015–2020. IoT-enabled devices (currently low, about 5% of white goods) are expected to grow dramatically, and the number of sensors is expected to increase six-fold by 2020. So, according to the International Energy Agency, by 2040 almost 1 billion households and 11 billion SA could participate in interconnected electricity systems.

Typically, DR policies can be classified between load-shifting strategies, which move the load from on-peak or event hours when demand and rates are the highest, to off-peak hours when rates are lower, and load-shedding strategies, which directly reduce or avoid energy use during on-peak hours altogether. Consequently, in the residential sector, the loads can be divided into non-shiftable, time-shiftable and energy “sheddable”. The time-shiftable loads are the appliances whose operation can be moved from peak to off-peak times with the minimal loss of comfort for the inhabitant. This is the category of 'wet' appliances, e.g. dishwashers (DW), washing machines (WM), and tumble dryers (TD). These appliances account for a significant proportion of household energy consumption. Alternatively, non-shiftable loads, such as lighting and brown appliances, cannot delay their operation [31]. At present, there is no deployed infrastructure that allows remote activation of these appliances. However, their behavior has been deeply studied and it is now possible to understand the potential of the DR in supporting the operation of the network [32].

Among household appliances, a special category is the thermostatically-controlled loads (TCL) (e.g., electric water heaters (EWH), HVAC systems, refrigerators, and freezers) as their thermal inertia allows for flexible load patterns (both shifting and shedding) while meeting their service requirement. Therefore, compared to other SA, TCL exhibit predictable behavior from the DR point of view, and even more when aggregated in large population clusters [33]. In recent work, a stochastic model has been presented for the generation of high temporal resolution synthetic profiles of the consumption of these domestic appliances [34]. However, its potential for flexibility remains virtually unknown. [35] presents the recent projects that are facilitating the transition from research to development. In general terms, and due to their inherent characteristics, there are two types of TCL, with different operating principles. First, resistive loads (i.e., heat generation equipment) and, second, compressor-driven loads (i.e., heat pumping equipment). Although this paper is particularly dealing with resistive loads, greater demand elasticities could be achieved if the control strategy achieved were extended to the rest of the residential TCL.

3.4. Structure of the smart appliance control testbed

The proposed control platform is composed of four main blocks that collect data and exchange information between each other aiming to implement the abovementioned DR policies through DLC. The platform architecture is shown in Figure 3. 1 , where LabVIEW works as the core application by handling the data provided by the outer blocks. This central block also has the highest priority from the call handling point of view, that is, LabVIEW follows the classical scheme where the main application deals with the so-called subVI to

allow modular designs. At the same time, this subVIs will be the interfaces with the rest of the blocks.

The block on the right side is related to the API that provides the testbed with both weather information (Ambient temperature and photovoltaic (PV) production forecast) and the price of the energy.

Finally, these DR policies must be mathematically translated into an optimization model which includes several constraints related to the people's habits, the availability of energy from different sources and the household appliances features among others. The model should also offer a certain degree of flexibility with respect to the number of invokes and formulation changes. All these reasons have contributed to opt for General Algebraic Modeling System (GAMS) as the software used to solve the proposed model. Furthermore, another component including the functions given by the GAMS API is used to integrate this software into LabVIEW using a dynamic link library (DLL). The following sections will describe these previous blocks and their interactions in more detail.

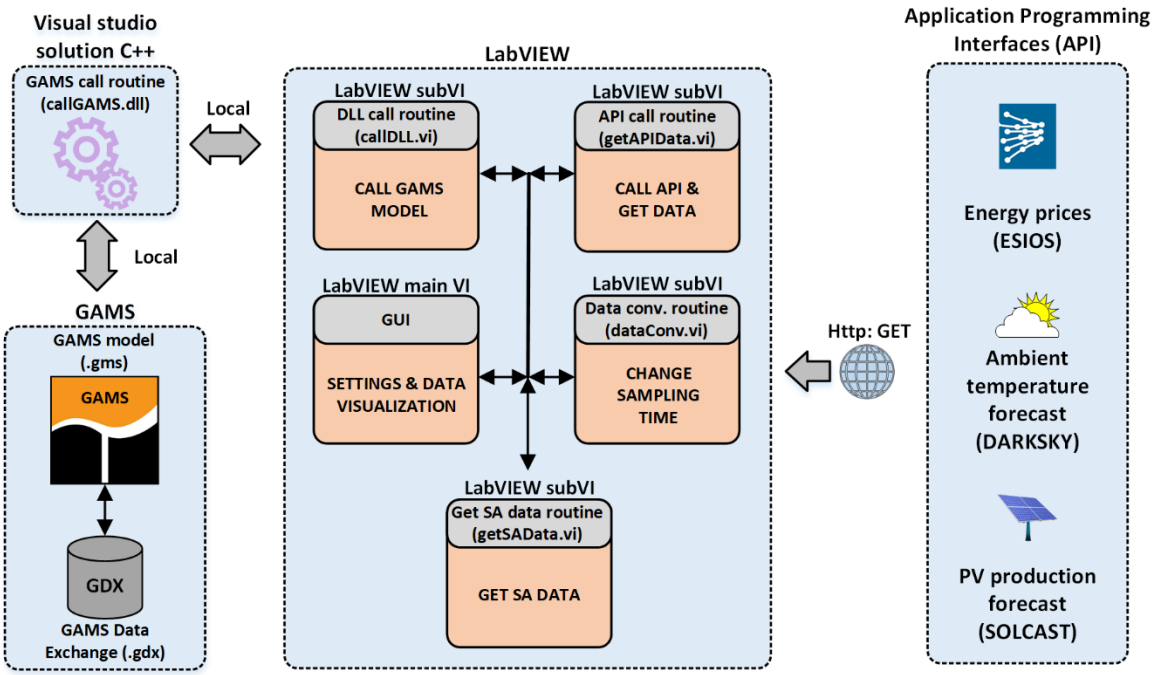

Figure 3. 1. Smart appliances control testbed overview.

3.4.1. LabVIEW

LabVIEW has been the tool used to integrate and manage all blocks of the platform. Concretely, the developed LabVIEW application consists of two threads commonly known as while loops located in the block diagram. The first one implements the whole infrastructure necessary to parametrize and call the GAMS model and comprises the data collection from the API solcast [36], dark sky [37] and Spanish system operator information system (E-SIOS) [38], which is the information system of the Spanish electricity group Red Eléctrica de España (REE), using the subVI getAPIData.vi that implements an hypertext transfer protocol (HTTP) client. This loop also entails the data standardization with respect to the sampling times by means of dataConv.vi, the model call through callDLL.vi as will be described in the following section and the display of the results. However, the second

loop just converts the raw information of the scheduled SA (name, operation mode, and time) into a recognizable information by the model through getSAData.vi.

The graphic user interface (GUI) or front panel is shown in Figure 3. 2 and has three main parts, namely, the SA scheduler (part A) including at the top the EWH section where the parameters that model this appliance (Minimum and maximum temperatures, tank capacity, nominal power, initial temperature, loss factor, inlet water temperature, and the hourly hot water consumption) are set up. The rest of SA under analysis in this study (WM, DW, and TD) are modeled according to their average power consumption and are scheduled at the bottom of part A where both the time and mode of operation as well as the cycle time can be selected. Two modes of operations have been evaluated: The fixed mode is used to launch the SA at a fixed time while the variable mode enables a certain degree of flexibility since the SA is scheduled over a time interval. As a result, the platform is forced to decide the start time within this interval once the model is solved. This part also includes information (Name, operation mode and time) about the scheduled SA.

Figure 3. 2. LabVIEW graphic user interface.

At the top of the part B are the parameters that model the energy storage system (ESS) such as the initial state of charge (SOC), capacity, minimum, and maximum SOC allowed as well as maximum power flow and a maximum ratio of change. At the middle, some features of the nanogrid under study can be found: Geographical coordinates (Longitude and latitude), tilt angle, power and efficiency in the case of the PV system or maximum power and tariff type with respect to the grid connection. The last section in part B includes the local directories required by GAMS, on the left half, and the personal keys that API administrator provides to establish a secure connection, on the right half.

Finally, part C shows the results of the optimization process divided into three graphs. From top to bottom, the first graph plots the hourly price of the energy according to the selected tariff, the optimal power consumption from the grid and thus the cost once these two previous ones are known. The second graph shows profiles such as the SOC and power taken from the batteries, the PV production and the amount of such power that would be injected into the nanogrid, the power usage of the SA and the consumption to be considered non-shiftable. The last graph describes the whole state of the EWH depicting its power consumption as well as the water and ambient temperatures.

3.4.2. Linking GAMS and LabVIEW

This section describes the communication between GAMS and LabVIEW. Some papers show the integration of GAMS into Matlab [39] or other software like LabVIEW through Matlab as an intermediary interface [40]. In this sense, the novelty of this work is the direct coupling of both tools without using any intermediate software. On the one hand, the inner communication between the GAMS model and its GAMS Data Exchange (GDX) file has been included under the subsection GAMS as appears in Figure 3. 1. This file is often used to store the parameters with which the model is called, as well as the model results, however, such interaction does not take place directly but will have to be handled by means of the appropriated classes and methods that the GAMS object-oriented API [41] provides resulting in the seamless integration of GAMS into any application such as LabVIEW in this case. This architecture employs the C++ API in a DLL format which is the interface that makes the linkage possible. The flowchart is shown in Figure 3. 3. First, system and working directories have been set; the system directory refers the path where all GAMS installation files are located while the working directory refers to the path where the GAMS models and GDX files will be stored (also shown in part B of Figure 3. 2). The second stage aims to create a database object where the parameters used in the model will be stored, but this will be carried out in the third stage. The model execution options, such as the names of the database object and the exchange file to be used are subsequently specified. The last stages are in charge of executing the model, returning the optimal values of the decision variables.

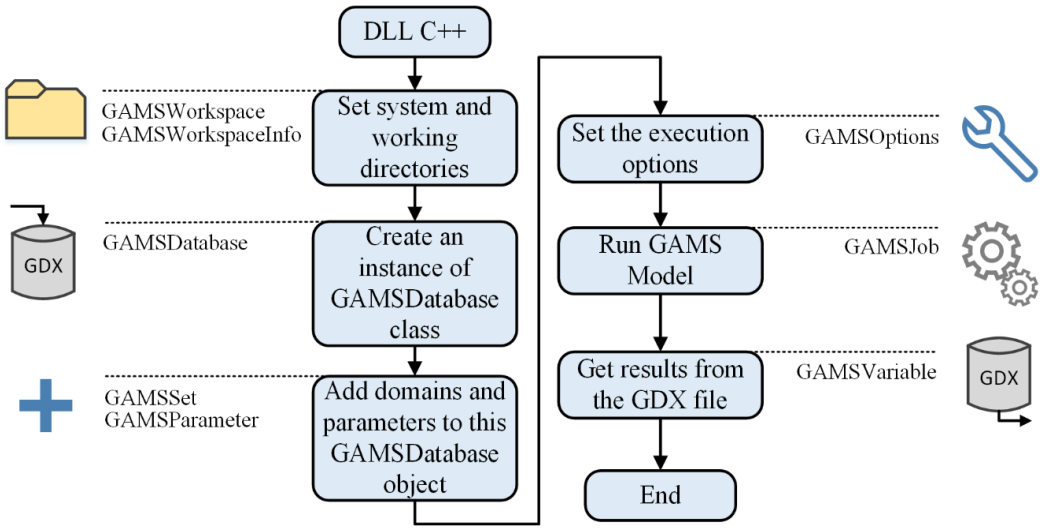

Figure 3. 3. Dynamic-link library flowchart for linking both environments.

3.4.3. An optimization model for demand side management

While most of the proposed models address this issue as a task scheduling problem using heuristics algorithm to make decisions on shifting, shedding or even disconnecting the load, this paper proposes a novel mixed-integer linear programming (MILP) model that uses the price-based DR programs to optimize the power consumption using the potential flexibility that TCL provides to the demand. The proposed model involves a smart home as shown in Figure 3. 4 with its own ESS, distributed energy resources (DER) based on PV panels as well as a scenario with SA managed through the DLC strategy.

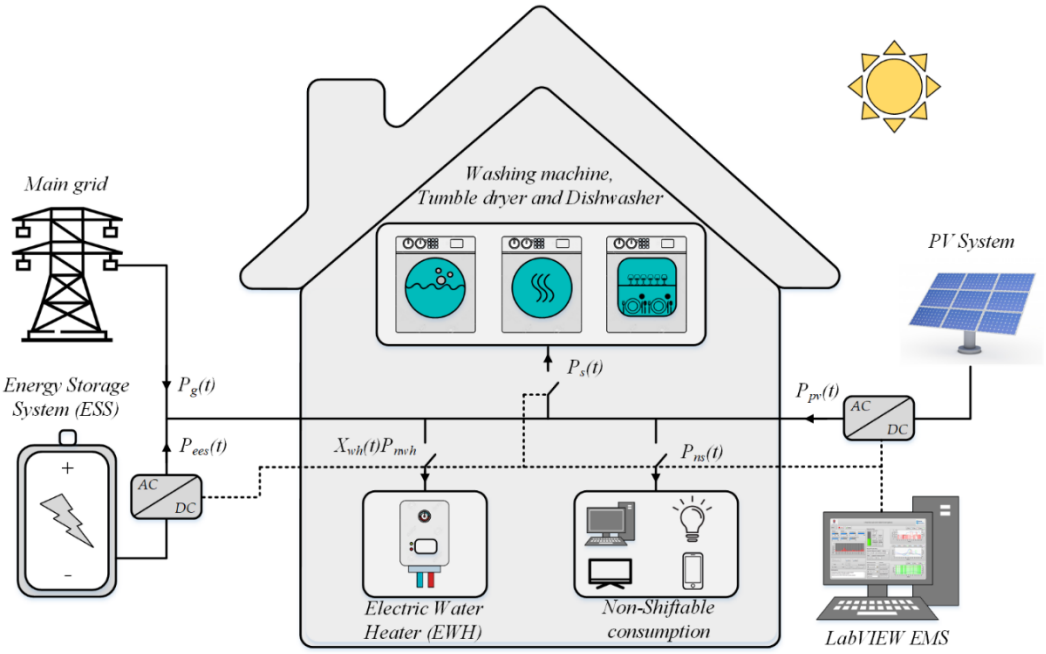

Figure 3. 4. Smart home topology employed in the case study.

In terms of mathematical formulation, equation (3. 1) refers to the objective function f (in €) where $P_g(t)$ (in kW, as all the powers henceforth) and $Pr(t)$ (in €/kWh) are the power consumption from the grid and the price of the energy respectively at time slot $t \in [1,2,\dots T]$. The rest of the equations are constraints related to the power balance, the user preferences and the energy availability from the sources. Equation (3. 2) denotes the global power balance at each time slot t with $P_g(t)$, the power taken from the PV panels $P_{pv}(t)$ as well as the power given by the energy storage system $P_{ess}(t)$ on the generation side. On the demand side is the non-shiftable power $P_{ns}(t)$, which involves the stand-by consumption coming from non-dimmable devices, such as lighting, low power DC adapters used to supply small devices and also the consumption from the SA scheduled in fixed mode, $P_s(t)$ is the power consumption of the common-use SA such as the WM, DW and TD scheduled in variable mode and the consumption of the EWH expressed as the product of its nominal power P_{wh} and the binary variable $x_{wh}(t)$ that indicates its state each time slot.

Equations (3. 3), (3. 4) and (3. 5) set the limits for $P_g(t)$, $P_{pv}(t)$ and $P_{ess}(t)$ respectively, where P_g^{max} denotes the maximum power that can be taken from the grid and P_{ess}^{max} the maximum power that can be injected into or extracted from the ESS. Moreover, the ratio of change of this variable has also been constrained in equation (3. 8) through the parameter dP_{ess}^{max} (in kW/h) to ensure a lifetime of the batteries as long as possible. Finally, $f_{pv}\left(P_{pv}^{pk}, \eta_{pv}, \alpha, \lambda, \phi, t\right)$ refers to the function that implements solcast to provide the PV production each time slot t and thus has been taken as the maximum power available to be injected into the system from the PV panels. Parameters such as the installed peak power P_{pv}^{pk}, the efficiency η_{pv}, the tilt angle α or the location, through the latitude λ and longitude ϕ will be required by this API in each HTTP request.

Equations (3. 6) and (3. 7) describe the dynamic of the ESS by means of a simple kWh counter to compute the current state of charge $SOC(t)$ (in %) based on the previous one $SOC(t-1)$ and $P_{ess}(t)$ and setting the $SOC(t)$ limits between SOC_{min} and SOC_{max} not to allow deep charges and discharges which is also a condition to ensure a long lifetime of the system.

The SA scheduling process using the variable mode is modeled by equations (3. 9) and (3. 10) and has been conceived as a decision-maker who chooses the optimal SA operation from among the possible ones that could be generated between the selected start and end times, by shifting the original consumption one-time slot. In this context, let us define j as the index that refers to each SA to be scheduled and k_j the index associated with each shifted consumption that may be generated for each j, being N_j the number of SA and N_k^j the number of possible consumption profiles. This family of shifted consumptions builds each matrix $\Gamma_j(k_j, t)$ which has as many rows as possible scenarios and as many columns as considered time slots T. Moreover, for the decision-making process, all the shifted consumptions have been associated with a binary variable $x_j(k_j)$ and thus, the optimal scenario will be indicated once the model is solved by means of the state of these decision variables. Finally, to ensure just one shifted consumption operates, equation (3. 10) forces the sum so that just one binary variable is equal to 1.

The EWH has been considered as a special SA due to its thermal inertia and therefore has its own power balance equation as it is apparent from (3. 11). From left to right, this balance involves the energy stored inside the EWH tank characterized by the current and previous average water temperature $T_{wh}(t)$ and $T_{wh}(t-1)$ (in ℃, as the rest of temperatures hereafter), the tank capacity C_{wh} (in m3) and the parameters that model essential features of the supply water like its density ρ (in kg/m3) and its specific heat C_p (in kJ/kg℃). The following terms are the thermal losses taking place in the tank walls given by the loss factor g_{wh} (in kW/℃) and the ambient temperature profile $T_{amb}(t)$ besides the energy provided by the water entering the tank as a consequence of the usage events and defined by means of the hot water consumption $D_{wh}(t)$ (in m3/s) and the temperature of this water, T_{inlet}. Finally, the discrete energy due to the heater element can be found. Once the EWH dynamic has been well-defined, the model for this appliance is fully completed with equation (3. 12) where the upper and lower limit of $T_{wh}(t)$ are constrained according to the normal operation temperatures T_{wh}^{min} and T_{wh}^{max}.

$$Min\ f = \frac{24}{T}\sum_{t=1}^{T} P_g(t)\, Pr(t) \tag{3. 1}$$

$Subject\ to$:

$$P_g(t) + P_{pv}(t) + P_{ess}(t) = P_{ns}(t) + P_{sa}(t) + x_{wh}(t)P_{nwh} \tag{3. 2}$$

$$0 \le P_g(t) \le P_g^{max} \tag{3. 3}$$

$$0 \le P_{pv}(t) \le f_{pv}\left(P_{pv}^{pk}, \eta_{pv}, \lambda, \phi, t\right) \tag{3. 4}$$

$$-P_{ess}^{max} \le P_{ess}(t) \le P_{ess}^{max} \tag{3. 5}$$

$$SOC(t) = SOC(t-1) - 100\left(\frac{24}{T}\right)\frac{P_{ess}(t)}{C_{ess}} \tag{3. 6}$$

$$SOC^{min} \le SOC(t) \le SOC^{max} \tag{3. 7}$$

$$-dP_{ess}^{max} \leq \frac{P_{ess}(t) - P_{ess}(t-1)}{24/T} \leq dP_{ess}^{max} \tag{3. 8}$$

$$P_{sa}(t) = \sum_{j=1}^{N_j} \sum_{k_j=1}^{N_k^j} x_j(k_j)\, \Gamma_j(k_j, t) \tag{3. 9}$$

$$\sum_{k_j=1}^{N_k^j} x_j(k_j) = 1 \tag{3. 10}$$

$$\begin{aligned} C_{wh}\rho C_p \frac{T_{wh}(t) - T_{wh}(t-1)}{86400/T} &= g_{wh}[T_{amb}(t) - T_{wh}(t-1)] \\ &+ D_{wh}(t)\rho C_p[T_{inlet} - T_{wh}(t-1)] + x_{wh}(t)P_{nwh} \end{aligned} \tag{3. 11}$$

$$T_{wh}^{min} \leq T_{wh}(t) \leq T_{wh}^{max} \tag{3. 12}$$

3.5. Case study

This section aims to evidence the effectiveness of the above-described DLC platform by testing it under cases which consist of minimizing the cost of the energy imported from the grid over a 24-hour time horizon, as was stated in the previous section, with a time resolution of 5 minutes, so that, $T = 288$. Concretely, two case studies based on the available electricity tariffs in the Spanish market are considered. One case is based on time discrimination in two periods (off-peak and peak) also known as tariff DHA, and another is a case using the default tariff or tariff A (without time discrimination). Both cases use the SA consumption models shown in Figure 3. 5 and based on 120 minutes working cycle divided into 8 slots of 15 minutes provided by [42]. Additionally, to give the case study a more realistic approach, the component of the non-shiftable power that represents the standby consumption was obtained by acquiring the active power in one of the laboratory circuits for a 24-hour workday.

Under this framework, a typical dwelling including a small scale ESS and PV installation has been chosen as the topology of this case study (see Figure 3. 4). More in detail, the PV system is modeled by a nominal power of 2 kW, an efficiency of 90% and mounted with a tilt angle of 30°. With respect to the location, southern Spain has been considered for both cases, concretely at 37.88° and −4.79° of latitude and longitude respectively. On the other hand, the ESS has a capacity of 6 kWh, a maximum charge/discharge power of 2 kW with a ratio of change limited to 0.5 kW/h and where the SOC can fluctuate in the range 35%–65%, the initial SOC was fixed to 50%. The EWH considered is the type which can be found in the residential environment, vertically mounted and cylindrical, with a capacity of 0.1 m3 as well as a nominal power of 2 kW. Its loss factor has been set to 2.10−3 kW/℃ and the inlet water temperature to 21 ℃ [43], while the water temperature inside the tank has been constrained in the range 60–85 ℃ with an initial condition of 65 ℃. In addition, an example of hot water consumption considering the water drawn from the EWH tank due to household use such as hand washing, showering, and dishwashing among others and based on [44] has been used. Finally, the capacity of the main grid has been fixed to 4.6 kW since it is a common value in Spain. Table 3. 1 summarizes the main parameters of the model as well as its values.

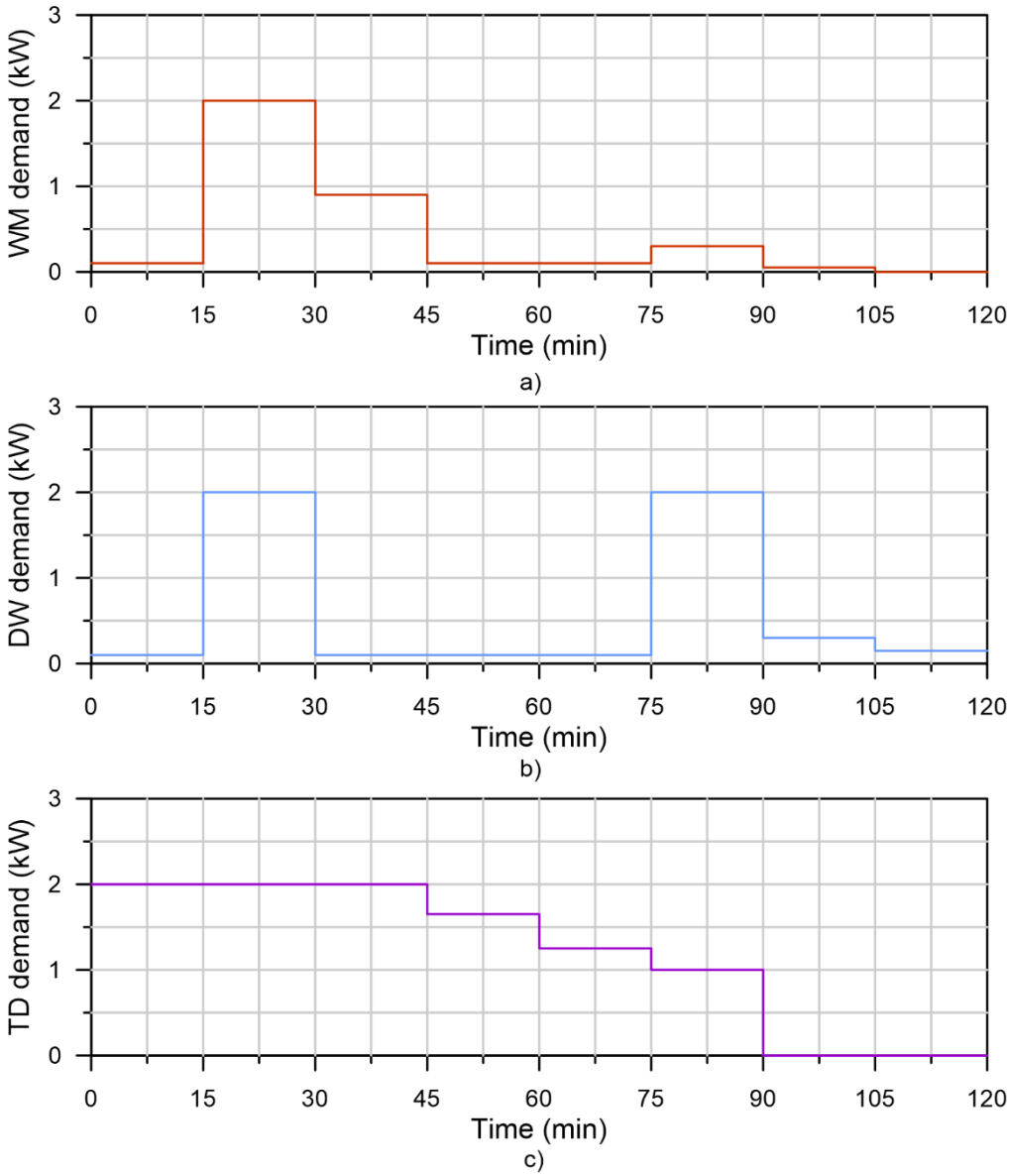

Figure 3. 5. Smart appliances models employed in the optimization: a) Washing machine demand, b) dishwasher demand, and c) tumble drier demand.

Table 3. 1. Main parameters of the model.

Subsystem	Parameter	Value	Subsystem	Parameter	Value
Main grid	P_g^{max}	4.6 kW	EWH	C_{wh}	0.1 m^3
ESS	P_{ess}^{max}	2 kW		g_{wh}	$2 \cdot 10^{-3}$ kW/℃
	C_{ess}	6 kWh		T_{inlet}	21 ℃
	dP_{ess}^{max}	0.5 kW/h		T_{wh}^{min}	60 ℃
	SOC^{min}	35%		T_{wh}^{max}	85 ℃
	SOC^{max}	65%		$T_{wh}(0)$	65 ℃
	$SOC(0)$	50%		P_{nwh}	2 kW
PV	P_{pv}^{pk}	2 kW		C_p	4.18 kJ/kg· ℃
	η_{pv}	90%		ρ	988 kg/m^3
	α	30°			
	λ	37.88°			
	ϕ	−4.79°			

Figure 3. 6 introduces the first case in which tariff A with both scheduling mode (variable and fixed) have been used, depicting a 24-hour horizon. Particularly, in this case, the scheduling configuration for the SA has been set as follows: Washing machine scheduled from 09:00 to 14:00, tumble dryer scheduled from 16:00 to 21:00 and dishwasher fixed at 14:00.

Note from Figure 3. 6 a) the result of the scheduling process and the times at which the SA start their operation cycles. As it is apparent from $P_{sa}(t)$, which is the decoupled consumption of all the SA scheduled in either fixed or variable mode, the washing machine starts almost at midday (at 11:45), around the peak of the prices although a large amount of this demand is covered by the PV system. The dishwasher at 14:00 (as was stated) and tumble drier is shifted until 18:00 where the second valley of the price can be found. This behavior shows a clear strategy of searching for the lowest price or the highest PV production to launch these SA. In view of the results, all the initial constraints related to the scheduling period are clearly satisfied.

The non-shiftable consumption is denoted by the red line of the same figure including the fixed consumption of the dishwasher at 14:00 and the experimentally measured example in which the period of highest activity falls in the range 09:00–18:00 according to the laboratory timetables. The green line shows the power injected into the system from the PV panels, which represents 9.78 kWh, and has not the same value that the PV production shown in orange (10.65 kWh) and provided by solcast. In this case, the system does not use all the energy to achieve the most economical way, however, the amount of this one taken from the main grid is greater than if the PV energy were fully employed.

Figure 3. 6 b) depicts the EWH behavior using the above-mentioned hot water demand (expressed in L/h instead of m3/s for easier comprehension) and the hourly temperature profile provided by dark sky (see purple and blue lines respectively). The EWH consumption shown in orange evolves in the range 0–2 kW due to it's on/off operation. Before 12:00, the water temperature is more or less constant and the power consumption behaves in agreement to the water consumption so that a water demand variation causes a proportional energy consumption, which means this energy is mainly used to warm the inlet water. In fact, the highest energy consumption in this interval takes place at the peak of water demand. On the contrary, at midday, the water consumption is not significative and thus, this energy is intended to increase the water temperature inside the tank from 60 ℃ to 83 ℃, considering multiple favorable conditions such as the greater availability of energy coming from the PV system, the high ambient temperature as well as the amount of charge already stored in the ESS. This temperature increment enables to face the future water drawn acts, which is a desirable strategy in response to DR events as it is the presence of high market prices in this interval. Later, the temperature slowly falls up to 60 ℃ at 20:00 due to the water consumption and remains constant the rest of the day.

The ESS shows a clear policy based on the energy price (red line in Figure 3. 6 d) and PV production. The initial SOC was set to 50% and quickly decreases to supply the non-shiftable power until 02:00 reaching almost 39% in a high-priced environment. Afterward, the off-peak of the prices can be found and $P_{ess}(t)$ go up as fast as possible (due to the slope of $P_{ess}(t)$ matches to dP_{ess}^{max}) to retrieve some charge previously lost, which is equivalent to shift the amount of energy that belongs to $P_{ns}(t)$, from the beginning of the day to the off-peak interval. During this interval $P_{ns}(t)$ is supplied by means of the main grid. At 04:30 the SOC drops again to repeat the same process with $P_{ns}(t)$ and reaches the minimum value allowed (35%) at 08:00. Once here, the PV system begins to inject power that goes directly to the ESS resulting in a charging process that carries the SOC from 35% to 65% to address the SA consumption with the help of $P_{pv}(t)$ during the most expensive interval (12:00–15:00). The rest of time follows the same principle as explained above: Charge process in

presence of the second off-peak of the price (15:00–17:30) and subsequent discharge to supply both the tumble drier and the non-shiftable power (17:30–00:00).

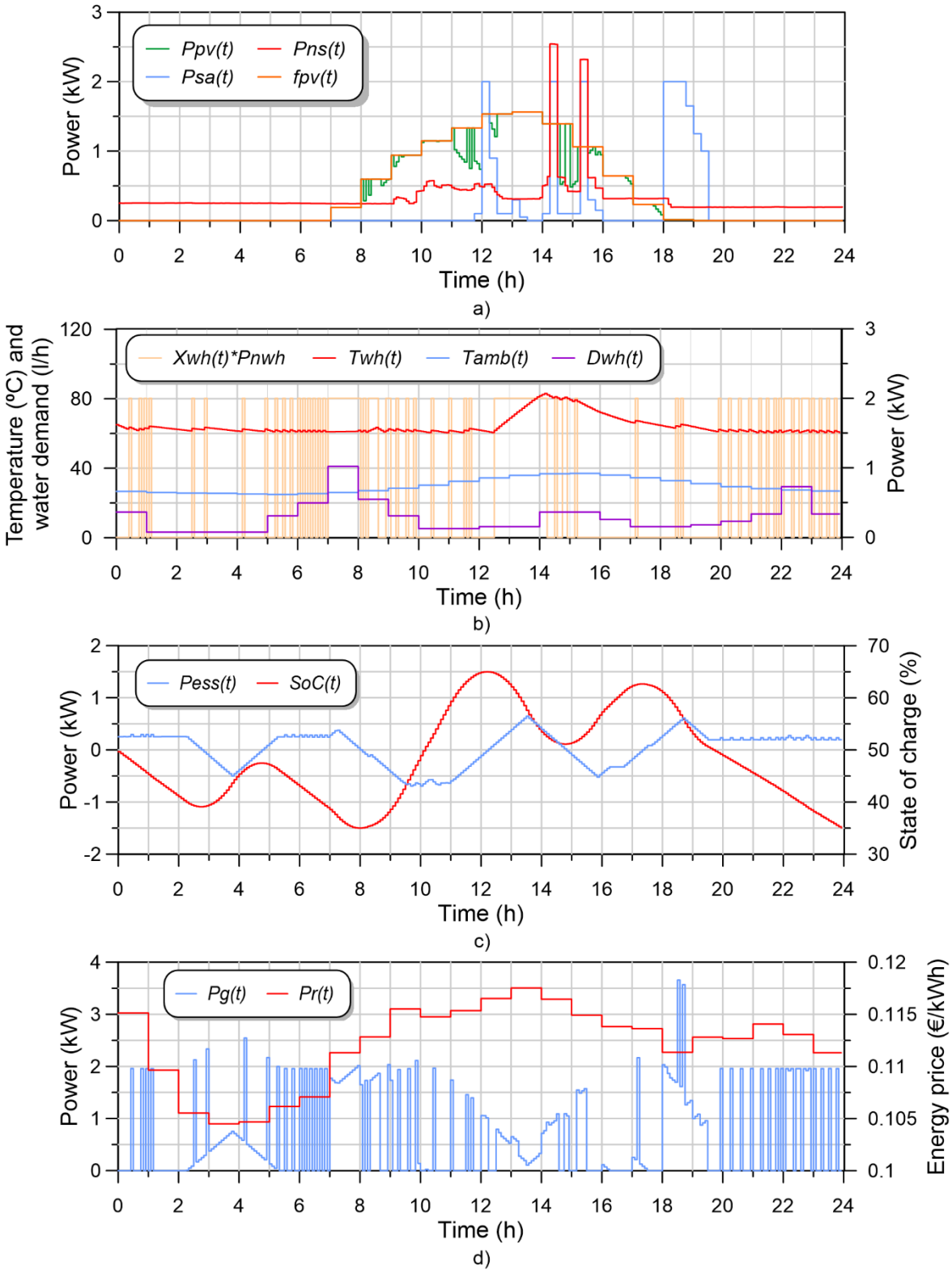

Figure 3. 6. Optimization results using tariff A: a) Power injected by the PV system, smart appliances consumption, non-shiftable consumption, and PV production, b) Electric water heater performance: Consumption, ambient and water temperature as well as hot water demand, c) energy storage system performance: Power and state of charge, and d) total consumption from the utility and energy prices.

The total energy exported and imported by the system was 3.89 and 3.00 kWh respectively. Another important detail is the effect of dP_{ess}^{max} over $P_g(t)$: Previous tests were done with a more relaxed value prove that a larger amount of the EWH energy can be absorbed by ESS as this would enable better tracking of demands with higher ratios of change. Finally, in Figure 3. 6 d) the hourly prices and the main grid consumption can be found. The foregoing description of this case is also reflected in $P_g(t)$ and makes it possible the main objective of avoiding and capitalizing the peak and off-peak of $Pr(t)$ respectively. The daily price for this case was 1.80 € with a total demand of energy that almost achieves 16.10 kWh.

For the following case, the configuration for the SA has been set as follows: Washing machine fixed at 10:00, tumble dryer scheduled from 12:00 to 20:00 and dishwasher scheduled from 14:00 to 19:00.

Figure 3. 7 a) (blue line) shows how the model has decided to launch the dishwasher and tumble drier at the lower limit of the scheduling period which allows the system benefits from the PV production (depicted in orange and kept constant from the previous case) and the ESS that also supplies part of this consumption, especially after 13:00, where the prices are much higher than in the previous half. The washing machine operates at 10:00 as expected. The PV production is not fully intended to be injected into the system (just 9.96 of 10.65 kWh) as is evidenced by $P_{pv}(t)$, in green, and which also took place in the case above. With respect to the non-shiftable demand, the previous part corresponding to the stand-by consumption has been used, including the demand of the washing machine at 10:00.

Both the ESS and EWH have similar behaviors with respect to the previous case but with some exceptions. Figure 3. 7 b) shows the performance of the EWH under the same assumptions as of the first case (water demand, ambient temperature, water temperature limits, and initial conditions) although the temperature increment begins one hour earlier and is more progressive. Furthermore, the temperature rises at one of the peaks of the water demand while the water was warmed up before this maximum in the first case. The ESS also performs similar, which evidences the PV production has a higher weight in its behavior than the energy price. Moreover, with respect to $Pr(t)$, it is more important the shape of the function, concretely the maxima and minima location, than the absolute values. The energy exported and imported in this case reaches 3.45 and 2.55 kWh. Finally, Figure 3. 7 d) introduces the prices, that splits the day in two well-defined half, and the consumption from the main grid where the most consumption is located in the cheapest region as desired and entails an amount of 15.75 kWh (11.8 kWh from 23:00 to 13:00 compared to 3.95 kWh the rest of time). The daily price was 1.30 €.

Once these previous cases have been presented, Table 3. 2 summarizes the results. Obviously, case 2 achieves a better performance with respect to the objective function and thus, tariff DHA enables to more efficient utilization of elements such as DER and ESS in presence of thermal loads that contribute to the flexibility of the system as in this case the EWH.

Table 3. 2. Result summary.

	ESS		**PV**		**Main Grid**	
Case	Imported energy (kWh)	Exported energy (kWh)	Injected energy (kWh)	Energy production (kWh)	Energy imported (kWh)	Objective function: Price (€)
Case 1: Tariff A	3.00	3.89	9.78	10.65	16.10	1.80
Case 2: Tariff DHA	2.55	3.45	9.96	10.65	15.75	1.30

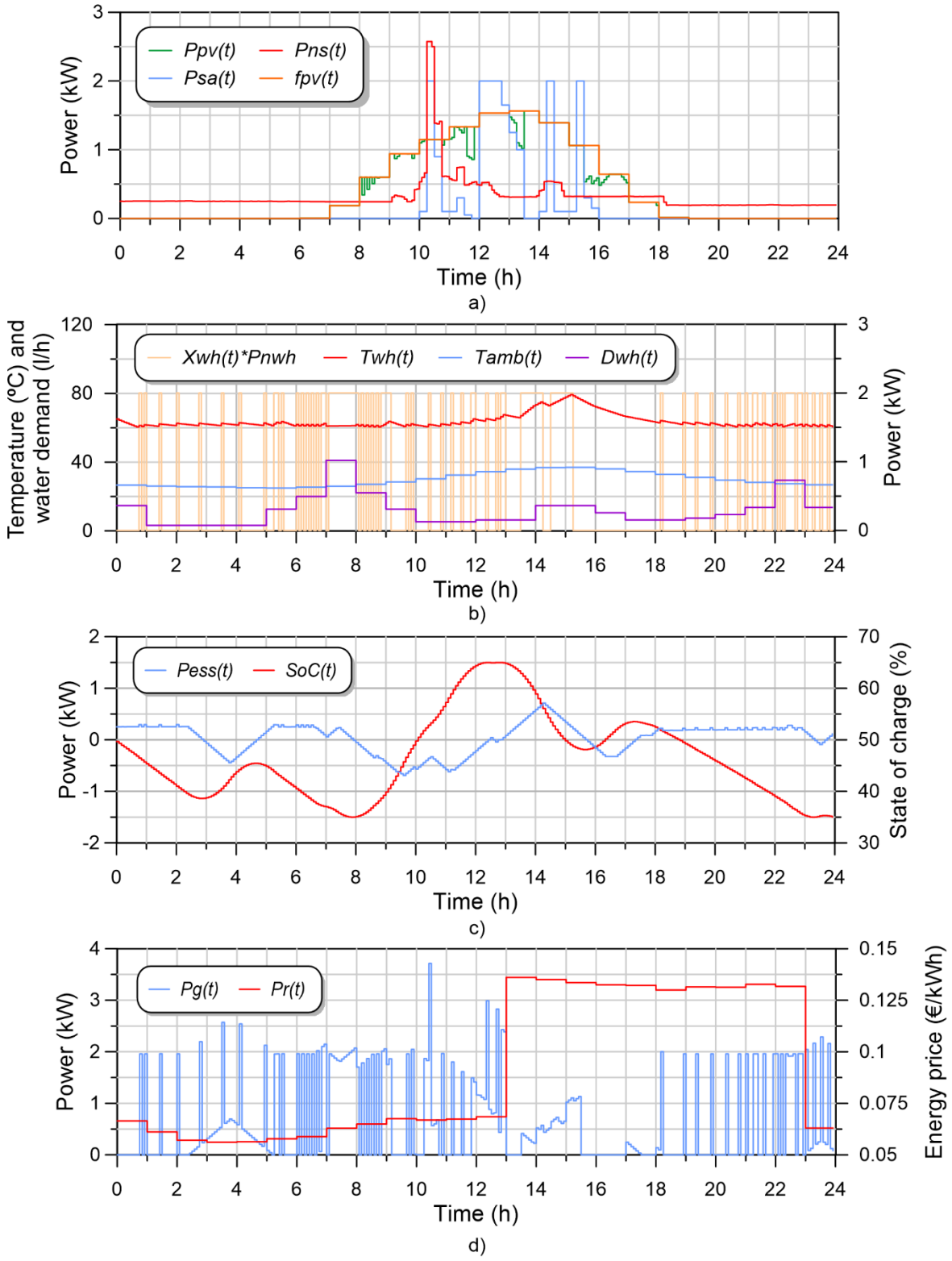

Figure 3. 7. Optimization results using tariff DHA: a) Power injected by the PV system, smart appliances consumption, non-shiftable consumption, and PV production, b) Electric water heater performance: Consumption, ambient and water temperature as well as hot water demand, c) ESS performance: Power and state of charge and d) total consumption from the utility and energy prices.

3.6. Conclusions and future work

In the current context of increasing energy use in the residential environment, where most consumption comes from the SA use, the employment of DR policies is essential to deal with this type of loads through a DLC paradigm with the goal of reaching higher efficient management of the energy resources. This paper has proposed an original architecture that supports research and development and integrates tools that are very diverse and complementary aiming to develop a platform that brings together the best features of all of them, such as the high mathematical performance of GAMS, the accuracy of the weather forecasting applications as well as the flexibility of LabVIEW as the linking tool. Later both cases studies have been carried out to prove the high capabilities of the testbed with successful results, placing the adopted solution as an attractive alternative towards a higher energy performance dwelling ambient.

Finally, as future work, the authors leave the real-time control of the DER, ESS, and loads in the primary and secondary control of a real MG. In this context, the developed platform would perform as a day-ahead demand scheduler in the tertiary control although additional communication channels would need to be deployed to enable the interface with the lower hierarchical level. Furthermore, the mathematical model written in GAMS and thus the developed DLL would also have to be adapted to the MG needs, however, due to the reconfigurable nature of the system, this would not take more than a few minutes. Hence, this platform could be migrated to be used in a real microgrid expecting the same performance, but these considerations must be deemed.

Acknowledgements

This research was supported by the Spanish Ministry of Economy and Competitiveness under Project TEC2016-77632-C3-2-R. The IMPROVEMENT project (Interreg SUDOE SOE3/P3/E0901) is acknowledged for partially funding this work.

References

[1] Amasyali, K.; El-Gohary, N.M. A review of data-driven building energy consumption prediction studies. Renew. Sustain. Energy Rev. 2018, vol. 81, pp. 1192–1205, doi: 10.1016/j.rser.2017.04.095.

[2] Alonso-Rosa, M.; Gil-de-Castro, A.; Medina-Gracia, R.; Moreno-Munoz, A.; Cañete-Carmona, E. Novel Internet of Things Platform for In-Building Power Quality Submetering. Appl. Sci. 2018, vol. 8, pp. 1320, doi: 10.3390/app8081320.

[3] Appliances and equipment Tracking Clean Energy Progress Available online: https://www.iea.org/reports/tracking-buildings/appliances-and-equipment / (accessed on 16 Janurary 2019).

[4] dSPACE Electrical Power Systems Simulation Package. Available online: https://www.dspace.com/en/inc/home/products/sw/impsw/epc-sim-pack.cfm (accessed on 22 April 2019).

[5] Typhoon HIL, Hardware in the Loop Testing Software and Hardware Available online: https://www.typhoon-hil.com/ (accessed on 22 April 2019).

[6] I.M. Moreno-Garcia, A. Moreno-Munoz, V. Pallares-Lopez, M.J. Gonzalez-Redondo, E.J. Palacios-Garcia, C.D. Moreno-Moreno. Development and application of a smart grid test bench. J. Clean. Prod. 2017, vol 162, pp. 45–60, doi: 10.1016/j.jclepro.2017.06.001.

[7] L. Barbierato et al., "A Distributed IoT Infrastructure to Test and Deploy Real-Time Demand Response in Smart Grids," in IEEE Internet of Things Journal, vol. 6, no. 1, pp. 1136-1146, Feb. 2019, doi: 10.1109/JIOT.2018.2867511.

[8] M. Thornton, M. Motalleb, H. Smidt, J. Branigan, P. Siano and R. Ghorbani, "Internet-of-Things Hardware-in-the-Loop Simulation Architecture for Providing Frequency Regulation With Demand Response," in IEEE Transactions on Industrial Informatics, vol. 14, no. 11, pp. 5020-5028, Nov. 2018, doi: 10.1109/TII.2017.2782885.

[9] M. Thornton, M. Motalleb, H. Smidt, J. Branigan, J. Ghorbani. Demo abstract: testbed for distributed demand response devices—internet of things. Comput. Sci. Dev. 2018, vol. 33, pp. 277–278, doi: 10.1007/s00450-017-0378-z.

[10] G.M. Shafiullah, M.T. Oo Amanullah, A.B.M. Shawkat Ali, P. Wolfs. Potential challenges of integrating large-scale wind energy into the power grid—A review. Renew. Sustain. Energy Rev. 2013, vol. 20, pp. 306–321, doi: 10.1016/j.rser.2012.11.057.

[11] H. Shareef, M. S. Ahmed, A. Mohamed, and E. Al Hassan, "Review on Home Energy Management System Considering Demand Responses, Smart Technologies, and Intelligent Controllers," in IEEE Access, vol. 6, pp. 24498-24509, 2018, doi: 10.1109/ACCESS.2018.2831917.

[12] B. Zhou, W. Li, K.W. Chan, Y. Cao, Y. Kuang, X. Liu, and X. Wang. Smart home energy management systems: Concept, configurations, and scheduling strategies. Renew. Sustain. Energy Rev. 2016, vol. 61, pp. 30–40, doi: 10.1016/j.rser.2016.03.047.

[13] S. Zhou, and M.A. Brown. Smart meter deployment in Europe: A comparative case study on the impacts of national policy schemes. J. Clean. Prod. 2017, vol. 144, pp. 22–32, doi: 10.1016/j.jclepro.2016.12.031.

[14] I. Abubakar, S.N. Khalid, M.W. Mustafa, H. Shareef, and M. Mustapha. Application of load monitoring in appliances' energy management—A review. Renew. Sustain. Energy Rev. 2017, vol. 67, pp. 235–245, doi: 10.1016/j.rser.2016.09.064.

[15] F. Babonneau, M. Caramanis, and A. Haurie. A linear programming model for power distribution with demand response and variable renewable energy. Appl. Energy 2016, vol. 181, pp. 83–95, doi: 10.1016/j.apenergy.2016.08.028.

[16] M. Killian, M. Zauner, and M. Kozek. Comprehensive smart home energy management system using mixed-integer quadratic-programming. Appl. Energy 2018, vol. 222, pp. 662–672, doi: 10.1016/j.apenergy.2018.03.179.

[17] G. Graditi, M. L. Di Silvestre, R. Gallea and E. Riva Sanseverino, "Heuristic-Based Shiftable Loads Optimal Management in Smart Micro-Grids," in *IEEE Transactions on* Industrial Informatics, vol. 11, no. 1, pp. 271-280, Feb. 2015, doi: 10.1109/TII.2014.2331000.

[18] M.A.F. Ghazvini, J. Soares, N. Horta, R. Neves, R. Castro, and Z. Vale. A multi-objective model for scheduling of short-term incentive-based demand response programs offered by electricity retailers. Appl. Energy, vol. 151, pp. 102–118, 2015, doi: 10.1016/j.apenergy.2015.04.067.

[19] A. Jindal, N. Kumar, and M. Singh. Internet of energy-based demand response management scheme for smart homes and PHEVs using SVM. Futur. Gener. Comput. Syst. Elsevier, vol. 108, pp. 1058-1068, 2020, doi: 10.1016/j.future.2018.04.003.

[20] M. Beaudin, and H. Zareipour. Home energy management systems: A review of modelling and complexity. Renew. Sustain. Energy Rev. 2015, vol. 45, pp. 318–335, doi: 10.1016/j.rser.2015.01.046.

[21] *Smart Appliances. Government Response to Consultation on Proposals regarding Smart Appliances*. Department for Business, Industrial Strategy. The consultation and Impact Assessmentcan be found on the BEISsection of GOV.UK. 2018. Available online: https://assets.publishing.service.gov.uk/government/uploads/system/uploads/attachment_data/file/748115/smart-appliances-consultation-government-response.pdf (accessed on 28/08/2019)

[22] Bertoldi, P.; Serrenho, T. Smart appliances and smart homes: recent progresses in the EU. Energy Effic. Domest. Appliances Light. In Proceedinds of the 9th international conference on Energy Efficiency in Domestic Appliances and Lighting, Irvine, CA, USA, 2017; pp. 970.

[23] Ectors, D.; Gerard, H.; Rivero, E.; Vanthournout, K.; Verbeeck, J.; Virag Viegand Maagøe, A.A.; Huang, B.; Viegand, J. Preparatory study on Smart Appliances (Lot 33) Task 7-Policy and Scenario analysis. Available online: https://eco-smartappliances.eu/sites/ecosmartappliances/files/downloads/Task_7_draft_20170914.pdf (accessed on 28/08/2019)

[24] techUK. State of the Connected Home 2018. Available online: https://www.techuk.org/insights/news/item/13914-connected-home-device-ownership-up-but-consumers-remain-sceptical (accessed on 28/08/2019)

[25] Šajn, N. Briefing Smart appliances and the electrical system *; 2016. Available online: http://www.europarl.europa.eu/RegData/etudes/BRIE/2016/595859/EPRS_BRI(2016)595859_EN.pdf (accessed on 28/08/2019)

[26] Martin, C., Starace, F., & Tricoire, J. P.. The Future of Electricity New Technologies Transforming the Grid Edge; World Economic Forum: Cologny, Switzerland, 2017.

[27] A. Fensel, D.K. Tomic, and A. Koller. Contributing to appliances' energy efficiency with Internet of Things, smart data, and user engagement. Futur. Gener. Comput. Syst. 2017, vol. 76, pp. 329–338, doi: 10.1016/j.future.2016.11.026.

[28] ETSI. TS 103 264 - V2.1.1 - SmartM2M; Smart Appliances; Reference Ontology and oneM2M Mapping; 2017. Available online: https://www.etsi.org/deliver/etsi_ts/103200_103299/103264/02.01.01_60/ts_103264v020101p.pdf (accessed on 28/08/2019)

[29] ETSI. TS 103 410-1 V1.1.1 SmartM2M; Smart Appliances Extension to SAREF; Part 1: Energy Domain; 2017. Available online: https://www.etsi.org/deliver/etsi_ts/103400_103499/10341001/01.01.01_60/ts_10341001v010101p.pdf (accessed on 28/08/2019)

[30] Electricity aggregators: starting off on the right foot with consumers. Available online: https://www.beuc.eu/publications/beuc-x-2018-010_electricity_aggregators_starting_off_on_the_right_foot_with_consumers.pdf (accessed on 28/08/2019)

[31] E.J. Palacios-Garcia, A. Chen, I. Santiago, F.J. Bellido-Outeiriño, J.M. Flores-Arias, and A. Moreno-Munoz. Stochastic model for lighting's electricity consumption in the residential sector. Impact of energy saving actions. Energy Build. 2015, vol. 89, pp. 245–259, doi: 10.1016/j.enbuild.2014.12.028.

[32] E.J. Palacios-García, A. Moreno-Munoz, I. Santiago, J.M. Flores-Arias, F.J. Bellido-Outeiriño, and I.M. Moreno-Garcia. Modeling human activity in Spain for different economic sectors: The potential link between occupancy and energy usage. J. Clean. Prod. 2018, vol. 183, pp. 1093–1109, doi: 10.1016/j.jclepro.2018.02.049.

[33] A. Kleidaras, A.E. Kiprakis, and J.S. Thompson. Human in the loop heterogeneous modelling of thermostatically controlled loads for demand side management studies. Energy, vol. 145, pp. 754–769, 2018, doi: 10.1016/j.energy.2017.12.120.

[34] E.J. Palacios-Garcia, A. Moreno-Munoz, I. Santiago, J.M. Flores-Arias, F.J. Bellido-Outeirino, and I.M. Moreno-Garcia. A stochastic modelling and simulation approach to heating and cooling electricity consumption in the residential sector. Energy, vol. 144, pp. 1080–1091, 2018, doi: 10.1016/j.energy.2017.12.082.

[35] P. Kohlhepp, H. Harb, H. Wolisz, S. Waczowicz, D. Müller, and V. Hagenmeyer. Large-scale grid integration of residential thermal energy storages as demand-side flexibility resource: A review of international field studies. Renew. Sustain. Energy Rev, vol. 101, pp. 527–547, 2019, doi: 10.1016/j.rser.2018.09.045.

[36] Detailed data with the Simple Radiation API Tool Available online: https://solcast.com.au/solar-data-api/api/solar-radiation-data/ (accessed on 13 March 2019).

[37] Dark Sky API: Documentation Overview Available online: https://darksky.net/dev/docs (accessed on 13 March 2019).

[38] API esios Documentation Available online: https://api.esios.ree.es/ (accessed on 13 March 2019).

[39] P. Wimmer, C. Kandler, and J. Honold. Potential of demand and production shifting in residential buildings by using home energy management systems. Build. Simul. 2015. Available online: http://www.ibpsa.org/proceedings/BS2015/p2821.pdf (accessed on 28/08/2019)

[40] A. C. Luna, L. Meng, N. L. Diaz, M. Graells, J. C. Vasquez and J. M. Guerrero, "Online Energy Management Systems for Microgrids: Experimental Validation and Assessment Framework," in IEEE Transactions on Power Electronics, vol. 33, no. 3, pp. 2201-2215, March 2018, doi: 10.1109/TPEL.2017.2700083.

[41] GAMS Application Programming Interfaces. Available online: https://www.gams.com/latest/docs/API_MAIN.html (accessed on 13 March 2019).

[42] Bilton, M.; Aunedi, M.; Woolf, M.; Strbac, G. Smart appliances for residential demand response (Report A10, for the Low Carbon London, LCNF project). Imp. Coll. London 2014. Available online: https://pdfs.semanticscholar.org/e3b8/ebf700ca1317b98dca21f04bd1e3629288b7.pdf (accessed on 28/08/2019)

[43] IDEA. Guía Técnica Agua Caliente Sanitaria Central. Available online: https://www.idae.es/uploads/documentos/documentos_08_Guia_tecnica_agua_caliente_sanitaria_central_906c75b2.pdf (accessed on 28/08/2019)

[44] Heating, A.S. of; Refrigerating; Engineers, A.-C. ASHRAE handbook: HVAC applications; American Society of Heating, Refrigerating and Air Conditioning Engineers; American Society of Heating, Refrigerating and Air-Conditioning Engineers: Atlanta, GA, USA, 2007, ISBN 1078-6074.

Chapter 4

Load scheduling strategy to improve power quality in electric-boosted glass furnaces

Joaquin Garrido-Zafra[1], Aurora Gil-de-Castro[1], Rafael Savariego-Fernandez[1], Matias Linan-Reyes[1], Felix Garcia-Torres[2] and Antonio Moreno-Muñoz[1]

[1]Departamento de Ingeniería Electrónica y de computadores, Escuela politécnica superior, Universidad de Córdoba, Córdoba, Spain

[2]Departamento de Ingeniería Eléctrica y Automática, Escuela politécnica superior, Universidad de Córdoba, Córdoba, Spain

Abstract

In glass furnace boosting, particularly in the tin bath and annealing Lehr heating systems, an AC-AC power converter is normally employed by the industry. This Triac-based converter driven by integral cycle control (ICC) is employed to provide highly accurate power to the resistive heating elements distributed into the furnace. The advantages of ICC include low inrush current and increased reliability; although its impact on power quality (PQ), due to the subharmonic distortion produced, is significant. While different strategies for energy demand management have been implemented to date, they have not adequately addressed this PQ issue. Thus, the goal of this research is to establish an optimal electrical load scheduling strategy considering criteria about PQ and thermal behavior through a mixed-binary quadratic programming (MBQP) problem which exploits the ICC advantages avoiding PQ degradation.

4.1. Introduction

The glass industry is a well-established industry that manufactures a wide variety of products, including food and beverage containers, fiberglass insulation, windows for cars and buildings, video screens, kitchen utensils, and light bulbs. Glass production can be divided into six primary sectors: container glass, flat glass, domestic glass, special glass, continuous filament fiberglass, and insulating glass wool. Although the diversity of glass products, with different properties and characteristics, involves different manufacturing processes, practically all glass plants provide for five basic steps: (a) raw material selection, (b) batch preparation (i.e. weighing and mixing), (c) melting and refining, (d) conditioning and forming (e.g. in a flotation bath) and (e) post-treatment (i.e. annealing, tempering, coating, drilled or polished). The glass industry relies on electricity and natural gas to meet most of its energy needs. Glass melting consumes most of the energy of all production processes, and is done using natural gas, a combination of natural gas and electricity (electric boosting), or all electricity[1], although other alternatives are also being proposed[2]. Each glass sector has its specificity and manufacturing process, but the glass melting process is common to all-glass sectors. This physical process involves raw materials, energy, and state-of-the-art manufacturing facilities. As a result, the glass industries have an excellent track record in reducing energy needs and the associated CO_2. Thus, in recent decades, the energy intensity of glass manufacturing was reduced by 77% and CO_2 emissions by 50%, even as production increased[3]. Continued efforts in process innovation are essential to increase reduction in energy consumption. Future trends for the glass sector are still unclear, but, increasingly, fossil fuel-based furnaces are boosted electrically. The electric furnaces are built as a box-shaped container lined with refractory materials. Electrodes are inserted from the top or bottom of the furnace and energy is supplied by resistance heating while the current flows through the molten glass. The raw materials are usually fed in a layer at the top of the bath so that they slowly melt inside. The thermal efficiency of electric furnaces is two to three times higher than that of fossil fuel-fired furnaces. This recent paper [4] discusses the opportunities and limitations of all-electric melting furnaces to produce glass containers. Such innovation would not only benefit the glass industries themselves but for all downstream industries and help ensure a smooth transition to a low-carbon economy.

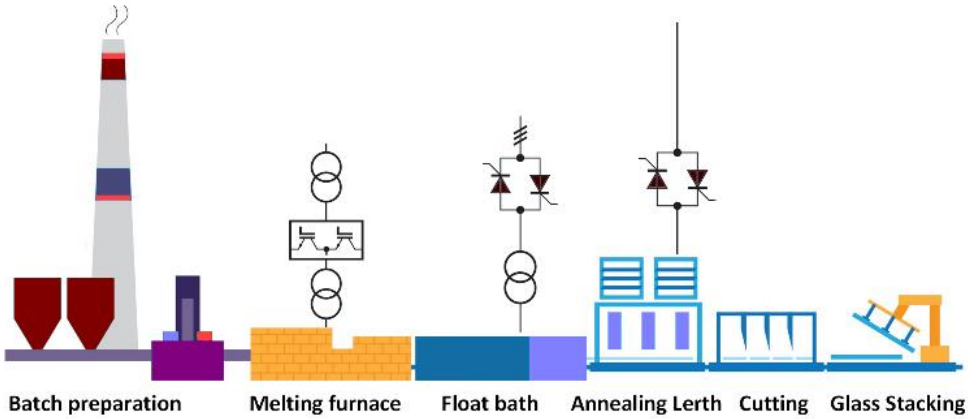

Figure 4. 1. Glass pane melting process.

4.2. State of the art review

One of the most representative examples of this industry, and where our research could be applied with great advantages, is float glass manufacturing. The float glass process, invented by Sir Alastair Pilkington in 1952 [5], allows the manufacture of clear, tinted and coated glass for buildings, and clear and tinted glass for vehicles. The basic physics of the continuously operating fuel-fired furnaces supplemented with electric boosting is analyzed

in [6] This paper aims to provide glass manufacturers with a tool to monitor, compare, and optimize furnace performance through retrospective analysis of daily production data, as well as to provide guidelines for furnace construction. The integrated glass furnace model of combustion space and glass tank is established in [7] to analyze the float glass melting at the furnaces with or without electric boosting. It has been found that with the optimal design of the electric boosting system, better glass melting quality, more homogenization, and increased melting efficiency would be achieved. The paper [8] [simulates float glass furnaces with a higher melting capacity by increasing the fuel supply and including electric boosting. The temperature distribution, heat flow from the combustion chamber to the glass tank, and the flow patterns of the glass are evaluated. As shown in Figure 4. 1, while electrical heating systems found in glass furnace boosting can employ other power converters, in a *tin bath* and *annealing lehr heating systems* a triac-based AC-AC voltage converter is normally employed. The triac is made up of two antiparallel connected thyristors, allowing a bidirectional current. In [9] figures 5 and 6 show typical schematic diagrams employed. In these figures, each AC-AC converter may be directly coupled through an electrode pair to glass loads at voltages of 1000 V or less or coupled by a transformer to supply voltages of 600 V or less, typically providing around 400 kVA to the furnace. This converter is used to provide continuous phase-angle control of voltages to the glass load or the primary of a transformer connected to the glass load. It may also supply time-proportioned bursts of full cycles of the supply voltage (also called on/off control, zero-crossing control mode, or integral cycle control, ICC) to resistance heaters supplying radiant heat to the glass. Besides this full-wave ICC, there are other complementary control methods like half-wave control, soft-starts, and soft-downs.

The phase-angle controller produces low-order integer harmonics, and heavy inrush currents while switching on in a cold start. In contrast, the advantages of the ICC include low inrush current and increased reliability (as the device is switched on at zero voltage and current), easy construction, and low hardware cost. However, they produce frequencies which are non-integer multiple and below the fundamental of the mains under consideration, so-called subharmonics. Undoubtedly the main disadvantage of the ICC furnaces regarding the impact on power quality (PQ) is subharmonics [10]. This impact can become more severe in multiple triac-controlled applications such as *tin bath heating* or *annealing lehr* when driving numerous heating electrodes distributed over multiple heating zones. These systems can easily contain more than 40 zones running at different power levels and variable set points. Moreover, if not properly supervised, this may lead to large uncontrolled peaks of power.

The harmonics and interharmonics of a waveform can be mathematically defined in terms of spectral components in a quasi-steady state over a range of frequencies. Harmonics are spectral components at an integer multiple frequencies of the system fundamental frequency, and interharmonics at frequencies that are not integer multiple. However, subharmonics belong to a special class of interharmonics where frequency components in voltage and current waveforms are less than power system frequency [11]. IEC 61000-4-7 and other PQ international standards define methods to measure harmonics and interharmonics in power systems, but at present, there is neither an official definition of this concept nor a standard method to measure subharmonics. The main problem is that the frequency range up to 100 Hz remains very sensitive to spectral leakage problems caused by an also small error in synchronization [12].

Compared to harmonics and interharmonics, subharmonics present a much more serious problem in practice as they cannot readily be filtered. Further, they are responsible for an excessive flow of subharmonic current causing e.g. a low frequency pulsating torque in motor drives. Some of the most significant effects of power system subharmonics on

lighting systems, transformers, induction motors, and turbogenerators are reported in [10]. The PQ impact of different switching strategies of ICC has been studied in detail in [13]. As in other applications, when it comes to further reducing harmonic distortion, techniques based on the PWM AC chopper controller can be used [14][15][16], this choice has been accomplished in [17]. However, the most important suppliers of automation and process control for the thermal treatment industry have preferred to innovate by taking advantage of the distributed characteristics of the heating process itself and the maturity of the ICC, thus adopting a "divide and conquer" strategy [18][19]. So, instead of choosing a local and independent controller for each heating element, a coordinated supervisory control with load balancing and shedding functionality was adopted in [20] and improved in [21]. Definitively, they have applied a heuristic strategy of energy demand management through shaving peaks[22][23] but they have not addressed particularly the PQ issue, nor the subharmonic content.

Thus, against this background, the main objective of this research is to establish an optimal, and scientifically justified strategy, through a mixed-binary quadratic programming (MBQP) problem. While similar approaches like mixed-integer nonlinear programming formulations have been used for the optimization of other energy applications [24], to our knowledge, it has never been used in the industry of glass melting to achieve a PQ improvement, especially in the subharmonic content. This paper is a thorough revision of the previous conference paper [25], as the section materials and methods has been updated, including the mathematical background and a detailed formulation of the problem, as well as an extension of the thermal considerations. Additionally, the results section has been unfolded in two new case studies. The remainder of the paper is organized as follows: Section II is devoted to materials and methods, including the mathematical background, the thermal considerations, the problem formulation as well as the description of the hardware implemented. Results are included in Section III and Section IV puts forward several conclusions.

4.3. Materials and methods

4.3.1. Laboratory setup

Figure 4. 2 shows the scenario where the tests were carried out. To measure the current waveform and analyze its power profile and frequency emissions, a Pearson current probe model 411 was used. This current probe has a transfer ratio of 100 mV/A with a higher 3 dB cut-off frequency at 20 MHz and the low cut-off at 1 Hz. The instrument used to acquire and store these measurements was the 12-bit resolution Yokogawa DL50E oscilloscope and data-logger. Moreover, the Tektronix MDO3024 oscilloscope was also used in parallel to compute the spectrum of the current as will be shown in section III. Both devices were used with 1 MS/s sampling frequency by acquiring a window length of 1 MS resulting in 1-Hz frequency resolution. The latter must always be lower than the distance between interharmonics in the Fourier analysis to be able to distinguish each of them correctly. Moreover, the Agilent E3631A DC power supply was used to provide the necessary input voltage for each power converter as well as a laptop equipped with LabVIEW where the communications with each power controller are executed. The software GAMS (General Algebraic Modeling System) linked to LabVIEW as was described in [26] has also been used to solve the optimization problem proposed in subsection B.

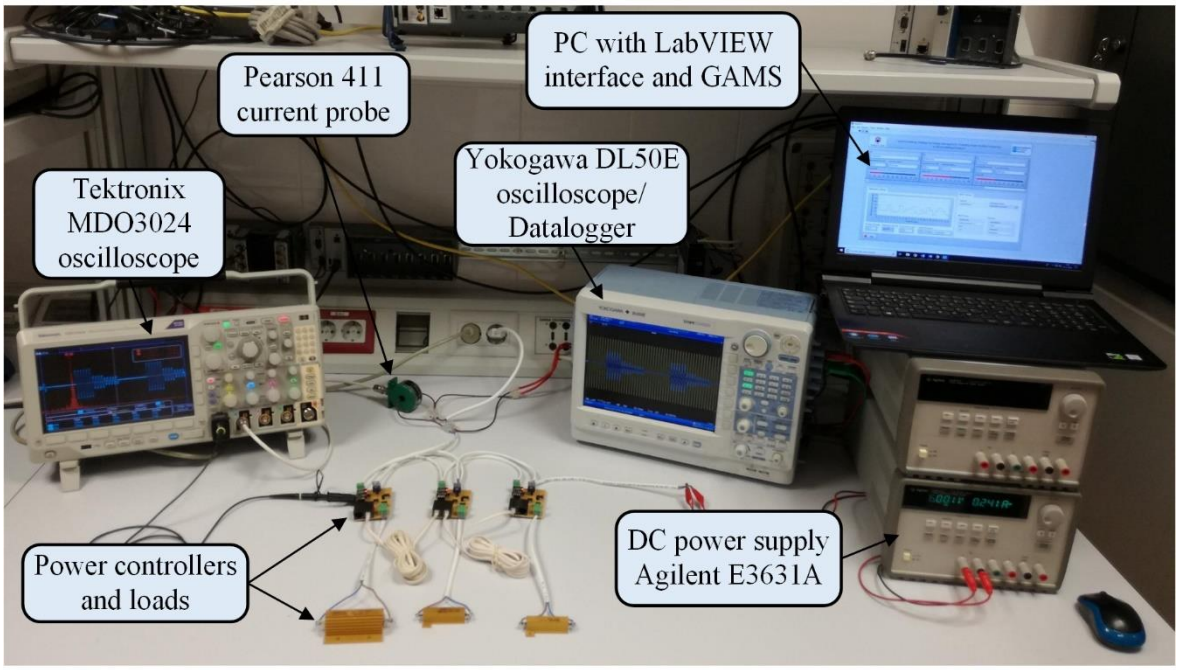

Figure 4. 2. Laboratory setup.

Finally, for laboratory testing, the prototype shown in Figure 4. 3 has been developed with several single-phase power converters based on the first of the abovementioned topologies in [9] and also [21].

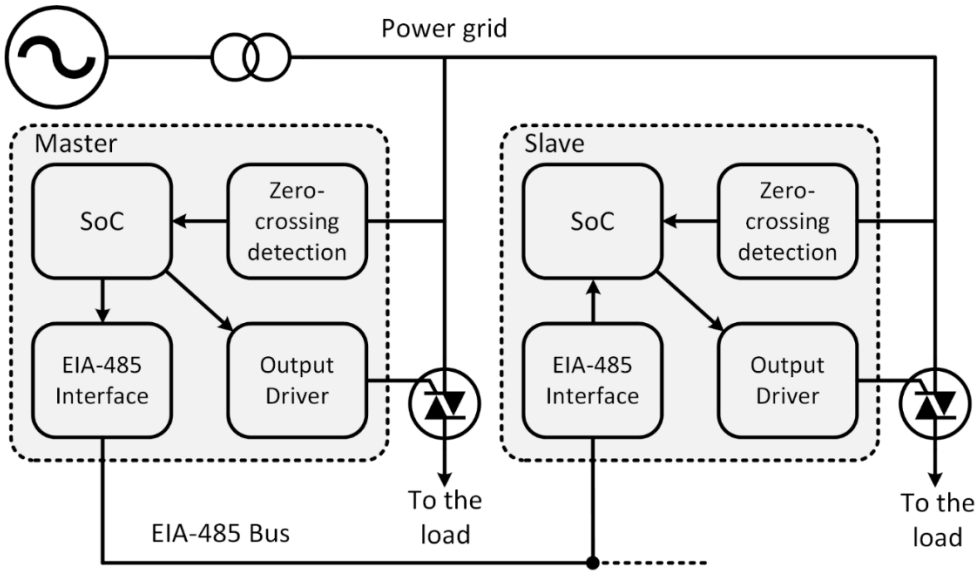

Figure 4. 3. Developed prototype.

Additionally, such devices also include an EIA-485 interface that performs synchronization tasks between the master and the slave converters and ensures that all triggering signals have a common time origin and thus, also take place within the same modulation period N. According to this protocol, the master node sends a synchronism frame in the last cycle of the modulation period to order the rest of the nodes to start a new one after receiving this message. Meanwhile, each slave is listening to the bus until a new message is received. It is important to emphasize that these prototypes detect the voltage zero crossings by using an optocoupled purpose-built circuit for synchronization whereby

the cycles along N can be easily identified by counting zero crossings. Converters also integrate the output driver that triggers the power switch.

At the same time, this group of power converters and the GAMS optimization engine linked to LabVIEW are connected through an MQTT network. In this way, each power converter behaves completely dependent on the LabVIEW client that sends to each prototype the number of cycles within the modulation period and the trigger pattern of the main power switch within N after execution.

4.3.2. Mathematical background

The mathematical formulation which supports the developed strategy from the PQ point of view is shown in this section. While the following formulation would be easily extrapolated to inductive loads, as this paper is devoted to the electric boosting, it is focused on resistive loads, which is what electrodes immersed in the molten material ultimately are.

First, as shown in Figure 4. 4, if T_c is the period corresponding to the mains supply voltage, for a full modulation period T_P, $i_p(t)$ is the current obtained when applying the ICC to a resistive load j of nominal active power P_j with the lowest energy delivery. The modulation period can also be expressed as the number of full cycles of the mains supply, N.

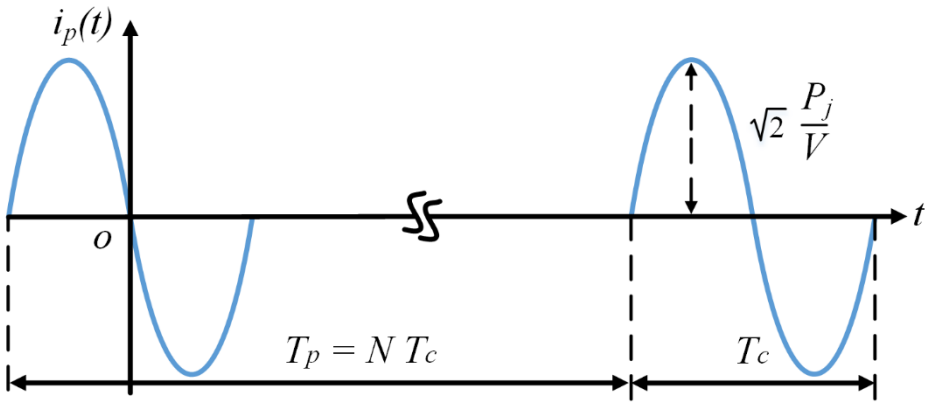

Figure 4. 4. Primitive current waveform.

As the current $i_p(t)$ corresponds to the minimum energy that can be supplied to a load j, any other $i_j(t)$ obtained by the ICC could be expressed by a finite sum of this primitive current, with different time delays, as (4. 1) shows. Where $\delta_i \in \{0, 1\}$ are logical variables that indicate the state of the main switch at each i-position. In this sense, $i_j(t)$ would be fully characterized by $i_p(t)$ and by the group of values $\delta_1 \ldots \delta_N$.

$$i_j(t) = \sum_{i=1}^{N} \delta_i \, i_p[t - (i-1)T_c] \qquad (4.\ 1)$$

Therefore, the following steps will be related to the study of $i_p(t)$. Concretely, this current will be analyzed in the frequency domain by using the Fourier series as a well-known tool for characterizing periodical waveforms. From Figure 4. 4, with the appropriate reference, $i_p(t)$ is an odd function, therefore it can be expressed just with sine terms.

$$b_h^j = \frac{4}{T_P}\int_0^{\frac{T_p}{2}} -\sqrt{2}\left(\frac{P_j}{V}\right)\sin(2\pi f t)\sin(2\pi f h t)\,dt$$

$$b_h^j = \begin{cases} \dfrac{2\sqrt{2}P_j\sin(\pi h)}{\pi NV(h^2-1)}, & h \neq 1 \\ \lim\limits_{h\to 1}\dfrac{2\sqrt{2}P_j\sin(\pi h)}{\pi NV(h^2-1)} = -\dfrac{\sqrt{2}P_j}{NV}, & h = 1 \end{cases} \quad (4.\ 2)$$

The variation of their coefficients b_h^j to the harmonic index h is a piecewise function given by (4. 2), where f is the mains frequency. This harmonic index must take integer values of $1/N$ which means that, theoretically, the spectrum of any current generated by combining several shifted primitive currents $i_p(t)$ will have only subharmonics, interharmonics and the fundamental component since the coefficients b_h^j take the value zero with integer multiples of h but the unity.

Once $i_p(t)$ is characterized in the frequency domain, $i_j(t)$ in (4. 1) could be rewritten in (4. 3) in terms of each frequency component to be $i(t)$, which includes all the loads involved in the scheduling process, L. In this regard, let us define I_h and φ_h in (4. 4) and (4. 5) as the magnitude (RMS value) of each frequency component and its phase angle respectively, as well as extend δ_i to $\delta_i^j \in \{0, 1\}$ for each load j. Moreover, I_h has been obtained regarding its vertical and horizontal components I_h^q and I_h^p as it is shown in (4. 6) and (4. 7) respectively. Note that both projections of I_h are computed considering the contribution of each load j at each position i where the angular distance $2\pi h$ refers to the angle between contiguous components. That is, if the lowest frequency component, $h = 1/N$, in the Fourier analysis is considered to have a period of 2π, its components will be spaced an angular distance of $2\pi/N$ and therefore any other whose harmonic index is h, will be spaced $2\pi h$.

$$i(t) = \sum_{h=1}^{\infty}\sqrt{2}\,I_h\sin(2\pi f h t - \varphi_h) \quad (4.\ 3)$$

$$I_h^2 = I_h^{p\,2} + I_h^{q\,2} \quad (4.\ 4)$$

$$\varphi_h = \tan^{-1}\left(I_h^q \big/ I_h^p\right) \quad (4.\ 5)$$

$$I_h^q = \sum_{i=1}^{N}\sin(2\pi h i)\sum_{j=1}^{L}\left(\frac{b_h^j}{\sqrt{2}}\right)\delta_i^j \quad (4.\ 6)$$

$$I_h^p = \sum_{i=1}^{N}\cos(2\pi h i)\sum_{j=1}^{L}\left(\frac{b_h^j}{\sqrt{2}}\right)\delta_i^j \quad (4.\ 7)$$

Without any loss of generality, Figure 4. 5 shows an example of the complex plane for $N = 5$ and $h = 1/N$ to explain graphically how I_h is found and its relationship with the rest of the variables.

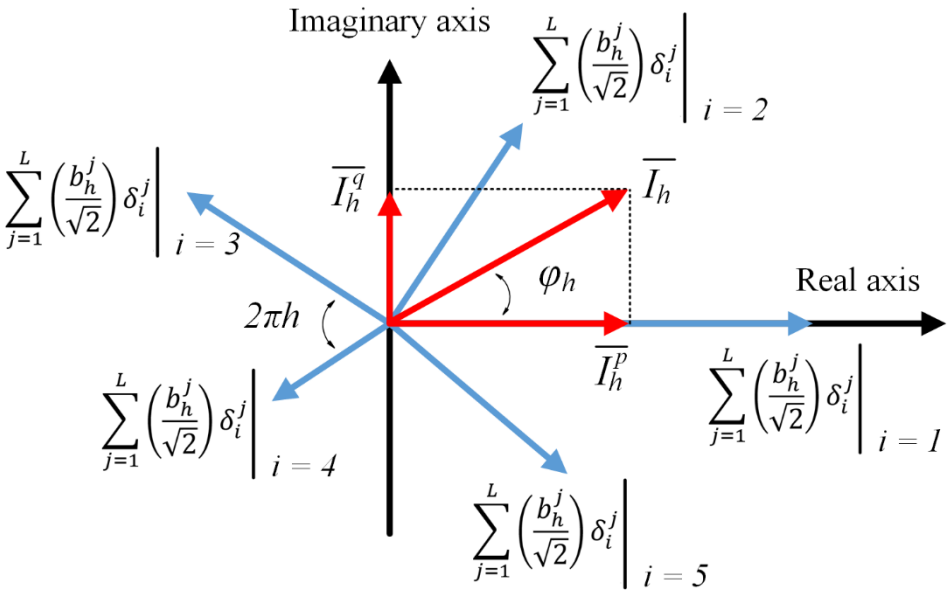

Figure 4. 5. An example of a complex plane for $N = 5$ and $h = 1/N$ to show how the resultant component is built.

4.3.3. Thermal considerations

It is relevant to introduce and discuss several details from the thermal point of view. In this application, where end loads will be power electrodes of the melting furnaces, the power converter must be able to provide the energy as uniform as possible because the steady-state temperature ripple is a sensitive aspect to be considered, particularly the impact that cycles' distribution has on it [27], [28]. In this work, ICC is used to control the supplied energy, however, this technique may cause a large ripple due to this intermittent power flow to the load. Therefore, there are periods where energy consumption is the nominal one as well as periods with zero energy consumption, causing temperature fluctuations around the mean. As for the relationship between instantaneous heat flow and temperature difference with ambient temperature, this is because its behavior can be expressed as a first-order model [8]. As a result, if the input is considered as a power pulse train, the output will vary exponentially around the set point. This PQ strategy should thus schedule this output cycle pattern for each load aiming to keep the temperature ripple to a minimum.

Currently, ICC is widely used in heating applications and, in this sense, different techniques to dispense the cycles along the period have been developed from a thermal point of view. The quality of these techniques is often measured by comparison with the regular distribution where each cycle is allocated at positions θ_k^j given by (4. 8) where α_j is the number of active cycles to be distributed in N, and k denotes each cycle among the α_j. Notice that all cycles are regularly distributed for any combination of parameters, however, it can only be implemented when α_j divides N as during these instants the position of the cycles matches and thus θ_k^j can be expressed as an integer number.

$$\theta_k^j = k\left(\frac{N}{\alpha_j}\right), \quad k \in \{0, 1 \dots \alpha_j - 1\} \tag{4. 8}$$

A more sophisticated approach described in [29] is the so-called accumulator-based method which achieves the best feasible distribution. This technique optimally computes the position of each cycle as shown in (4. 9) to avoid a fractional index θ_k^j adding new advantages. When α_j divides N the output cycles pattern is the same that the previous technique: Cycles are regularly distributed. Nevertheless, when this condition is not met, the output pattern must be implemented by allowing some level of irregularities related to the distance between contiguous active cycles. In this scenario, (4. 9) ensures that this magnitude is kept to a minimum value as the difference between the minimum and the maximum distances, in cycles, resulting in a unity value between active cycles. Furthermore, by distributing cycles as regularly as possible, the lowest frequency component in Fourier analysis is as high as possible, meaning that low-frequency ripple in the temperature is also minimized.

$$\theta_k^j = round\left(k\frac{N}{\alpha_j}\right), \quad k \in \{0, 1 \dots \alpha_j - 1\} \tag{4. 9}$$

4.3.4. Problem formulation

Once these two previous aspects have been properly established, this section proposes an MBQP problem in (4. 10)-(4. 12) to approach both PQ improvement and temperature ripple minimization based on (4. 9). The cost function J_{Sub} is given by (4. 10) and refers to the energy present in the subharmonic range, that is, the sum of I_h^2 for all harmonic orders below the unity $(h < 1)$. Equation (4. 11) is a power constraint. It is well-known that the power delivered to the load in ICC systems is controlled by varying the number of active cycles α_j along the modulation period. Concretely, this power, per unit, is given by the ratio α_j/N; however, this output power varies according to the resolution, which means that there will be set points that would not be reached as they are not integer multiples from the latter. Thus, α_j will be found as the nearest integer to the term within the rounding function, where P_j^{sp} is the power setpoint for each load j.

$$J_{Sub} = \sum_{h=1/N}^{N-1/N}\left[\left(\sum_{i=1}^{N}\sum_{j=1}^{L}\left(\frac{b_h^j}{\sqrt{2}}\right)\delta_i^j \sin(2\pi hi)\right)^2 + \left(\sum_{i=1}^{N}\sum_{j=1}^{L}\left(\frac{b_h^j}{\sqrt{2}}\right)\delta_i^j \cos(2\pi hi)\right)^2\right] \tag{4. 10}$$

$subject\ to$:

$$\sum_{i=1}^{N}\delta_i^j = \alpha_j = round\left(N\frac{P_j^{sp}}{P_j}\right) \qquad \begin{matrix}\forall P_j^{sp} \le P_j \\ \forall j\end{matrix} \tag{4. 11}$$

$$\frac{100}{\alpha_j}\sum_{i=1}^{N}\delta_i^j \ge \gamma \qquad \begin{matrix}\forall j | \alpha_j \ne 0 \\ \forall i = \theta_k^j\end{matrix} \tag{4. 12}$$

Finally, (4. 12) must be understood as a goal in this multi-objective context: PQ and thermal behavior improvement. It is in charge of modulating the weight of the accumulator-based distribution where $\gamma = 100\ \%$ forces the most regular distribution of (4. 9) and $\gamma = 0\ \%$ prioritizes the PQ objective in the problem. Broadly speaking, this constraint ensures that at least the fraction γ of α_j is in the positions given by (4. 9).

4.4. Results and discussion

This section aims to validate and evaluate the performance of the proposed MBQP problem and the developed hardware. To this aim, several indices such as the total power factor (TPF), computed as the ratio between the fundamental of the current and the RMS, and the total subharmonic content (TSC), computed as the ratio between the energy present in frequencies below 50 Hz (J_{Sub}) and the fundamental of the current, as well as some statistical parameters as mean and standard deviation are provided. The fit between the optimal cycles and the accumulator-based scheduling as well as the current spectrum and aggregated power profiles are also shown. The methodology adopted can be summarized as follows: Section A arises a case study regarding four scenarios of the previously formulated problem with a randomly generated population of 15 loads while sections B and C were carried out under the same load conditions (3 loads) but from two different points of views: Some results issued by the proposed optimization problem are discussed in section B and then the developed prototype is tested in section C for validation purposes.

4.4.1. Case study 1: A large-scale subharmonic minimization

First of all, Figure 4. 6 introduces the dataset to be employed in this section consisting of 15 different loads ($L = 15$). This dataset was generated by a random uniform distribution with nominal powers ranging from 0.4 to 1.0 pu. In the case of the power setpoints, each load *j* works with a power between zero and its nominal value which is also generated by a random uniform distribution. The deemed baseline was 500 kW.

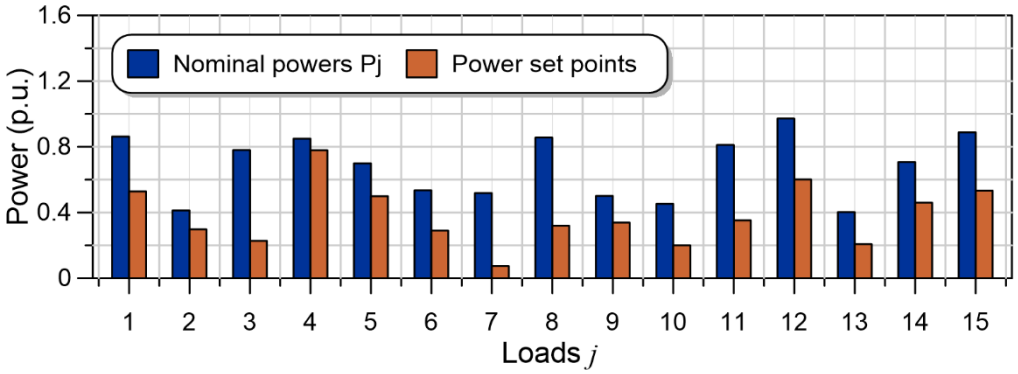

Figure 4. 6. Nominal powers and setpoints dataset to be used in the case studies.

Moreover, to reproduce very close conditions to those of the industry [22], a voltage level of $V = 230\ V$ was considered resulting in a fundamental component of the current of 0.548 pu (12.23 kA) which remains constant in both cases as the fundamental component is just in charge of delivering the total active power requested and this is also kept constant as the constraint (4. 11) indicates. Consequently, the mean value of the power profile is also constant in all cases, 0.548 pu (2.81 MW), corresponding to the total active power given by the product between V and the fundamental of the current. Similarly, the considered baseline for aggregated magnitudes as the total current or power was 22.31 kA and 5.12 MW

respectively, corresponding to the maximum values that may be reached according to the loads' population generated. Before describing the results issued by the proposed problem, loads from this dataset have been scheduled by the conventional ICC and accumulator-based techniques using a modulation period of 10 cycles ($N = 10$) to plot in Figure 4. 7 the current spectrum (a), removing the fundamental component for better visualization, the percentage of fit with the accumulator-based scheduling (per load) (b), and the scheduled power profile (c), for comparison purposes. Note that the spectrum in Figure 4. 7 a) has components that are spaced f/N, that is, 5 Hz in this case.

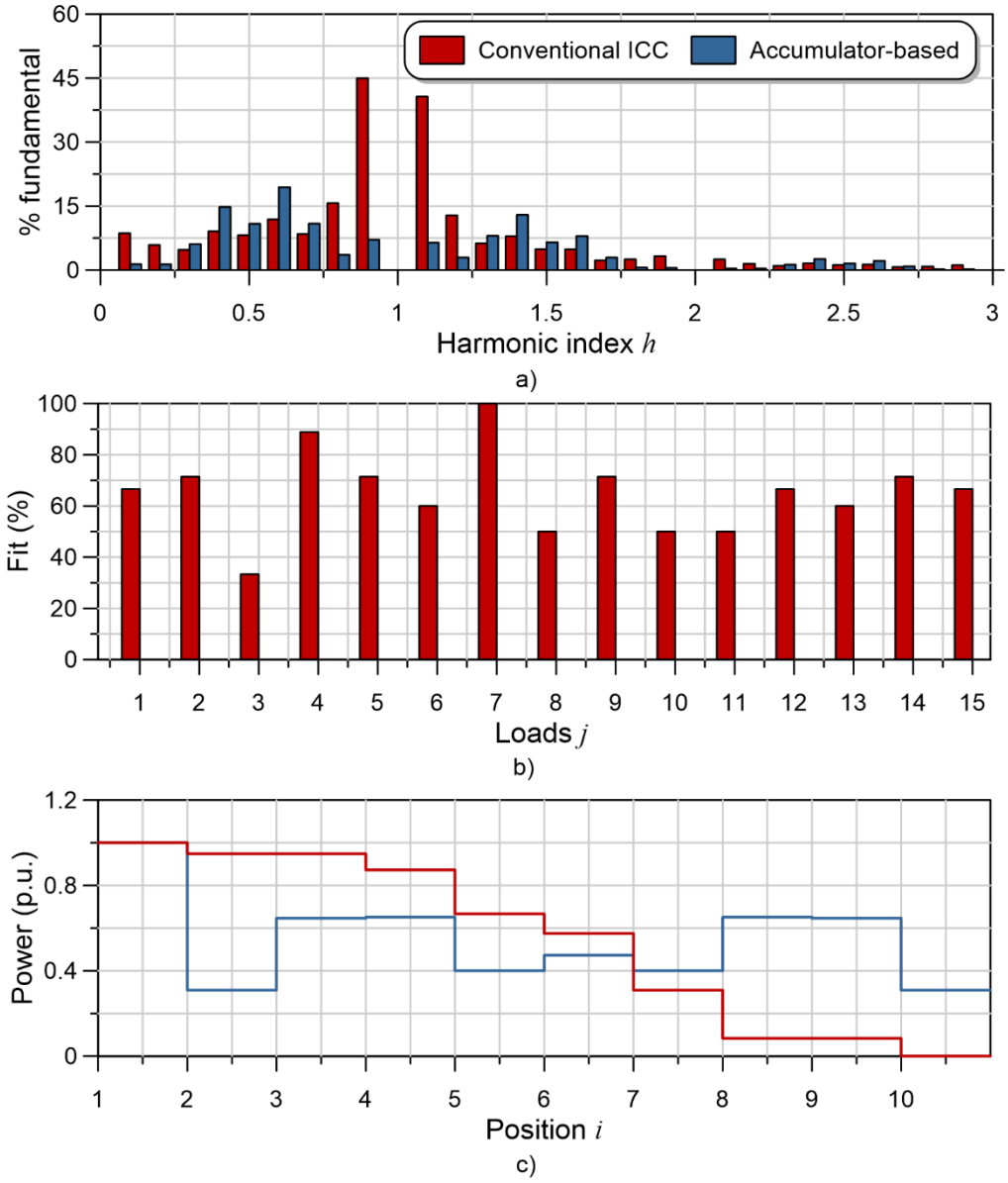

Figure 4. 7. Results for the ICC and accumulator-based methods (case study 1): a) Current spectrum (without the fundamental component), b) percentage of fit for each load in the ICC method and c) aggregated power profile.

As expected, when conventional ICC is employed, results are much poorer than in the accumulator-based method in several aspects that will be now described. For example, in terms of the subharmonic current spectrum, ICC shows higher magnitudes reaching up to 44.94 % @ 45 Hz ($h = 0.9$) of the fundamental while in the accumulator-based method the highest component reaches 19.41 % @ 30 Hz ($h = 0.6$). The energy presents in subharmonic

components is also higher in the results issued by ICC (TSC 43.21 %) compared to the accumulator-based method (TSC 28.70 %). Furthermore, it can be seen that the energy presents in non-fundamental harmonics with ICC is higher than in the accumulator-based method, which is supported by both TPF, 0.8228, and 0.9384 respectively.

The percentage of fit with the distribution given by (4. 9) has been plotted in Figure 4. 7 b) just for ICC as the distribution of the cycles for each load using the accumulator-based method is the reference case, giving 100 % in all cases. Traditional ICC reports a rate of fit in the range 33.33-100 % (although with other power setpoints can even reach 0 %) which is quite low and as a consequence, cannot be modulated due to its nature.

It is also possible to see in Figure 4. 7 c) the scheduled profile in both considered cases where the power profile corresponding to the ICC shows power peaks of up to 1.0 pu representing an increment of 82.20 % to the mean value (0.548 pu). The standard deviation (SD) of the distribution of 15 loads with a modulation period of 10 cycles reaches 0.398 pu in conventional ICC, showing that the values are spread out over a wide range over the mean value. For the accumulator-based technique, these values remain almost constant, except for the SD, showing a lower value than ICC, 0.213 pu as can be seen from Figure 4. 7 c), where the power profile shows less deviation to the average (0.548 pu). Besides the inefficient PQ results of both methods, these power distributions cannot be assumed by this energy-intensive industry, where the occurrence of high-power peaks could lead to high financial penalties on the electricity bill. The previous results show the comparison between traditional methods, however, Figure 4. 8 depicts the results when the abovementioned dataset (see Figure 4. 6) is used as an input of the proposed MBQP problem formulated in (4. 10)-(4. 12). The solver GAMS was used running inside an Intel ® Core ™ i5-6300HQ CPU @ 2.3 GHz. The execution time was approximately 3.76 s in each scenario.

To study the distribution of the cycles and their impact on PQ, four scenarios have been proposed for all case studies, for which γ will be 0 %, 50 %, 60 %, and 80 % respectively. As can be seen, scenarios 1 and 2 are very similar, even for an increase of 50 %. On the other hand, in scenarios 3 and 4, for an increase in γ of 20 %, the difference is remarkable. The spectrum is shown in Figure 4. 8 a). Although a substantial degradation between scenarios is noted as the proposed PQ indices TPF and TSC report, these results are much better than in the traditional ICC and accumulator-based scheduling (see the differences in vertical scale between Figure 4. 7 a) and Figure 4. 8 a)). In scenarios 4 and 3 the highest magnitude within subharmonic range reaches 17.20 % and 11.17 % @ 30 Hz ($h = 0.6$), while in the other scenarios is below 2 % of the fundamental (1.80 % and 1.68 % @ 35 Hz or $h = 0.7$ respectively in scenarios 2 and 1). These results are significantly better compared to 44.94 % @ 45 Hz ($h = 0.9$) for the ICC method, or 19.41 % @ 30 Hz ($h = 0.6$) in the accumulator-based method. Concerning the PQ indices, TSC achieves 22.29 % and 16.73 % in scenarios 4 and 3 compared to 3.49 % and 2.31 % in scenarios 2 and 1 respectively, which suggests a clear increase in subharmonic content for higher values of γ, as the feasibility region is reduced. However, they are even lower than the TSC in the two previous methods, 43.21 % in the ICC and 28.70 % in the accumulator-based method. The TPF drops slightly from scenarios 1 to 4 providing values of 0.9995, 0.9991, 0.9789, and 0.9634 while the ICC and accumulator-based methods reported TPF of 0.8228 and 0.9384 which shows a higher efficiency of the proposed method over the traditional ones.

In Figure 4. 8 b), it can be seen how the last constraint of the problem (12) sets effectively the minimum degree of fit with the accumulator-based distribution (per load) leading to scenarios where the worst case, understood as the load with the lowest percentage of fit and thus the most irregular cycles distribution, provides percentages greater than or equal to the parameter γ. Unlike the results shown in Figure 4. 7, this parameter enables the MBQP problem to keep this level of irregularity to a certain value. Scenario 1 is in the range

0-100 %, scenario 2 within 50-100 %, scenario 3 within 66.66-100 % and scenario 4 within 83.33-100 %.

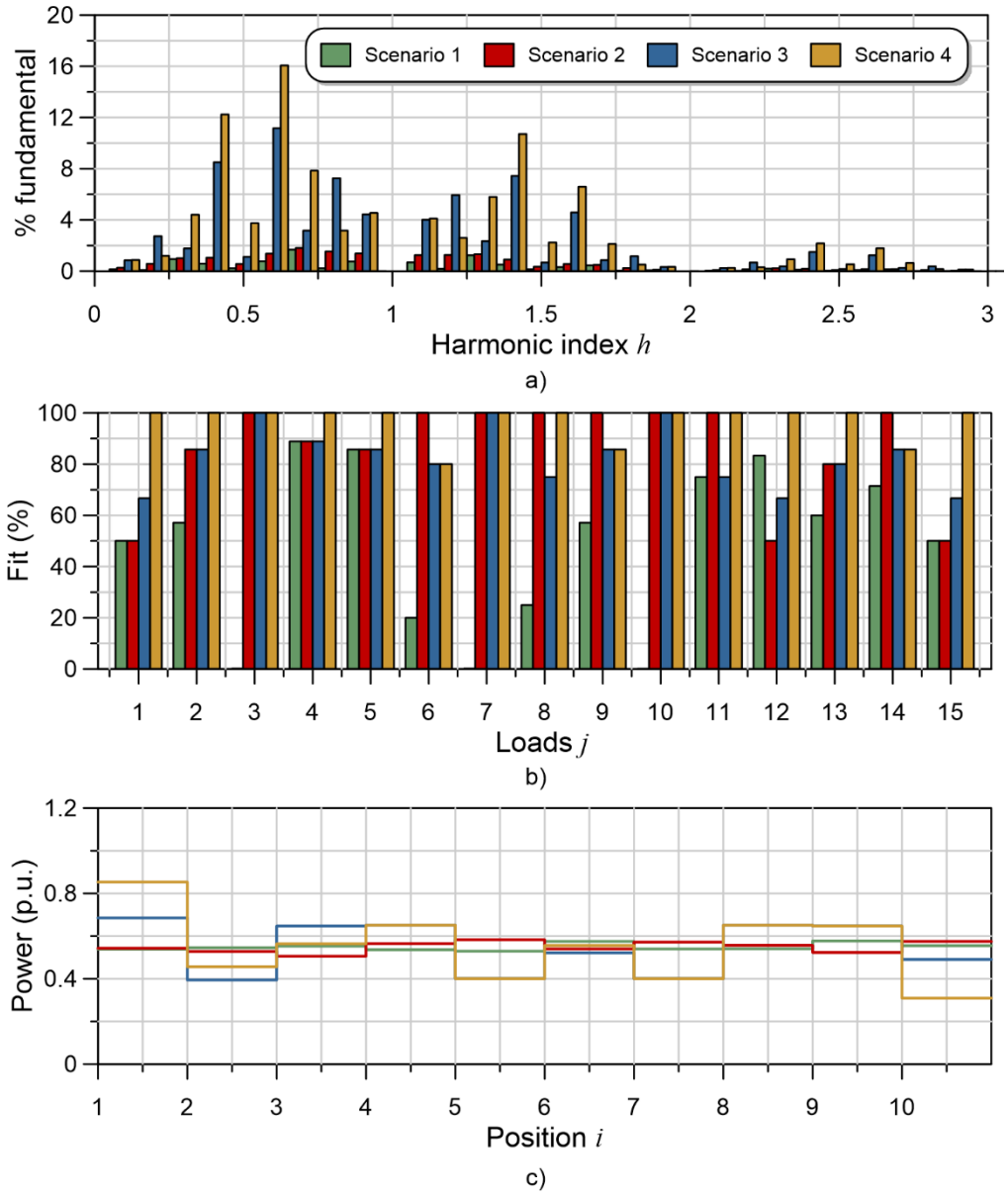

Figure 4. 8. Results for the proposed MBQP problem in four scenarios of the case study 1: a) Current spectrum (without the fundamental component), b) percentage of fit for each load and d) aggregated power profile.

Concerning the power profile shown in Figure 4. 8 c), although these scheduled profiles show signs of worsening from scenarios 1 to 4 as their standard deviations support: 0.023, 0.025, 0.115 and 0.160 pu respectively, results are much better than in case of Figure 4. 7, with SD equal to 0.398 in the ICC and 0.213 pu in the accumulator-based method. As expected according to the SD of each method, the power peaks reached when dispatching cycles represent other advantage of the proposed technique over the traditional methods: While the latter is not able to reduce their power peaks from the maximum achievable, 1.0 pu, the proposed one provides power reductions of up to almost the half, 0.577 pu, or 0.853 pu when the thermal factor becomes more important due to γ. Finally, Table 4. 1 summarizes the main results of this case study.

Table 4. 1. Results summary for case study 1.

Scenario	TPF	TSC (%)	Max. Subh. (%)	Max. Power (pu)	SD (pu)	Min. fit (%)
Conv. ICC	0.8228	43.21	44.94	1.0	0.398	33.33
Accu.-based	0.9384	28.70	19.41	1.0	0.213	100
1	0.9995	2.31	1.68	0.577	0.023	0
2	0.9991	3.49	1.80	0.582	0.025	50
3	0.9789	16.73	11.17	0.685	0.115	66.66
4	0.9634	22.29	17.20	0.853	0.160	83.33

4.4.2. Case study 2: A small-scale subharmonic minimization

For validation purposes, this case study considers the loads that will be employed for testing the laboratory hardware in the subsequent case study. In this regard, the main goal of this section is to provide the theoretical results from which the experimental ones will be validated. Three loads ($L = 3$) of nominal powers 0.307, 0.448, and 1.0 pu, power set points of 0.123, 0.135, and 0.60 pu, as well as a modulation period of $N = 10$, has been deemed. The considered baseline was 78 W for the previous loads as well as 137 W and 595.6 mA for aggregated magnitudes, which also represents the maximum achievable values. The execution time is considerably reduced due to the lower number of loads and falls up to 1.27 s in each scenario using the same solver. With this dataset, Figure 4. 9 a) shows the current spectrum (removing the fundamental component for better visualization) when applying the conventional methods and the proposed one with $\gamma = 50$ %. The subharmonics range contains a large number of components of which the following can be stand out: ICC, 56.87 % @ 45 Hz (171.35 mA), accumulator-based, 42.19 % @ 30 Hz (127.12 mA) and the proposed method achieves a significant reduction of 75.71 % and 67.27% (13.81 % @ 35 Hz, 41.61 mA) concerning the previous ones. However, a reduction in this frequency component does not involve less energy in subharmonics range (TSC) as shown in Table 4. 2 (scenarios 1 and 2).

Concerning the TSC, similar behavior can be seen: While traditional methods result in currents with more than a half of the distortion located in frequencies below to 50 Hz (64.88 % and 59.31 %), this percentage falls up to 22.64 % with the suggested method. The TPF shows signs of increasing when the proposed method is applied which means that the energy of non-fundamental harmonics tends to decrease. Concretely, the TPF (0.9625) is improved by 26.69 % or 18.14 % when regarding the ICC (0.7597) or the accumulator-based (0.8147) respectively.

As in the previous case study, in terms of dispatching cycles, the proposed optimization problem also provides a control mechanism by means of γ which is depicts from Figure 4. 9 b): While load with the most irregular distribution reaches 33.33 % of fit in ICC, the proposed method effectively set the minimum fit to 50 %.

Finally, Figure 4. 9 c) depicts the power profile when the mains cycles are dispatched by these three methods considered: While the results provided by ICC and accumulator-based techniques often show positions with powers far from the mean (0.506 pu) reaching up to 1.0 pu, and therefore result in a high SD (0.433 and 0.360 pu for ICC and accumulator-based method respectively), the suggested approach successfully achieves the power profile to be as uniform as possible providing an SD of 0.143 pu and a maximum 0.744 pu which means a variation of -66.97 and -25.6 % as well as -60.27 and -25.6 % over the conventional techniques.

Although, Figure 4. 9 only depicts the results for the proposed method when $\gamma = 50$ % (scenario 2), in Table 4. 2, more experiments with the same values of γ as those considered in case study 1 have been reported. Notice that the proposed method always provides better

results than traditional ones and enable furnace zones to operate at different quality levels as well as reduce the temperature ripple indirectly through the parameter γ. Likewise, these results lead to the accumulator-based ones when γ approaches 100 % which also takes place with the results presented in Table 4. 1.

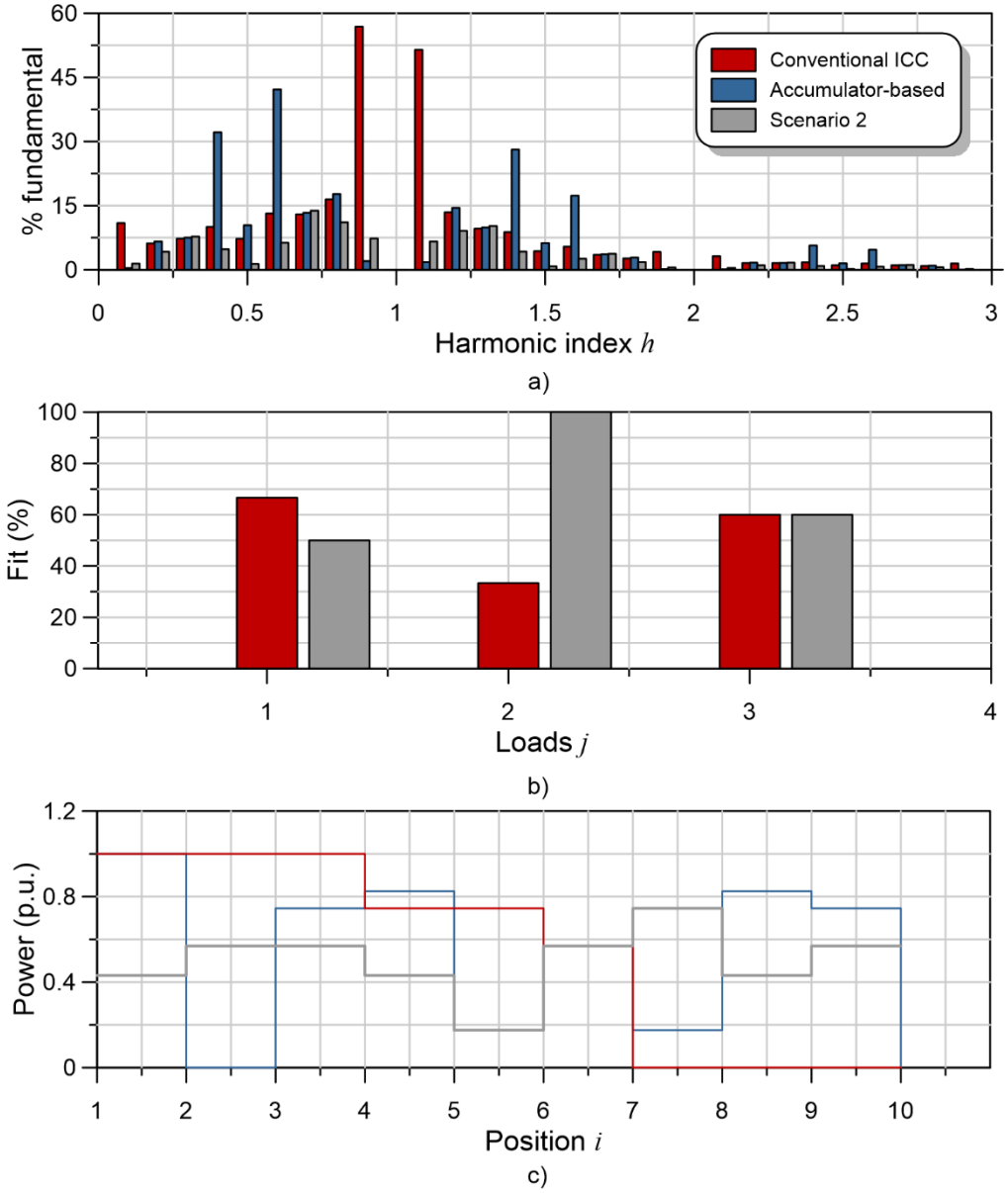

Figure 4. 9. Results for ICC and accumulator-based methods as well as the proposed problem with $\gamma = 50$ % (scenario 2) in case study 2: a) Current spectrum (without the fundamental component), b) percentage of fit for each load and d) aggregated power profile.

Table 4. 2. Results summary for case study 2.

Scenario	TPF	TSC (%)	Max. Subh. (%)	Max. Power (pu)	SD (pu)	Min. fit (%)
Conv. ICC	0.7597	64.88	56.87	1.0	0.433	33.33
Accu.-based	0.8147	59.31	42.19	1.0	0.360	100
1	0.9625	22.46	14.48	0.744	0.143	0
2	0.9625	22.64	13.81	0.744	0.143	50
3	0.9292	32.54	16.71	0.825	0.201	66.66
4	0.8991	39.52	23.87	0.825	0.246	80

4.4.3. Case study 3: Lab testing

A laboratory scale test has been done with the same conditions as the previous case to test the performance and show the operation of the small-scale prototype described in section II. Furthermore, this case study was carried out at the same voltage level as the previous ones, 230 V. Figure 4. 10 shows the current waveform and spectrum taken from the Tektronix oscilloscope, as well as the corresponding power profile according to the used method in each case. Two vertical cursors (a, b) in the spectrum quantify the fundamental of the current (cursor a, which is independent of the method as was stated, in the range 0.487-0.494 pu @ 50 Hz (301.3-305.4 mA) while the theoretical one would be 0.506 pu) and the low order subharmonic (cursor b) representing the highest amplitude in the frequency range below 50 Hz, which varies in magnitude and frequency with the used method as was also seen in the previous section. Additionally, one modulation period among the 5 acquired has been highlighted in blue to identify it and show how the three loads are scheduled.

Figure 4. 10 a) shows the results when all power converters operate under the traditional ICC method. Notice that this technique achieves the highest power ripple as all loads are scheduled at the beginning of the modulation period and thus, the peak demand matches the summation of each P_j. Hence, ICC provides the poorest power profile and PQ with TPF, TSC, and peak demand values of 0.7654, 64.52 %, and 1.0 pu respectively. In this case, the low order subharmonic (cursor b) is located at approximately 45 Hz, reaching 56.86 % of the fundamental (170.6 mA). Moreover, this method also reaches the highest SD, 0.413 pu, and one of the lowest percentages of fit with the regular distribution, 33.33 %, which is in line with the trends shown in the above case study.

On the other hand, the results produced by the accumulator-based method are shown in Figure 4. 10 b), which allows a better energy distribution at a local level, so the power ripple reached is lower than in the previous technique. Despite this advantage, the demand and PQ of the aggregate current are not enhanced in the same degree, resulting in a TPF, TSC, and peak demand values of 0.8169, 57.51 %, and 1.0 pu respectively, which is a moderate improvement compared to the ICC. The peak demand is not improved as it is 1.0 pu as the worst case. Moreover, it is observed in the spectrum that the low order subharmonic is in this case 42.10 % of the fundamental (126.2 mA @ 30 Hz), lowering the amplitude of the component and the frequency compared to the ICC method. Concerning the power distribution, this method provides a lower SD than the traditional ICC as expected (0.344 pu).

The last scenario refers to the proposed MBQP problem for $\gamma = 50$ %. Figure 4. 10 c) displays the results where the improvement can be seen graphically due to the low distortion exhibited by the current and shows better results in terms of power profile and PQ than the previous methods, providing a TPF of 0.9645, TSC of 21.87 % and power peak of 0.736 pu. These values describe an improvement of 26.01 %, -66.10 % and -26.4 % as well as 18.07 %, 61.97 % and -26.4 % with respect to the conventional ICC and the accumulator-based methods respectively. Looking at the spectrum, in this case, the reduction is even more significant (-76.81 % and 68.71 %), as the low order subharmonic reaches 13.17 % @ 35 Hz (39.77 mA). Under the proposed optimization problem, the SD (0.133 pu) also decreases by 67.80 % and 61.34 %, compared to the ICC and the accumulator-based method respectively. Furthermore, the percentage of fit with the regular distribution is kept within the range 50-100 % as expected. All these results discussed above are reported in Table 4. 3.

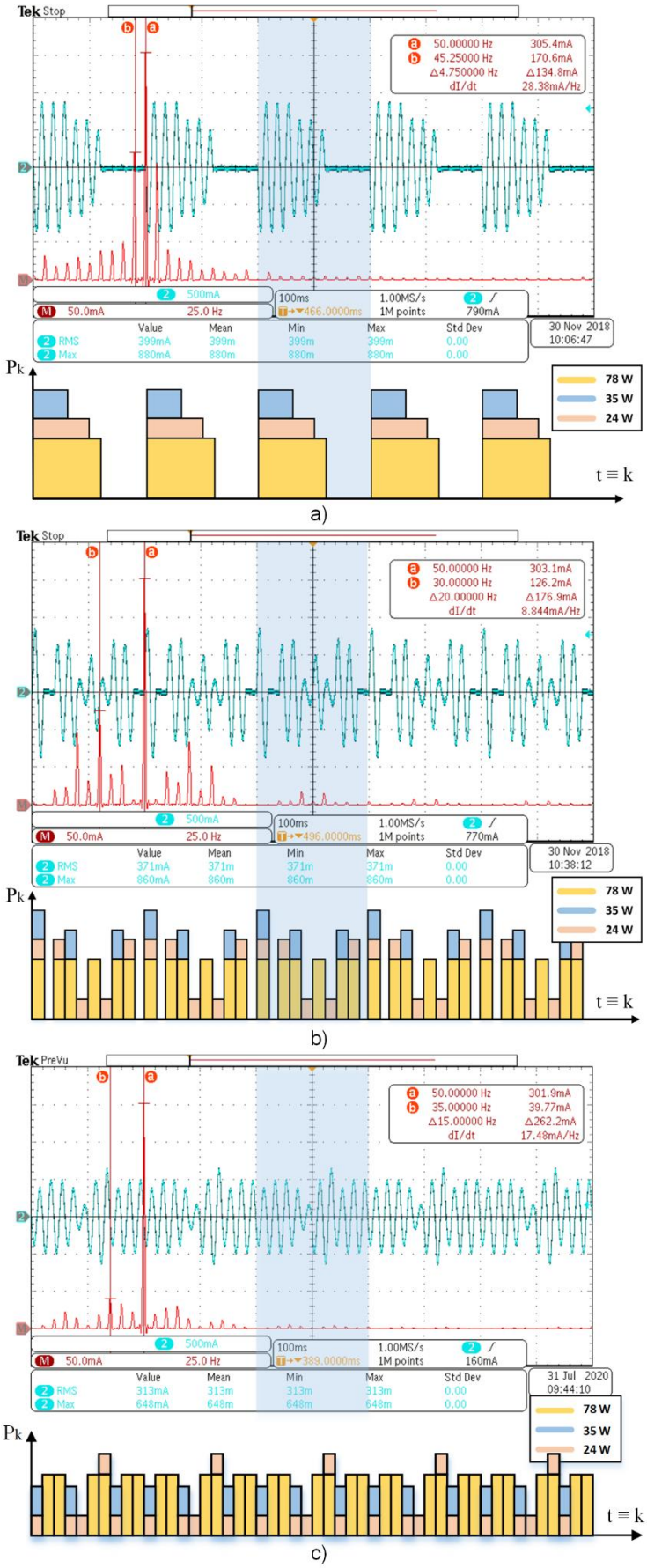

Figure 4. 10. Experimental current waveform, spectrum, and power profile when applying: a) The ICC, b) Accumulator-based method, and c) the proposed MBQP problem (scenario 2).

Table 4. 3. Results summary for the experimental results.

Scenario	TPF	TSC (%)	Max. Subh. (%)	Max. Power (pu)	SD (pu)	Min. fit (%)
Conv. ICC	0.7654	64.52	56.86	1.0	0.413	33.33
Accu.-based	0.8169	57.51	42.10	1.0	0.344	100
1	0.9627	21.93	14.00	0.736	0.136	0
2	0.9645	21.87	13.17	0.736	0.133	50
3	0.9297	31.96	16.54	0.800	0.191	66.66
4	0.9018	38.13	23.10	0.809	0.233	80

Finally, a comparison table (see Table 4. 4) is included to show the variation of the experimental results with case study 2 as reference. Notice the small variation in all indices proposed, especially in the minimum fit which does not show signs of change because the position of the mains cycles remains constant between both case studies. Therefore, in view of the successful results, where the maximum variation is around 5 %, the proposed optimization problem can be validated as an appropriate solution that helps to improve the energy efficiency in the glass melting process.

Table 4. 4. Results validation with case study 2 as reference.

Scenario	TPF	TSC (%)	Max. Subh. (%)	Max. Power (pu)	SD (pu)	Min. fit (%)
Conv. ICC	0.750	-0.555	-1.774	0	-4.619	0
Accu.-based	0.270	-3.035	-0.213	0	-4.444	0
1	0.021	2.360	-3.365	-1.075	-4.895	0
2	0.208	-3.401	-4.611	-1.075	-6.993	0
3	-0.054	-1.782	-0.977	-3.030	-4.975	0
4	-0.300	-3.517	-3.205	-1.939	-5.284	0

4.5. Conclusions

To improve the glass melting process, increase productivity, improve glass quality and reduce CO2 emissions, electrical melting is often employed in different stages of the process. While furnace boosting can employ self-commutated electronic power converters, in tin bath and annealing lehr heating systems a classical Triac-based AC-AC voltage converter continued to be normally employed. Although ICC overcome the inefficient low power factor of the phase angle firing mode, it brings the inconveniences of subharmonics as well as a high-temperature ripple. What is more, it is needed to avoid any peak power demands to assure the highest efficiency. Thus, this paper establishes a novel solution derived from the ICC that offers an MBQP problem to minimize the subharmonic content of the current waveform and keep the temperature ripple of each furnace zone under control. Finally, the results provided by the proposed case studies validate this strategy and demonstrate the improvements over other traditionally adopted methods, which paves the way towards a more efficient and decarbonized glass-melting sector.

Acknowledgements

This research is supported by the Project IMPROVEMENT (grant SOE3/P3E0901) co-financed by the Interreg SUDOE program and the European Regional Development Fund (ERDF), and partially funded by the Spanish Ministry of Economy and Competitiveness under Project TEC2016-77632-C3-2-R.

References

[1] E. Worrell, C. Galitsky, E. Masanet, and G. Wina, “Energy efficiency improvement and cost saving opportunities for the glass industry. Environmental Energy Technologies Division,” 2008, doi: 10.2172/927883.

[2] S. Q. S. Ahmad, C. Wieckert, and R. J. Hand, “Glass melting using concentrated solar thermal energy,” *Glas. Technol. J. G*las. Sci. Technol. Part A, vol. 58, no. 2, pp. 41–48, 2017, doi: 10.13036/17533546.58.2.012.

[3] A. Marcu, S. Roth, and W. Stoefs, “Composition and Drivers of Energy Prices and Costs in Energy-Intensive Industries The Case of the Flat Glass Industry,” 2014.

[4] L. Biennek, “All-electric melting prospects for glass container production,” *Glas. Worldw.*, no. 88, pp. 76–80, 2020.

[5] L. A. B. Pilkington, “Review lecture: the float glass process,” *Pro*c. R. Soc. Lond. A, vol. 314, no. 1516, pp. 1–25, 1969, doi: doi.org/10.1098/rspa.1969.0212.

[6] R. Conradt, “Prospects and physical limits of processes and technologies in glass melting,” J. Asian Ceram. Soc., vol. 7, no. 4, pp. 377–396, 2019, doi: 10.1080/21870764.2019.1656360

[7] L. Li, H.-J. Lin, J. Han, J. Ruan, J. Xie, and X. Zhao, “Three-Dimensional Glass Furnace Model of Combustion Space and Glass Tank with Electric Boosting,” Mater. Trans., vol. 60, no. 6, pp. 1034–1043, 2019, doi: 10.2320/matertrans.M2019044.

[8] L. Li, J. Han, H. Lin, J. Ruan, J. Wang, and X. Zhao, “Simulation of glass furnace with increased production by increasing fuel supply and introducing electric boosting,” Int. J. Appl. Glas. Sci., vol. 11, no. 1, pp. 170–184, Jan. 2020, doi: 10.1111/ijag.13907.

[9] "Introduction to ANSI/IEEE standard 668-1987: IEEE recommended practice for electrical heating applications to melting furnaces and forehearths in the glass industry," in IEEE Transactions on Industry Applications, vol. 24, no. 4, pp. 682-684, July-Aug. 1988, doi: 10.1109/28.6121.

[10] A. Testa and R. Langella, "Power system subharmonics," IEEE Power Engineering Society General Meeting, 2005, 2005, pp. 2237-2242 Vol. 3, doi: 10.1109/PES.2005.1489461.

[11] “IEC 60050 - International Electrotechnical Vocabulary - Details for IEV number 103-07-29: "sub-harmonic component"” [Online]. Available: https://www.electropedia.org/iev/iev.nsf/display?openform&ievref=103-07-29. [Accessed: 27-Nov-2018].

[12] A. Testa, D. Gallo and R. Langella, "On the Processing of harmonics and interharmonics: using Hanning window in standard framework," in IEEE Transactions on Power Delivery, vol. 19, no. 1, pp. 28-34, Jan. 2004, doi: 10.1109/TPWRD.2003.820437.

[13] Yong Nong Chang, G. T. Heydt and Yazhou Liu, "The impact of switching strategies on power quality for integral cycle controllers," in IEEE Transactions on Power Delivery, vol. 18, no. 3, pp. 1073-1078, July 2003, doi: 10.1109/TPWRD.2003.813642.

[14] K. J. Ferreira and A. E. Emanuel, "A Digitally Controlled Unity Power Factor Compensator for Pulse-Burst-Modulated Loads," in IEEE Transactions on Power Electronics, vol. 25, no. 7, pp. 1888-1893, July 2010, doi: 10.1109/TPEL.2010.2043446.

[15] N. A. Ahmed, K. Amei and M. Sakui, "A new configuration of single-phase symmetrical

PWM AC chopper voltage controller," in IEEE Transactions on Industrial Electronics, vol. 46, no. 5, pp. 942-952, Oct. 1999, doi: 10.1109/41.793343.

[16] F. Jahani and M. Monfared, "A Multilevel AC/AC Converter With Reduced Number of Switches," in IEEE Transactions on Industrial Electronics, vol. 65, no. 2, pp. 1244-1253, Feb. 2018, doi: 10.1109/TIE.2017.2733495.

[17] K. A. Nigim and G. T. Heydt, “Power quality improvement using integral-PWM control in an AC/AC voltage converter,” Electr. Power Syst. Res., vol. 63, no. 1, pp. 65–71, Aug. 2002, doi: 10.1016/S0378-7796(02)00098-6

[18] O. Krapp, “Energy efficiency, process safety and transparency assured,” Glass Worldwide, 2016.

[19] A. Breitkopf, “More power to your Glass Plant: Saint Gobain trusts in Power Controllers from AEG SVS for their plant upgrade. (Plant Untilities),” Int. Glas. Rev., vol. 15, pp. 68–70, 2002.

[20] R. Meuleman, “How can predictive strategies contribute in a better power control and decreased energy consumption?,” Glass machinery plants & accessories, 2009.

[21] H. Kröhler, “Smoothing the peak: Integrated optimization algorithms save heating costs,” ABB Review, 2015.

[22] R. Meuleman, “The only future for glass industry will be ‘all-electric,’” in 14th International Seminar on Furnace Design, Vsetin, Czech Republic, 2017.

[23] I. Papadogeorgos and K. M. Schure, Decarbonisation Options for the Dutch Container and Tableware Glass Industry. PBL Netherlands Environmental Assessment Agency;© ECN part of TNO, 2019.

[24] F. Teng and G. Strbac, "Full Stochastic Scheduling for Low-Carbon Electricity Systems," in IEEE Transactions on Automation Science and Engineering, vol. 14, no. 2, pp. 461-470, April 2017, doi: 10.1109/TASE.2016.2629479.

[25] J. Garrido-Zafra, A. Moreno-Munoz, A. Gil-de-Castro, F. Bellido-Outeirino, R. Medina-Gracia and E. G. Ballesteros, "Load Scheduling Approach for Energy Management and Power Quality enhancement in Glass Melting Furnaces," 2019 IEEE International Conference on Environment and Electrical Engineering and 2019 IEEE Industrial and Commercial Power Systems Europe (EEEIC / I&CPS Europe), 2019, pp. 1-6, doi: 10.1109/EEEIC.2019.8783727.

[26] J. Garrido-Zafra, A. Moreno-Munoz, A. Gil-de-Castro, E. J. Palacios-Garcia, C. D. Moreno-Moreno, and T. Morales-Leal, “A Novel Direct Load Control Testbed for Smart Appliances,” Energies, vol. 12, no. 17, p. 3336, Aug. 2019, doi: 10.3390/en12173336.

[27] N. Barry and E. McQuade, "Temperature control using integer-cycle binary rate modulation of the AC mains," in IEEE Transactions on Industry Applications, vol. 31, no. 5, pp. 965-969, Sept.-Oct. 1995, doi: 10.1109/28.464505.

[28] E. P. McCarthy and J. Danesh, "A Novel Method of Direct Digital Integral-Cycle Power Control," in IEEE Transactions on Industrial Electronics and Control Instrumentation, vol. IECI-25, no. 2, pp. 149-154, May 1978, doi: 10.1109/TIECI.1978.351526.

[29] J. Nieznanski, "The accumulator in integral-cycle AC power control," in IEEE Transactions on Industrial Electronics, vol. 42, no. 3, pp. 331-334, June 1995, doi: 10.1109/41.382146.

Chapter 5

IoT cloud-based power quality extended functionality for grid-interactive appliance controllers

Joaquin Garrido-Zafra[1], Aurora Gil-de-Castro[1], Rafael Savariego-Fernandez[1], Matias Linan-Reyes[1], Felix Garcia-Torres[2] and Antonio Moreno-Muñoz[1]

[1]Departamento de Ingeniería Electrónica y de computadores, Escuela politécnica superior, Universidad de Córdoba, Córdoba, Spain

[2]Departamento de Ingeniería Eléctrica y Automática, Escuela politécnica superior, Universidad de Córdoba, Córdoba, Spain

Abstract

Due to the myriad of loads that are collected into commercial Grid-interactive Efficient Buildings (GEBs) focused on the industry 4.0 paradigm, it is important to ensure their proper electrical operation. The power quality (PQ) here requires a granular monitoring approach, reaching a point where each device connected to the microgrid can diagnose whether its power supply is optimal. Otherwise, it can participate cooperatively in decision-making to avoid anomalies or faults in the microgrid. In this work, we present cloud-based extended functionality to make smart appliances (SA) responsive to the grid, either autonomously or managed under the open automated demand response (OpenADR) standard. Further to acting as a switch, the main strength lies in its PQ monitoring via the Fiware Internet of Things (IoT) platform with data-driven analytics capabilities. It identifies and even predicts a broad spectrum of electrical disturbances, far exceeding the capabilities of previous solutions such as the grid-friendly appliance controller, so it is possible to customize a battery of alarms at will (e.g., according to IEEE 1547 standard). Moreover, although it can act autonomously, its main mission will be to act in a coordinated manner, either cooperatively or under the supervision of the GEB Energy Management System (EMS). Finally, different case studies are presented to show their capabilities. With the integration of these distributed sub-metering systems, under standards IoT wireless communication protocols, a further step will be taken in the advent of the digital utility paradigm.

5.1. Introduction

The market for large household appliances is expected to grow annually by 1.8% (CAGR 2019-2023), reaching 368 billion dollars in 2023 [1]. This increasing pace is being driven by several trends, such as the expansion of digitization in everyday life, the citizen interest in sustainability, and the increase in the purchasing power of the average consumer. Meeting these expectations requires investments and economies of scale, but on the other hand, it can bring new opportunities for innovation. Thus, in recent years we have witnessed the appearance and proliferation of SAs. Popularly SAs are recognized for having some electronic processing capability and wireless connectivity. For example, smart washing machines can independently regulate the washing powder and the detergent to be used depending on the weight of the load and the type of fabric. They can also automatically send alerts when the detergent runs out. However, in the energy field, within the framework of Smart Grids (SG), the term "smart" refers to those appliances capable of modulating their electricity demand in response to signal requests from the electrical system. Thus, household appliances could incorporate different Demand Response (DR) strategies. DR has already proven to be a resource that the grid operator can use in several ways to provide system reliability, stability, and security services such as voltage and frequency support. Typically, DR policies can be divided into direct (explicit DR) through aggregation or virtual power plants (VPP), or indirect (implicit DR) [2]. Explicit DR (also called incentive-based DR program) is divided into traditional-based (e.g., direct load control, interruptible pricing) and market-based (e.g., emergency DR programs, capacity programs, demand bidding programs, and ancillary services market programs). On the other hand, implicit DR (sometimes called price-based DR program) refers to the voluntary program in which consumers are exposed to time-varying electricity prices, e.g. time-of-use pricing, critical peak pricing, and real-time pricing. For the appliances, this would materialize into load-shifting strategies, which shift their operating period from peak to off-peak hours, or load-modulation strategies, which directly reduce or avoid energy use during peak hours.

In the context of the SG, technological advances that enable demand-side resource utilization include bilateral grid-device communication, local and centralized smart controllers, IoT-based coordination and negotiation architecture, controlled and communicated SAs [3]. A different solution is represented by what is known as a grid-friendly or Grid-Interactive Appliance controller (GIAC) [4], [5]. A GIAC can monitor the power frequency and shed the appliance after the under-frequency alarm is triggered, to support the stability of the system. The paper [6] proposes to use appliances equipped with GIAC to address this issue under the umbrella of the IEEE 1547-compliant inverters [7], tripping off-line when operating as part of a microgrid in islanded mode. Finally, the paper [8] introduces a novel approach to establish real-time demand information for a sector of the distribution network. The proposed approach makes it possible to identify the peak and off-peak periods, based on the voltage measured at the electrical panel of the end-users' buildings.

Nowadays in many countries, due to the three electricity tariff periods, and the price difference between the off-peak time band compared to the peak time, the electricity over cost when using a normal instead of a responsive appliance is even more visible. As an example, taking into consideration the consumption of a normal appliance as a washing machine[9], it is almost twice the price of using this appliance in one- or another-time band.

Thus, the present work aims to design a new controller that combines both approaches expanding their possibilities: it can act on DR schemes as well as monitor PQ disturbances for the establishment of a wide and eligible range of alarms and restrictions. The idea is also to be connected to the appliance and managed by the EMS according to the presented values.

Based on a previous IoT sensor development [10], real-time status information, configuration, consumption data, and even diagnostic data from the appliances can be analyzed and recorded while in operation, and simultaneously transferred to the cloud for machine learning processing.

This paper is a thorough revision of the conference paper [11] focused on PQ that expands the integration of OpenADR [12], [13] together with the IoT flexible devices and platform to deploy protective functionalities according to PQ constraints. This is the main novelty of the present paper, as to our knowledge, there is no previous research combining them all to provide PQ functionalities supporting the power system under anomalies or faults.

The rest of this paper is organized as follows: Section 2 presents a review of the IoT and the OpenADR standard employed. Section 3 is devoted to the design of the controller, including hardware devices employed and their configurations and discussing the communications environment. The main features of the developed IoT platform are stated in Section 4 and the tests are then discussed in Section 5. Finally, the conclusions and future work are reported in Section 6.

5.2. Overview

5.2.1. IoT communication protocols

IoT has become one of the most significant trends in the information and communication technology (ICT) world. IoT applications are proliferating in all industries. Although there is no universal definition, several authors have provided definitions of the term [14], [15], [16]. The general idea refers to all those everyday objects connected to the Internet. Standardization is the current problem with IoT protocols, as there are too many protocols and aspirants to be standardized. While their consolidation is coming, what is currently being created is more confusion with each new device that is launched onto the market. There have been many attempts to review all protocols [17], [18], [19]. In the paper [20], the authors even name the technologies of the future as the 5G. In [21], the author makes a good attempt to classify all existing protocols into layers similar to ISO levels of communications. IEEE 802.15.4 and IEEE 802.15.4e are among the most widespread communication protocols: They define access to the physical layers as well as access control levels for Wireless Personal Area Networks (WPANs), and they are mainly used for networks with low transmission rates and low power consumption. Based on the standard IEEE 802.15.4 of WPAN, ZigBee is a high-level wireless communication protocol, operating at 2.4 GHz and its bandwidth is up to 250 kbps, to be used in ultra-low power wireless communications. LoRaWan [22] is a non-cellular low-power wide-area network (LPWAN) wireless communication network protocol, particularly intended for low power devices. LoRaWAN is mainly used within the IoT for connections among devices. Some characteristics are secure bi-directional, low power consumption, long communication range, low data rates, low transmission frequency, mobility, and location services. SigFox is also a protocol for IoT which rewards low power consumption, 12-byte messages are used and are valid for networks up to 50 km. One of its main advantages is that has compatibility with major manufacturers in the market. Another option is the use of the existing mobile phone network itself, like GSM, UMTS or LTE network. The main advantage is that can use a network that is already in service, while the main disadvantage is the cost of using a network which is not oriented to low consumption.

5.2.2. IoT data protocols

The most used IoT data protocols today are as follows: Message Queuing Telemetry Transport (MQTT) (and its variant MQTT-S), Simple Object Access Protocol (SoAP), Constrained Application Protocol (CoAP), Extensible Messaging and Presence Protocol (XMPP), and Representational State Transfer (REST).

The MQTT [23] protocol permits an extremely lightweight publication/subscription messaging model, using Machine to Machine (M2M) communication mainly with a star network topology. Typically used for bi-directional communications in unreliable networks and battery-powered devices with low power consumption. The MQTT-S variant is useful for devices requiring more time on standby mode, allowing up to ten times more scalable devices.

The SoAP was created by the UserLand company in 1998. It oversees structuring the message so that it can be sent from or to the server and put into an Extensible Markup Language (XML) file, an extensible frame language used to store data legibly. As such, it is not tied to or linked to any programming language. It was highly accepted by companies when it came to light, but today it competes against other modern languages. SoAP is an information exchange protocol based on XML, designed for the Internet, and is used to encrypt information from the requirements of Web Services and respond to messages before sending them to the network. SoAP uses Web Service Description Language (WSDL) which is an independent platform, is an extension of the XML language that stores and locates Web Service applications.

The CoAP protocol is an improved protocol version from MQTT-S oriented to Web Services instead of messages as MQTT. It also provides support for integration and content discovery, sends, and receives UDP packets, and is designed to request and receive information via the hypertext transfer protocol (HTTP) with methods like GET, PUT, POST, and DELETE. It also adapts to the node-sensor format with 8-bit controllers and allows the use of 6loWPAN networks that fragment IPv6 packets into small layer frames.

REST relies on HTTP to exchange information and does not need extra encapsulation to do so. It is lighter and easier to use but with some limitations. Instead of making requests encapsulated in an "envelope SOAP" to request a service for which the WSDL is necessary, in REST the requests are made through the HTTP protocol with GET, POST methods without the need to encapsulate it. It uses a single communication path between the device and the cloud and prioritizes Network Address Translation (NAT) address crossing.

XMPP allows an extensive number of uses, including instant messaging or voice and video calling, redistribution of contents, and generalized routing of XML data. Massive real-time scalability for approximately 100,000 nodes. It is also used when traffic messages are large and potentially complex for each device. Also used when extra security is demanded.

5.2.3. OpenADR standard

Several studies have been conducted on OpenADR as a communication data model for automatic DR. For example, the paper [24] introduces a multi-agent system (MAS) that aggregates consumers and prosumers and handles automatically OpenADR-compliant DR requests. The proposed framework ensures a 100% DR success rate through a dynamic, bi-directional DR matchmaking process that can mitigate observed deviations both internally and externally in real-time. Authors use OpenADR as the standard for encoding and communicating, e.g., DR events, energy-related reports, and availability schedules.

The paper [25] studies the layered architecture applied to automatic DR systems and presents an automatic DR hierarchical management system with client-server information

interaction pair as the basic unit. In the OpenADR framework, the clients and the server are better known as virtual end nodes (VEN) and virtual top nodes (VTN) respectively, and their roles will be discussed later. The paper [26] proposes the use of the OpenADR standard protocol in combination with a Decentralized Permissioned Market Place (DPMP) based on Blockchain. It shows the result of a real experimental case, which implements a Capacity Bidding Program (CBP) where the OpenADR protocol is used as a communication method to control and monitor energy consumption.

However, less attention has been paid to this concept in combination with IoT. One of the few researchers addresses DR load control in an SG using IoT technology [27]. Authors present the charging control of plug-in electric vehicles in response to real-time pricing from a utility. The Plug-in Electric Vehicle (PEV) charging is coordinated with real-time pricing and desired target State of Charge (SOC). Moreover, authors in [12] propose a solution based on the standard OpenADR, creating a platform based on IoT capable of turning on or off electrical devices based on a central decision process that meets the requirements of energy producers and consumers. Another example is found in [28], where an open-source platform is developed to allow sensing and control of heating, ventilation, and air conditioning (HVAC), lighting, and plug load controllers in small- and medium-sized commercial buildings.

5.3. Grid-interactive appliance controller extended functionality

This section describes the proposal of the GIAC shown in Figure 5. 1. According to this figure, the proposed GIAC includes the prototype board of the IoT PQ sensor besides an infrastructure based on the OpenADR standard. The following lines will describe both elements more in-depth: Firstly, the IoT sensor to monitor PQ and, secondly, the implemented OpenADR infrastructure.

This board includes the input connectors for current (left) and voltage (right) sensing. The current input circuit is intended to be driven by the split-core current transformer SCT 013-030 of YHDC® with a transfer ratio of 30 A/V and the voltage input is connected directly to the power grid. According to the signal conditioning circuits, the board can measure up to 21 A, 460 V, and 9.9 kVA with 2 W maximum power consumption. Moreover, the board was equipped with the thermistor MCP9700A for monitoring the temperature at the measurement point.

The signal acquisition is performed by a specific purpose integrated circuit (IC) for energy measurements. The device selected was the MCP3909. As in previous works [10], [29], [30], the implemented hardware architecture consists of an ESP32 system-on-chip (SoC) that retrieves data from the IC through a Serial Peripheral Interface (SPI) bus. However, in this design, the ESP32 SoC retrieves raw data (current and voltage samples) rather than traditional PQ indices computed by the IC such as the root mean square (RMS) values, Powers, total power factors (TPF), or total harmonic distortions (THD). This means that the workload has been transferred from the IC to the ESP32 SoC aiming to build and compute custom algorithms and PQ indices from the current and voltage waveforms. The waveforms are retrieved with 16 bits resolution from the delta-sigma analog to digital converters (ADCs) at the frequency of 12.8 kHz. As was stated, the ESP32 SoC includes an SPI bus to retrieve the samples provided by the IC, however, this is not the only communication interface: Once the data processing is performed over these waveforms, other communication channels must be set up to connect the board to the infrastructure detailed in section IV. In our research, the communication protocol involved in the data transmission was the MQTT protocol due to their lightweight implementation [31] to be used in low-resources devices with limited bandwidth.

The primary power source of the prototype is the power grid from which it is collecting the measurements. To accomplish this, a step-down transformer and a circuit based on a linear voltage regulator are employed to provide the DC power supply for the ICs. Also, the board includes an external backup 9 V input that is enabled when the main grid may be unstable (i.e., voltage sags) and is used to supply the ICs and avoid any disconnection or reset.

After the hardware description, the firmware architecture involved in obtaining the PQ indices from the current and voltage samples acquisition to the data transmission is noteworthy. The ESP32 SoC was equipped with the real-time operating system (RTOS) FreeRTOS [32] and organized as it is depicted in the task diagram of Figure 5. 2. While task 0 performs and queues the PQ indices, tasks 1, 2, and 3 just wake up when there is available data within their queues, verify the connection with the MQTT broker to avoid the loss of data, dequeue the PQ indices from the real-time queues and publish them. Otherwise, the PQ indices are not dequeued and will therefore be published once the connection is re-established. In this scenario, the reconnection functions are also triggered.

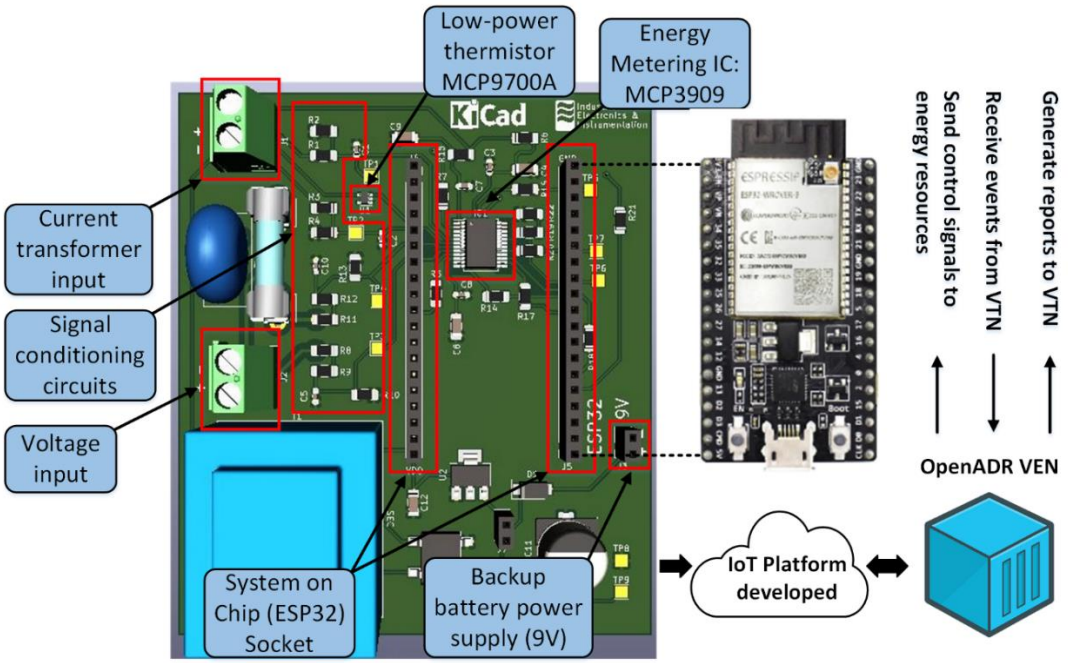

Figure 5. 1. GIAC overview.

The interrupt service routine (ISR) is triggered once current and voltage samples are converted by the ADCs of the IC. Furthermore, this routine fills up a certain buffer with the previous current and voltage samples and performs the RMS value of the voltage each cycle of the fundamental. Although this RMS value is not reported to the IoT platform, the device uses it internally to assess whether a voltage disturbance has occurred or not with a time response of one cycle of the main grid (approximately 20 ms). If so, the magnitude and duration of such a voltage disturbance are sent to task 1 using the real-time queue 0. As it is also evidenced from Figure 5. 2, several real-time queues available in FreeRTOS have been included for synchronization purposes between tasks according to the time intervals they are updated. The ISR also uses a wake-up signal to release the highest priority task (task 0) where the main PQ indices are computed with 10 cycles (approximately 200 ms) as stated in IEC 61000-4-30 for European networks. According to this standard, there are three-time aggregation intervals, 150-cycles (3 seconds approximately), 10-min, and 2 hours which are computed by aggregating these periods of 10 cycles. The device computes the following

indices: RMS value of the current and voltage; active, reactive, and apparent powers; current and voltage harmonics (up to 50 order), frequency, TPF, and THD for the voltage and current, as well as transients as voltage sags and swells (providing, in this case, their magnitudes and durations), and temperature at the measurement point. All the parameter magnitudes are 150-cycle aggregated except the voltage disturbances which are asynchronously reported due to their asynchronous nature. Moreover, RMS voltage and current values are reported with a 10 min aggregation as well.

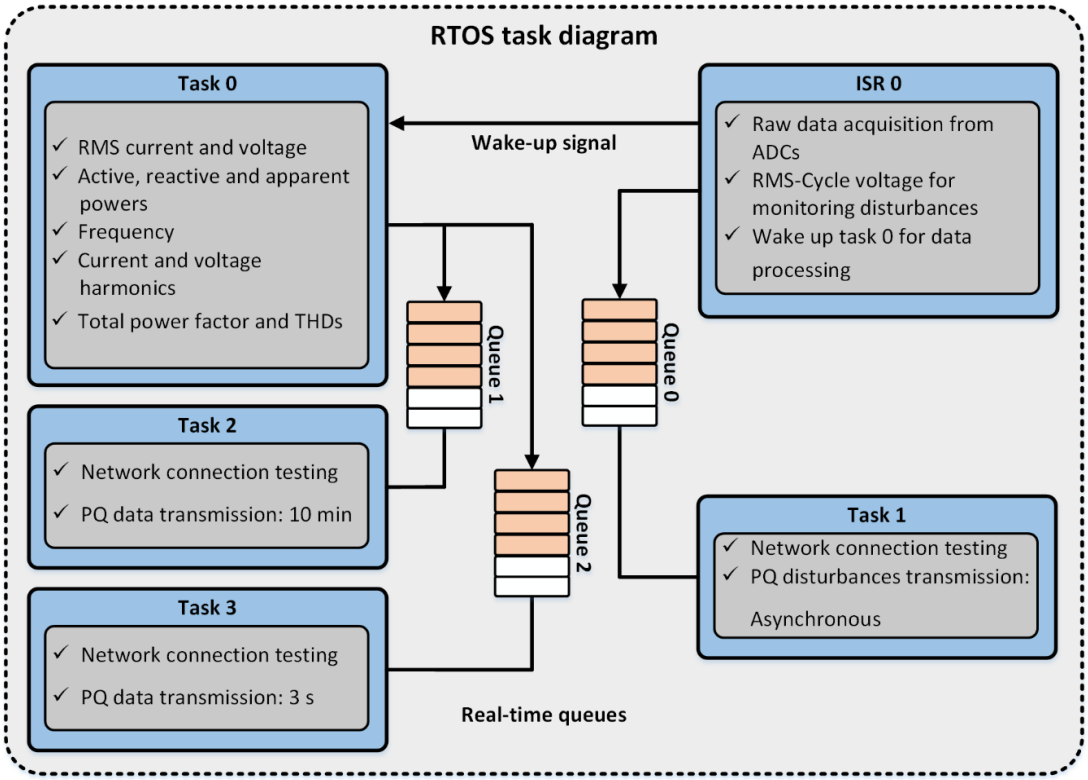

Figure 5. 2. RTOS task diagram.

Finally, OpenADR has been employed through its python implementation OpenLEADR [33] in this research and has also been deployed over the docker containers technology together with the IoT platform that will be described in section IV. OpenADR enables the development of non-proprietary and standardized interfaces that allow stakeholders in the electricity market (mainly utilities and aggregators) to automatize and simplify the management of the typical DR resources such as HVAC, lighting, electric water heaters, pool pumps, and factory equipment among others. OpenADR-based entities can send signals and exchange information so that other entities can change their electric load using a common language and the existing communications. As was stated previously in Section II, entities are organized based on a client-server topology in this standard, where clients and servers are better known as VEN and VTN respectively, and their functionality is well-differentiated: The main purpose of VENs is to generate reports that support the VTN decision-making process, as well as receive and acknowledge events from VTN to control the demand side energy resources. By contrast, the VTN has a complete diagnosis of the system whenever it is required thanks to reports delivered by VENs, and can, therefore, create and transmit events to manage the energy resources controlled by them after certain conditions. Although Figure 5. 1 illustrates the most likely case where a GIAC operates as a VEN, at least one GIAC must operate as a VTN as will be presented in section IV.

Regarding the reporting functionality, reports will be focused on PQ and therefore, parameters delivered by VENs are the same described above for the IoT PQ sensor. These reports will be scheduled with a period of approximately 3 seconds. On the other hand, a battery of custom events as well as events based on several standards related to frequency deviations or voltage disturbances will be configured into the VTN.

5.4. The internet of things platform developed

Once the GIAC has been introduced, the following lines will focus on the IoT platform deployed to collect PQ data to provide monitoring and protective functionality. This Fiware-based platform is shown in Figure 5. 3 together with the GIACs as well as the laboratory setup configured for the testing process.

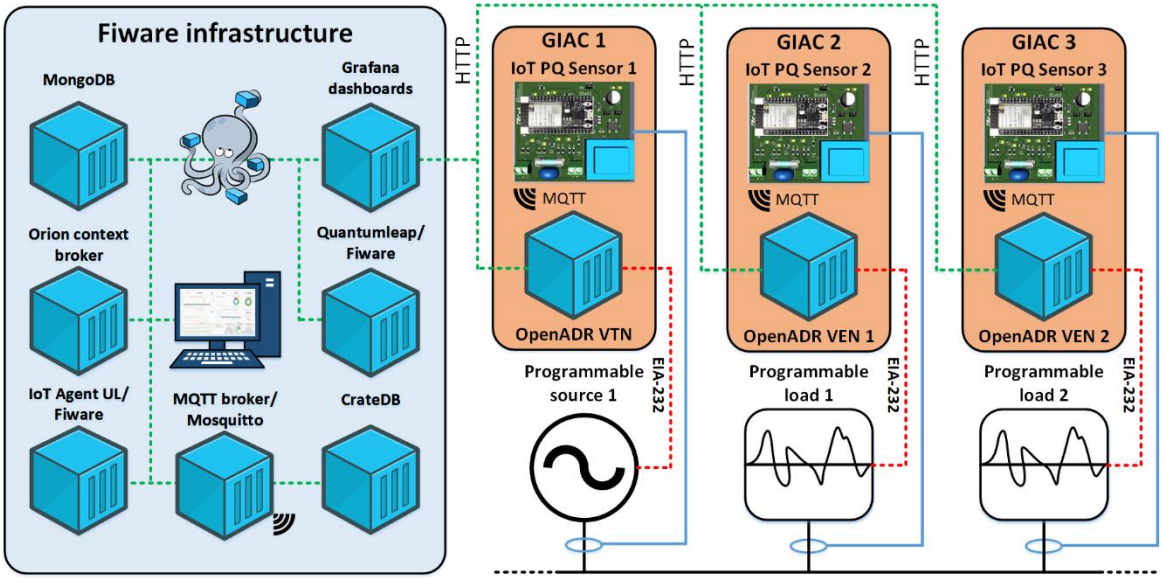

Figure 5. 3. Block diagram of the IoT platform with the GIAC and the laboratory equipment.

At its heart is FIWARE [34] which is an open-source framework that is widely used to speed up and facilitate the development of customized smart solutions for many sectors such as smart city, smart industry, or smart energy. Internally, it uses the next-generation service interface (NGSI) protocol which is aligned with the current ETSI-NGSI specifications and provides communication interfaces called IoT agents for most of the protocols used in IoT (i.e. MQTT, HTTP, LoRaWAN, or Sigfox) as well as seamless integration with third-party applications like popular databases or dashboards to promote interoperability.

For this research, a basic smart solution of six services has been deployed using the container technology provided by docker [35]. These services include the core of any FIWARE-based solution which consists of an instance of the MongoDB database and the so-called orion context broker (OCB) that exchange data through the NGSI protocol as well as with any other container. While this database stores all the defined entities (understood as a thing representation), their attributes structure, and the last value of them even other information related to the relationship between containers, the OCB manages these data. Besides this core, the well-known MQTT broker mosquito has also been used for connecting the IoT PQ sensors as well as the IoT agent for the ultralight 2.0 protocol [36] which is the bridge between the MQTT broker and the OCB to perform the conversion from MQTT to the NGSI protocol. Moreover, the platform also includes a couple of services in charge of managing the time series data: CrateDB and Quantumleap. CrateDB is a Structured Query

Language (SQL) distributed database optimized for large-scale IoT projects which makes it suitable for this research due to the large amount of data coming from the sensors. Quantumleap is the connector in charge of persisting the time series data into CrateDB. Finally, the open-source observability platform for data visualization, monitoring, and analysis, Grafana, has also been added.

5.5. Protective functionalities provided by the devices

This section aims to evaluate the effectiveness of the deployed platform and GIACs under several scenarios such as overconsumption, power system frequency deviations, voltage disturbances as well as the presence of certain harmonics or distortion to take corrective or protective actions.

As was stated in section I, this research is focused on the PQ aspects of the power grid and thus, the infrastructure is tested autonomously to evaluate its effectiveness in dealing with PQ deviations without a controller coordinating its operation. Nevertheless, the platform is intended to be driven by a decision-making entity located in the upper layer. In this regard, previous research such as [37], where an EMS for SAs is developed, or [38], where a load scheduling strategy with PQ constraints is presented, are very suitable for this purpose.

First of all, before discussing the experimental results, a schematic diagram of the corrective action taken by the infrastructure at certain PQ deviations will be presented in Figure 5. 4. Notice that, when power consumption from each load (P) is over the established limit (P_{max}), the VTN receives the corresponding report and generates the power curtailment event for this load (VEN1 or VEN2) to force it to reduce the consumption up to 98 % of Pmax. This 2 % hysteresis has been implemented to avoid the VTN is continuously sending power curtailment events. No corrective action is taken if consumption does not exceed Pmax. Regarding the power system frequency deviations, the balance between total generation and consumption would give a situation with constant frequency. However, this balance might be broken by two reasons: if consumption is over the generation, the frequency falls, and the other way around, it rises when generation is overconsumption. In our research, it is assumed that frequency variations are originated by non-flexible loads while programmable loads 1 and 2 are intended to compensate these deviations according to the following law: if the frequency is over the upper limit (f_{max}), the consumption of this load is then increased in a given percentage of its nominal power. Similarly, when the frequency is below the lower limit (f_{min}), its consumption is decreased by the same percentage. Otherwise, the consumption remains constant at the level at which the frequency is within the limit. So that, the presence of the loads leads to changes in frequency. The values of f_{max} and f_{min} have been established according to the standard EN50160 [39] as mentioned below. In case of a voltage disturbance occurrence, the loads will be disconnected from the programmable source whether there is a voltage disturbance that may cause permanent damage to it. To evaluate that, limits defined in standards such as IEEE 1547 [40], IEC 61727 [41], IEEE 929 [42], and VDE 0126-1-1 [43] have been employed so that a voltage disturbance defined with magnitude and duration within the permissible area would be ignored, otherwise, the load would be disconnected. To deal with the presence of voltage harmonics, the infrastructure evaluates the voltage THD as detailed in standards EN 50160 and IEEE 519 [44]. Consequently, the loads are disconnected when the measured THD is over the limits (THD_{max}) defined in such standards. On the other hand, the load returns to its normal operation when this parameter falls below the value THD_{min} (more restrictive than those defined in the standards). As mentioned below, the values THD_{max} and THD_{min} constitute a hysteresis to ensure that the loads' reconnection is performed with an acceptable

voltage quality. Finally, the infrastructure also detects which load may be a source of current harmonics or distortion and performs a disconnection to ensure the PQ within the grid. Otherwise, the load behavior is not modified. In this case, the standard IEC 61000-3-2 defines what should or should not be an acceptable current distortion by evaluating the absolute amplitude of the individual current harmonics (I_h). Concretely, the limits (I_{h-max}) defined for SA (class A within the standard) have been employed.

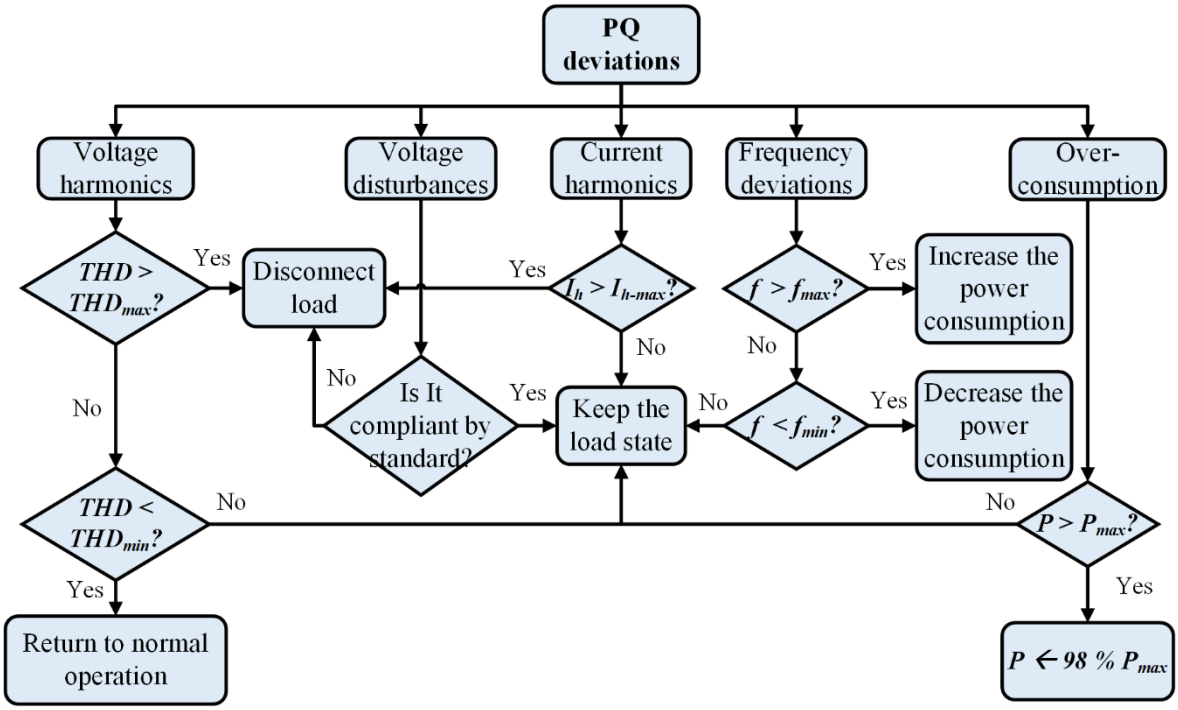

Figure 5. 4. Schematic diagram of the corrective actions for each PQ deviation.

Concerning the experimental results, the test bench of Figure 5. 5 has been employed. The power system of this laboratory setup includes the programmable power source California Instruments 3001 iX [45] and the programmable load California Instruments 3091LD [46]. The server Dell PowerEdge R220 connected to the local network was also used for running the Fiware and OpenADR services, as well as the scripts to control the programmable source and load for the tests. Moreover, the laboratory setup includes the prototypes of the IoT PQ sensors (see Figure 5. 1) in charge of collecting the measurements shown in the results, and the datalogger and oscilloscope Yokogawa DL850E [47] together with the Pearson 411 [48] current probe for visualization purposes. Finally, the DC power supply Agilent E3631A [49] was also employed as a backup power supply for these boards.

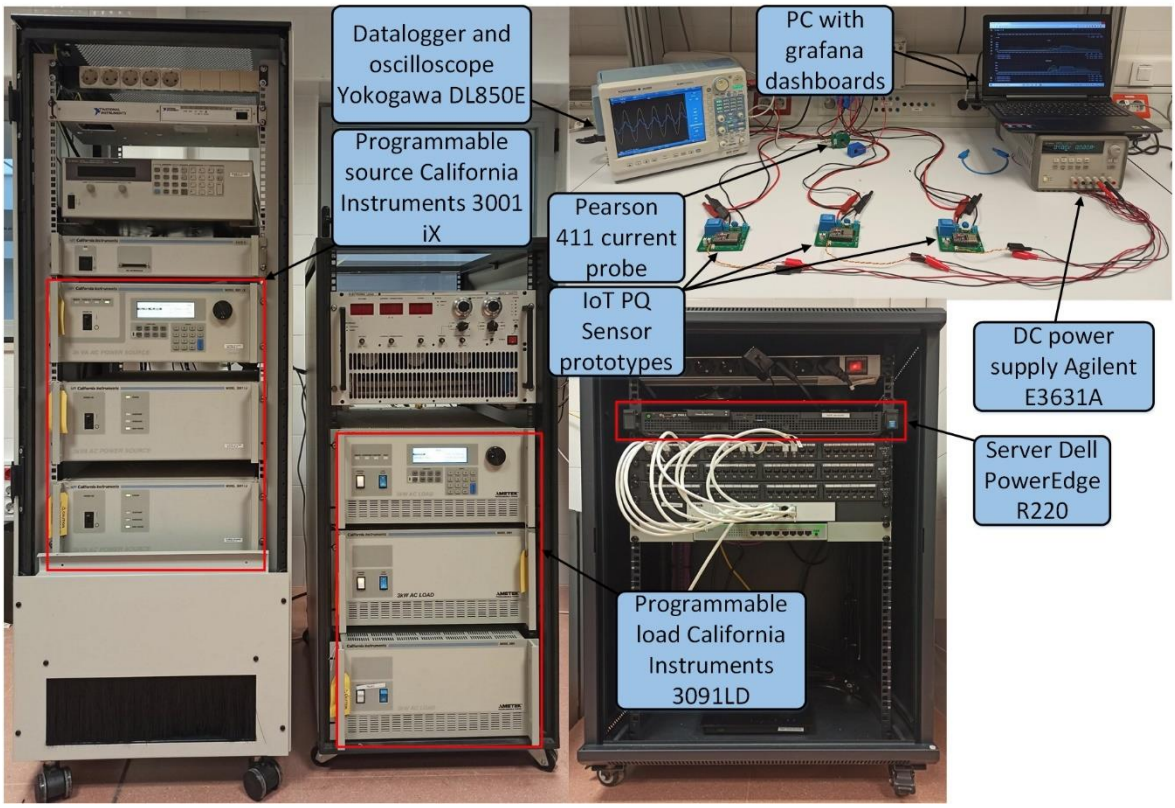

Figure 5. 5. Laboratory setup.

5.5.1. Overconsumption

Two tests were accomplished for overconsumption with different power limits, the first test with different power levels for both loads, and the second test with equal power levels. First, Figure 5. 6 a) introduces the power consumption profiles used as a reference for both programmable loads (loads 1 and 2). These 15 minutes dataset was generated as follows: First, 30 values between 0 and 1.5 kW were randomly generated to ensure that the maximum power of the programmable source was not exceeded, generating 30 seconds duration steps. Then, noise from the standard normal distribution with 0.25 kW of standard deviation was added.

Figure 5. 6 b) depicts the consumption behavior of loads 1 and 2 (blue and orange lines) when the power limits were set to 1.0 kW and 0.5 kW respectively (see red dashed lines in the figures). The power measured at the voltage source terminal (green line) is also shown. As expected, when power consumptions from each load are over those limits, the load is forced to reduce its consumption up to 98 % of the limit. The power consumption is not modified if it is below the limit. It is noteworthy to mention that as the GIAC computes the active power with 150 cycles of aggregation time (see section III), the corrective actions appear approximately 3-s after the actual change as seen in the spikes of the power consumption when it is over the set limits.

Another test was done, keeping, in this case, the same power limit for both loads. In the case of Figure 5. 6 c), the limit was set to 1.0 kW. Therefore, the power consumption in load 1 is the same as in the previous test while load 2 is allowed to increase its consumption 0.5 kW more. Likewise, the approximately 3-s response time previously detailed for Figure 5. 6 a) is also complied in this case as it is derived from the figure.

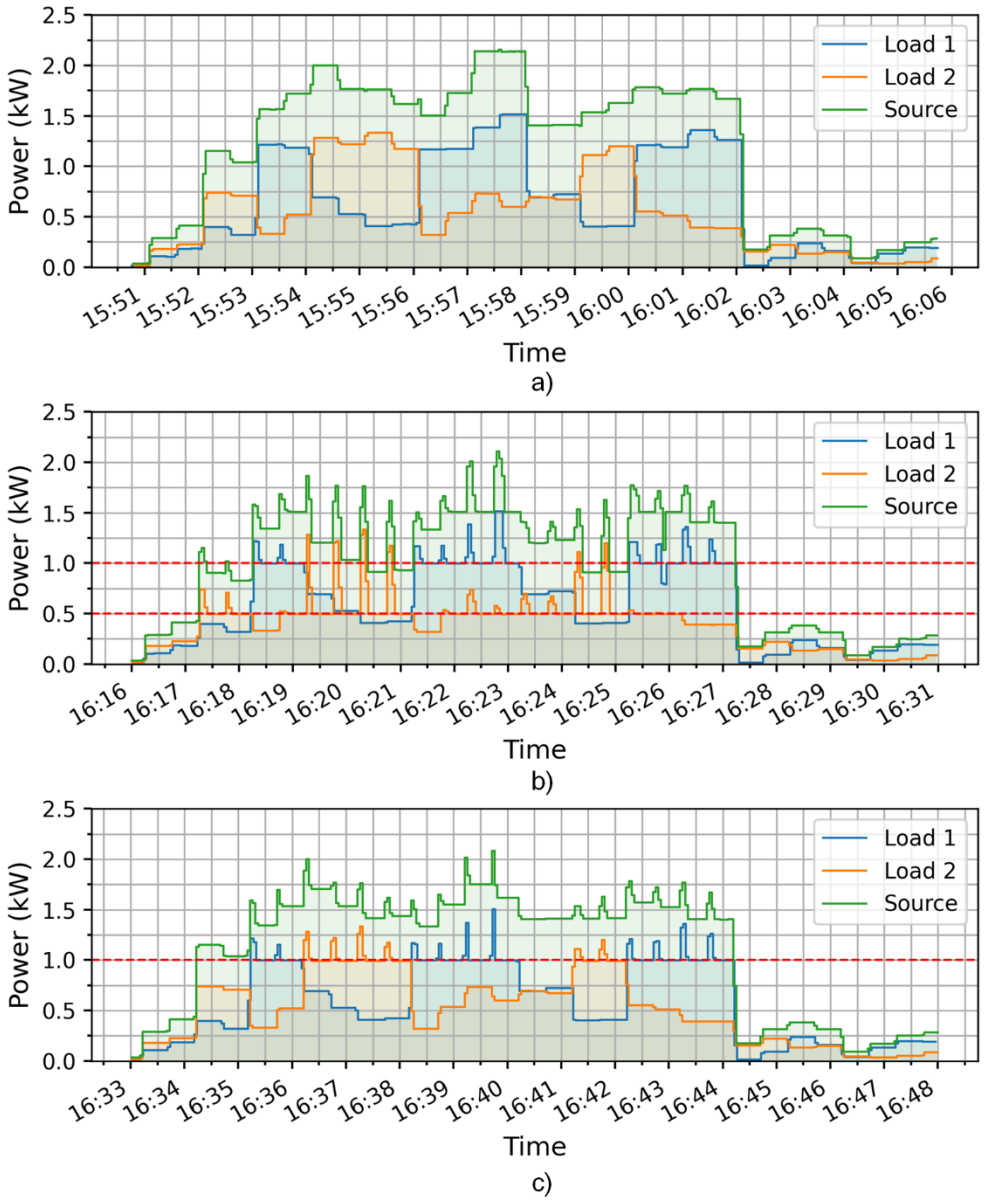

Figure 5. 6. a) Power profiles employed in the tests as a reference, b) Power consumption when loads 1 and 2 are limited to 1.0 kW and 0.5 kW respectively (Red dashed lines) and c) Power consumption when both loads are limited to 1.0 kW (Red dashed line).

5.5.2. Power system frequency deviation

Two tests have been carried out for corrective actions related to power system frequency, more specifically, this test accomplishes with standard EN 50160, where the limits for 99.5 and 100% of the time over a year have been implemented in Figure 5. 7 a) and b): 49.5-50.5 Hz and 47–52 Hz respectively (see red dashed lines that represent f_{max} and f_{min}) for grid-connected systems. Although a multitude of PQ disturbances may adversely impact the power system frequency, most of them do so for a very short time and do not depend on the demand side (i.e. voltage disturbances). Therefore, this case study is focused on the steady-state compensation of the frequency deviations by achieving a balance between the total generation and demand of the system. To do so, a couple of flexible loads were employed to modulate the total consumption of the system. Furthermore, the dataset shown in Figure 5. 7 (see black line) was considered to emulate the influence of non-flexible loads on the

frequency. Similar to section A, this dataset was built generating 90 random values varying from 46 to 54 Hz, creating then 10 seconds duration steps with those values, and then, adding noise from the standard normal distribution with 0.5 Hz of standard deviation. As a result, different slopes in the frequency variation have been emulated to test the GIAC under several conditions. Most of the reported frequencies in real grids are within the limit of 49.5-50.5 Hz, but some points have intentionally been selected to be outside it even reaching 54 Hz or 46 Hz as it has been recorded in a nanogrid in the southern part of Sweden [50]. EN 50160 establishes a larger margin for islanded grids (42.5-57.5 Hz during 100% of the time).

Figure 5. 7 a) shows the first scenario where the permissible region for the frequency goes from $f_{min} = 47$ to $f_{max} = 52$ Hz (red dashed lines). Loads 1 and 2 start from 0.2 and 0.5 kW, respectively, and increase their values with a rate of change of 2 % of their nominal power. Notice that the control rule is successfully applied to compensate the frequency deviations: From 11:42:30 to 11:43:45 the power consumption of both loads keeps growing so that when the frequency is over f_{max}, it can be compensated due to the increase in generation. Something similar but shorter in duration takes place at 11:44:30 and 11:52:15. On the contrary, the frequency falls below f_{min} twice: from 11:46:40 to 11:47:30 and from 11:49:50 to 11:50:25, however, the frequency does not keep below the limit within those intervals which leads to rising the power consumptions with several steps while they keep falling. For the rest of the test, the frequency is within the limits therefore the power on the demand side remains constant.

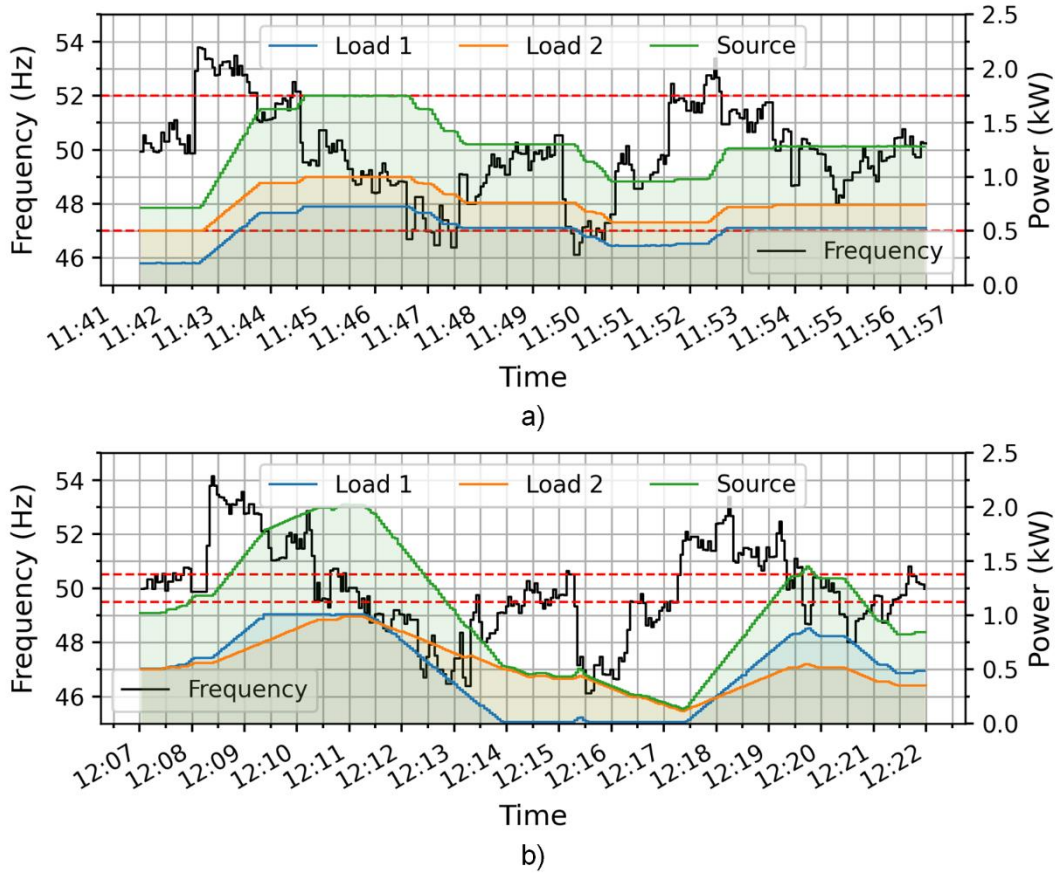

Figure 5. 7. a) Power consumption for loads 1 and 2 and measured at the source terminal when both loads are employed to compensate power system frequency deviations (47-52 Hz). b) Power consumption for loads 1 and 2 and measured at the source terminal when both loads are employed to compensate power system frequency deviations (49.5-50.5 Hz). Red dashed lines are the limits at EN 50160.

The second scenario is depicted in Figure 5. 7 b) where the permitted region is more restrictive ($f_{min} = 49.5$ to $f_{max} = 50.5$ Hz). Accordingly, the power consumption will suffer more variations compared to the previous scenario. Moreover, the initial power has been changed to 0.5 kW for both loads and the ratio of change for load 2 has been changed to 1 %. Note that frequency keeps above fmax from 12:08:15 to 12:10:25 and thus, the power consumption does rise, however, immediately load 1 reaches its nominal power while load 2 still does not. In this context, load 1 will opt out of the event transmitted by the VTN as cannot increase its consumption to reach a balance between consumption and generation. Although the period from 12:17:15 to 12:19:30 is similar, the consumption does not reach the nominal power. In contrast, this can also happen when the power system frequency drops below f_{min}. Notice the period from 12:11:20 to 12:14:00 in which the nominal power of load 1 falls up to 0.0 kW and remains constant even when the frequency is still below f_{min} as the disconnection of the power is necessary to keep the frequency.

5.5.3. Voltage disturbances

The voltage disturbances test was performed by generating several voltage sags and swells with different magnitudes and durations using the programmable voltage source. As in the previous tests, the main purpose is to check whether the deployed infrastructure can detect the voltage disturbance events and carry out a certain policy towards the loads.

Nevertheless, a simple test was performed to validate the measurement device before exposing the whole system to a more complex scenario. In this regard, Figure 5. 8 shows a screenshot of the Tektronix MDO3024 oscilloscope with the voltage and current waveforms of the load fixed at 230 V and 1 A during a test voltage sag (see red and purple waveforms respectively).

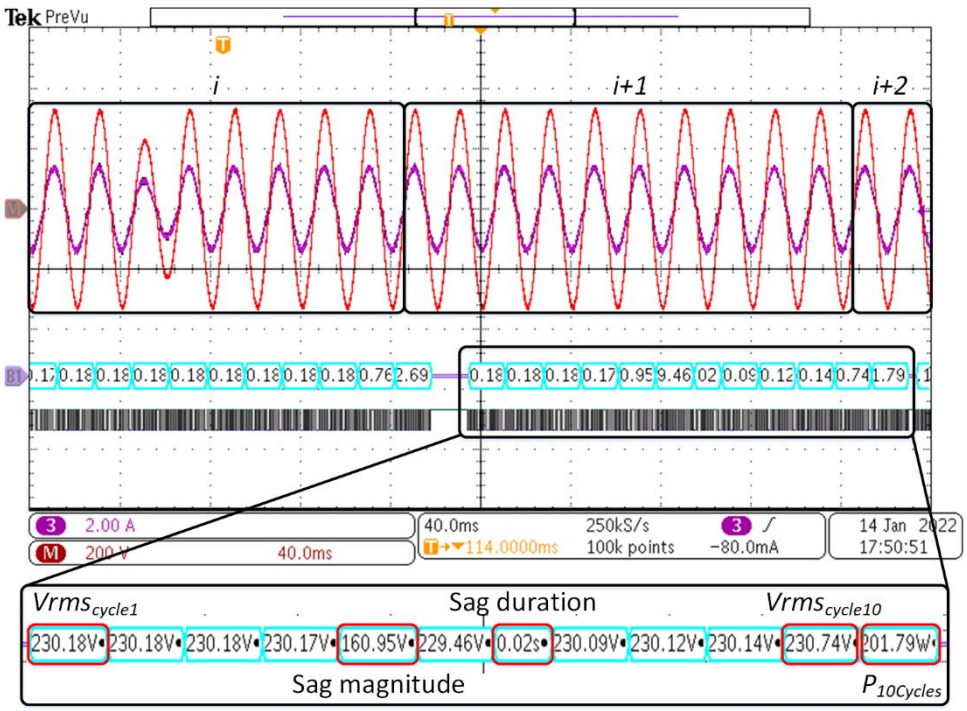

Figure 5. 8. Load voltage and current, as well as device measurements during a test voltage sag.

These waveforms in the screenshot have been separated in 10-cycle windows (i, $i + 1$, $i + 2$) (note that i window is not completed, and two cycles are missing in the left-hand side of the screenshot) since the device calculates parameter magnitudes over 10-cycle time

interval according to the abovementioned standards. Below these current and voltage waveforms, the decoded frame with the measurements from i window sent by the universal asynchronous receiver transmitter (UART) of the device can be found. It should be mentioned that measurements include the RMS voltage of each cycle of the window ($V_{RMS_{Cycle1}}$, $V_{RMS_{Cycle2}}$…$V_{RMS_{Cycle10}}$), the duration of the voltage disturbance (if any), and the power corresponding to this 10-cycles window ($P_{10Cycles}$) and appear at approximately the same time as the next window ($i + 1$) since the device processes a 10-cycles window while acquiring the next one. For a more detailed visualization, this communication frame has been expanded to show the measurements described.

Notice that a voltage sag (160 V and 0.02 s of magnitude and duration) is generated in the fifth cycle of i window by the programmable power source and consequently, a voltage sag of 160.95 V and 0.02 s of magnitude and duration respectively was detected by the device as it is derived from the figure. It is noteworthy that the voltage disturbances detection algorithm needs to recognize one cycle where RMS voltage is within the range of 90-110 % of the nominal voltage (230 V in this case) to detect the end of a voltage disturbance, that is why the sag magnitude and duration do not come together in the frame. Finally, an active power of 201.79 W for the i window is reported.

Once this device functionality has been validated, Figure 5. 9 shows scenario 1 where the standards IEEE 1547 and IEC 61727 have been employed as a reference for loads 1 and 2 respectively. Notice that these standards define different admissible limits or regions (see Figure 5. 9) and thus different criteria for what should or should not be an allowable voltage disturbance. Consequently, a certain voltage disturbance may cause the disconnection of one load while the other one remains connected since this voltage disturbance is evaluated according to different standards for loads 1 and 2.

Figure 5. 9 a) depicts the limits established by such standards (green and red areas for both standards) and a battery of thirteen voltage disturbances configured for this experimental test (230.0 V as reference) covering all areas within or outside the limits (crosses in the figure). While the shaded part denotes the prohibited area defined by one or both considered standards, and thus, voltage disturbances located here will cause the loads' disconnection; the remaining blank region between upper and lower limits indicates the safety area, where no actions are taken. Specifically, the voltage sags and swells have been configured to test all possible cases in a 10 min test: Load 1 disconnected, load 2 disconnected, none of them disconnected, and both loads disconnected. Those values have been selected considering the most often registered voltage sags in low voltage networks in countries reported at [51].

On the other hand, the loads' behavior when these disturbances are applied is depicted in Figure 5. 9 b). Concretely, both loads were set to a constant power of 0.5 kW for a more detailed visualization of the protective actions. Four voltage disturbances with 2.3, 2.1, 2.4, and 1.4 seconds of duration and 60.0, 120.0, 130.0, and 44.8 % of magnitude respectively led to the disconnection of both loads as they belong to shaded green and red areas and their durations and magnitudes were measured with less than 0.0 and 1.34 % of error by the devices. Moreover, five disturbances characterized by 0.75, 1.5, 0.02, 0.2, and 0.24 of duration and 114.8, 80.0, 80.0, 112.6, and 70.0 % of magnitude respectively did not cause the disconnection of any load as they belong to the blank area and were identified with less than 1.34 and 0.572 % of error. Those leading to the disconnection of loads 1 and 2 were detected correctly and also identified with a maximum error of 0.67 and 0.0 % in magnitude and duration.

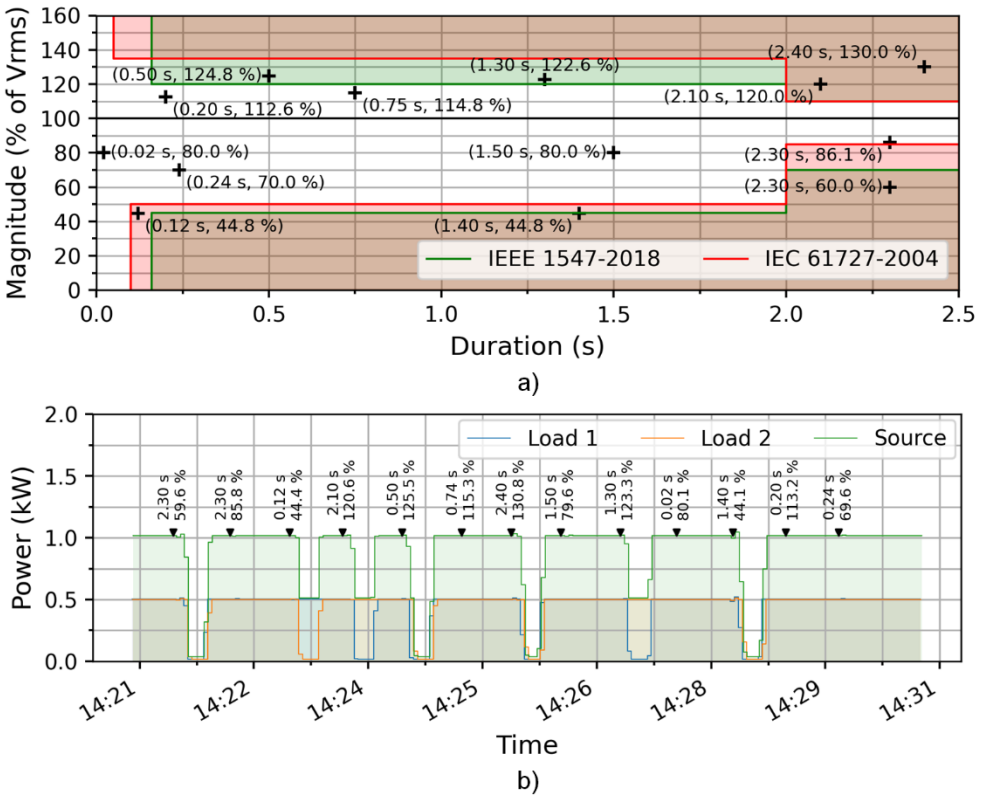

Figure 5. 9. a) Voltage disturbances configured for scenario 1 and limits defined by standards IEEE 1547 and IEC 61727. The shaded part denotes the prohibited region. b) Voltage disturbances identified by the GIAC and power consumption of loads in scenario 1.

Similarly, scenario 2 is depicted in Figure 5. 10, however, the standards IEEE 929-2000 and VDE 0126-1-1 were employed. Another thirteen voltage disturbances were also generated and shown in Figure 5. 10 a) to ensure that all possible cases abovementioned were tested.

The group of three disturbances that caused the disconnection of both loads –see Figure 5. 10 b)- was detected correctly and is characterized by 2.2, 2.3, and 1.0 seconds of duration and 70.0, 130.0, and 41.7 % of magnitude respectively. The maximum error was 1.44 and 0.0 % in magnitude and duration in this case. The three voltage disturbances located in the safety region –blank area- (0.75, 0.04, and 0.1 seconds of duration and 112.2, 84.8, and 114.8 % of magnitude) did not trigger any protective functionality as expected and were identified with a maximum error of 1.34 and 0.45 %. Finally, the other seven disturbances characterized by 2.1, 0.15, 0.5, 2.1, 1.6, 1.4, and 0.35 seconds of duration and 84.8, 44.8, 130.0, 112.2, 74.8, 121.7, and 70 % of magnitude (load 1 or load 2 disconnection) were successfully recognized and thus the protective functionality was triggered. In this latter case, the maximum error was 0.67 and 6.7 % in magnitude and duration.

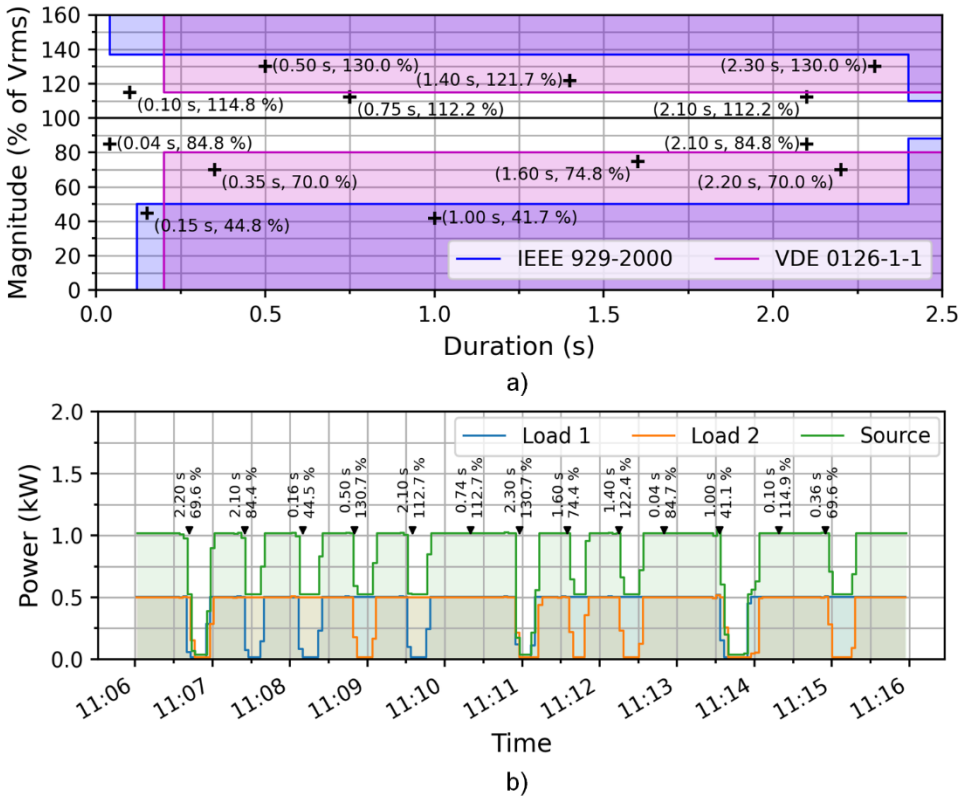

Figure 5. 10. a) Voltage disturbances configured for scenario 1 and limits defined by standards IEEE 929 and VDE 0126-1-1. The shaded part denotes the prohibited region. b) Voltage disturbances identified by the GIAC and power consumption of loads in scenario 2.

5.5.4. Voltage harmonic distortion

The voltage harmonic distortion test is presented in this section. As mentioned above, the voltage THD is employed to evaluate the voltage distortion (expressed in percentage of the fundamental). Therefore, the THD profile depicted in Figure 5. 11 (see black line) has been generated with a duration of 10 minutes from the standard normal distribution (3 % of standard deviation and 7 % of mean) to test the deployed infrastructure. The red dashed lines at 12, 8, and 6 % represent the limits defined by the standards IEEE 519, EN 50160 and the criterion for the load's reconnection respectively. Moreover, the standard IEEE 519 has been applied to load 1 and standard EN 50160 to load 2 and the power consumption was set to 1.0 and 0.5 kW respectively. As in section C, such standards define different limits of THD and thus a certain value of this parameter may cause the disconnection of one load while the other one remains connected.

Figure 5. 11 also depicts the power consumption of both loads as well as the power measured at the source terminal (see the blue, orange, and green lines respectively). Notice that load 1 is disconnected from the grid at 18:54:45 and 18:59:45 since the voltage THD rises above 12 %. However, load 2 is disconnected when the voltage THD is over 8 % which takes place at 18:52:45, 18:55:45, 18:57:45, 19:00:45 besides the previous instants when load 1 is disconnected since the standard EN 50160 is more restrictive than IEEE 519.

Furthermore, the reconnection of both loads must take place when the voltage THD falls below 6 % as was stated at the beginning of this section. In this regard, instants 18:53:45, 18:55:15, 18:56:45, 18:58:15 and 19:00:30 illustrate examples of this behavior. Given the results, it is possible to verify the effectiveness of the infrastructure.

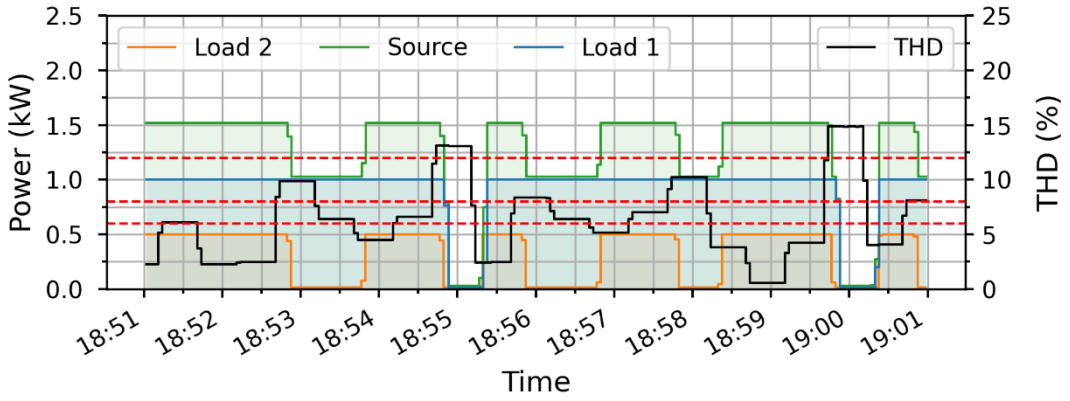

Figure 5. 11. Voltage THD profile configured for the test, power consumption for loads 1 and 2, and measured at the source terminal. Red dashed lines are the limits defined in IEEE 519 (12 %), EN 50160 (8 %), and the loads' reconnection criterion (6 %).

5.5.5. Current harmonic distortion

Finally, the performance of the infrastructure when dealing with the presence of current harmonics is reported in this section with a 10-minutes test. As a criterion, the absolute amplitude of the current harmonics up to order 50 has been considered according to the limits established in the standard IEC 61000-3-2.

The load control rule could be as complex as setting the load to a low harmonic emission mode or consumption (if applicable) when a certain harmonic amplitude I_h is over the threshold defined in the standard (I_{h-max}) or just disconnecting it in such a situation. Furthermore, the control rule adopted also depends on the dynamic of the load to be controlled and its operation modes. In this research, the load is disconnected from the grid (see the schematic diagram at the beginning of this section) to consider a general case since the key element of the research is the performance of the infrastructure when dealing with current harmonics rather than the development of a load control law. However, different control rules could be implemented due to the flexibility of the platform.

The test current employed is composed of harmonics 3 and 4 and their profiles are shown in Figure 5. 12 a) (See the green and black lines respectively) and have also been generated from the standard normal distribution with 0.5 and 0.1 A of standard deviation and 2.2 and 0.3 A of mean respectively. The red dashed lines are the limits defined by the standard for the considered harmonics: 2.3 A and 0.43 A respectively. Figure 5. 12 b) shows in blue the power consumption of the load.

Although the absolute value of the current harmonics is the only criterion employed for making decisions on whether the behavior of the load should be corrected or not, the THD of the current is also depicted in red for a more detailed view of the experiment. Moreover, notice that this magnitude is expressed as a percentage of the fundamental component (I_1), and therefore, when the load is disconnected, this component approaches zero and the THD increases rapidly regardless of how high the magnitude of the rest of the harmonics is.

As expected, the abovementioned behavior can be appreciated from the results. Notice that the 3rd harmonic is over the limit (2.3 A) at 17:50:00, 17:54:00, 17:56:00, and 17:57:00 while the 4th harmonic does it (limited to 0.43 A) at 17:53:00 and 17:58:00. Given the power consumption, the load is always disconnected from the grid at these instants. Nevertheless, the load remains constant in terms of power consumption when the considered current harmonics are within limits.

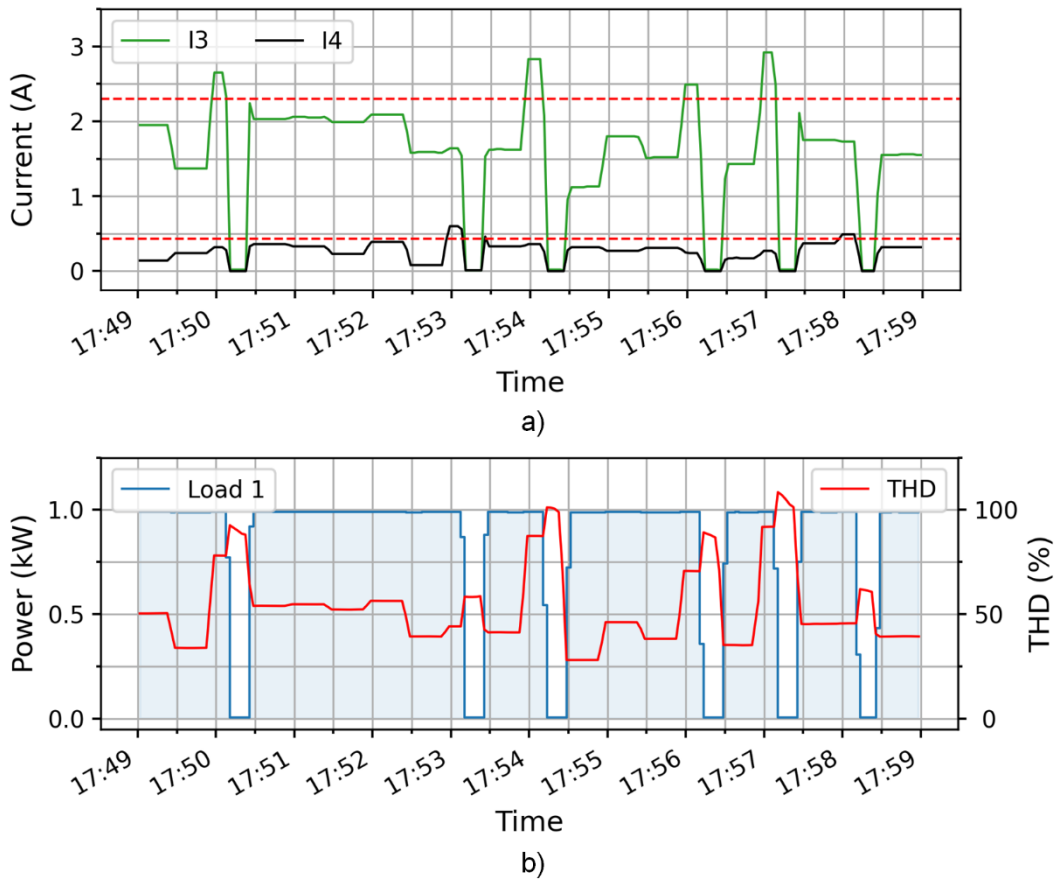

Figure 5. 12. a) Profiles employed for the 3rd and 4th harmonics and limits defined by the standard IEC 61000-3-2 (red dashed lines), b) Power consumption of load 1 and THD of the current.

5.6. Conclusions

Responsive appliances are those that, first, represents a significant load that can be reduced, increased, or moved over time, to provide useful support to the power grid, second, provided that the change in its operation is acceptable to the customer, if not imperceptible, and third, can respond to price, demand or certain grid conditions. This paper resolves many of the technical issues related to the design and construction of these devices, presenting a universal and ambivalent solution as demonstrated by the high-end IoT device, which can communicate and respond to information from the external environment within the framework of a cloud platform. While there are social, political, and economic barriers to the widespread acceptance and adoption of these flexible loads in the marketplace, they need to be addressed and reasonable approaches to overcome them.

Acknowledgements

This research is supported by the Project IMPROVEMENT (grant SOE3/P3E0901) co-financed by the Interreg SUDOE program and the European Regional Development Fund (ERDF).

References

[1] "Household Appliances Report 2019 - Major Appliances Statista Consumer Market Outlook - Segment Report." https://www.statista.com/study/48881/household-appliances-report-major-appliances/ (accessed Nov. 27, 2019).

[2] Z. Ma, J. Billanes, and B. Jørgensen, "Aggregation potentials for buildings—business models of demand response and virtual power plants," Energies, vol. 10, no. 10, p. 1646, 2017, doi: 10.3390/en10101646.

[3] H. Tang, S. Wang, and H. Li, "Flexibility Categorization, Sources, Capabilities and Technologies for Energy-Flexible and Grid-Responsive Buildings: State-of-The-Art and Future Perspective," Energy, p. 119598, 2020, doi: 10.1016/j.energy.2020.119598.

[4] Y. -Q. Bao and Y. Li, "FPGA-Based Design of Grid Friendly Appliance Controller," in IEEE Transactions on Smart Grid, vol. 5, no. 2, pp. 924-931, March 2014, doi: 10.1109/TSG.2013.2285178.

[5] D. J. Hammerstrom et al., "Pacific northwest gridwiseTM testbed demonstration projects; part ii. grid friendlyTM appliance project," Pacific Northwest National Lab.(PNNL), Richland, WA (United States), 2007.

[6] K. P. Schneider et al., "Enabling Resiliency Operations Across Multiple Microgrids With Grid Friendly Appliance Controllers," in IEEE Transactions on Smart Grid, vol. 9, no. 5, pp. 4755-4764, Sept. 2018, doi: 10.1109/TSG.2017.2669642.

[7] R. Real-Calvo, A. Moreno-Munoz, V. Pallares-Lopez, M. J. Gonzalez-Redondo, I. M. Moreno-Garcia, and E. J. Palacios-Garcia, "Intelligent Electronic System to Control the Interconnection between Distributed Generation Resources and Power Grid," RIAI - Rev. Iberoam. Autom. e Inform. Ind., vol. 14, no. 1, 2017, doi: 10.1016/j.riai.2016.11.002.

[8] C. Guzman, A. Cardenas and K. Agbossou, "Local Estimation of Critical and Off-Peak Periods for Grid-Friendly Flexible Load Management," in IEEE Systems Journal, vol. 14, no. 3, pp. 4262-4271, Sept. 2020, doi: 10.1109/JSYST.2020.2970001.

[9] M. Bilton et al., "Impact of energy efficient appliances on network utilisation," Rep. C2 "Low Carbon London" LCNF Proj. Imp. Coll. London, 2014.

[10] R. Medina-Gracia, A. d. R. G. de Castro, J. Garrido-Zafra, A. Moreno-Munoz and E. Cañete-Carmona, "Power Quality Sensor for Smart Appliance's Self-Diagnosing Functionality," in IEEE Sensors Journal, vol. 19, no. 20, pp. 9486-9495, 15 Oct.15, 2019, doi: 10.1109/JSEN.2019.2924574.

[11] J. Garrido-Zafra, A. Gil-de-Castro, R. Savariego-Fernandez, M. Linan-Reyes, A. Moreno-Munoz and F. García-Torres, "A Novel Microgrid Responsive Appliance Controller," 2020 IEEE International Conference on Environment and Electrical Engineering and 2020 IEEE Industrial and Commercial Power Systems Europe (EEEIC / I&CPS Europe), 2020, pp. 1-6, doi: 10.1109/EEEIC/ICPSEurope49358.2020.9160723.

[12] J. Ferreira, H. Martins, M. Barata, V. Monteiro, and J. L. Afonso, "OpenADR—intelligent electrical energy consumption towards internet-of-things," in CONTROLO 2016, Springer, 2017, pp. 725–736., doi: 10.1007/978-3-319-43671-5_61.

[13] "OpenADR." https://www.openadr.org/ (accessed Jun. 23, 2021).

[14] L. Atzori, A. Iera, and G. Morabito, "The internet of things: A survey," Comput. networks,

vol. 54, no. 15, pp. 2787–2805, 2010, doi: 10.1016/j.comnet.2010.05.010.

[15] D. Bandyopadhyay and J. Sen, “Internet of things: Applications and challenges in technology and standardization,” Wirel. Pers. Commun., vol. 58, no. 1, pp. 49–69, 2011, doi: 10.1007/s11277-011-0288-5.

[16] B. Hammi, R. Khatoun, S. Zeadally, A. Fayad, and L. Khoukhi, “IoT technologies for smart cities,” IET Networks, vol. 7, no. 1, pp. 1–13, 2017, doi: 10.1049/iet-net.2017.0163.

[17] O. Alvear, C. Calafate, J.-C. Cano, and P. Manzoni, “Crowdsensing in smart cities: overview, platforms, and environment sensing issues,” Sensors, vol. 18, no. 2, p. 460, 2018, doi: 10.3390/s18020460.

[18] A. J. C. Trappey, C. V Trappey, U. H. Govindarajan, A. C. Chuang, and J. J. Sun, “A review of essential standards and patent landscapes for the Internet of Things: A key enabler for Industry 4.0,” Adv. Eng. Informatics, vol. 33, pp. 208–229, 2017, doi: 10.1016/j.aei.2016.11.007.

[19] P. P. Ray, “A survey on Internet of Things architectures,” J. King Saud Univ. Inf. Sci., vol. 30, no. 3, pp. 291–319, 2018, doi: 10.1016/j.jksuci.2016.10.003.

[20] S. K. Goudos, P. I. Dallas, S. Chatziefthymiou, and S. Kyriazakos, “A survey of IoT key enabling and future technologies: 5G, mobile IoT, sematic web and applications,” Wirel. Pers. Commun., vol. 97, no. 2, pp. 1645–1675, 2017, doi: 10.1007/s11277-017-4647-8.

[21] A. Passemard, “The Internet of Things Protocol stack – from sensors to business value | Internet of Things (IoT) talks.” https://entrepreneurshiptalk.wordpress.com/2014/01/29/the-internet-of-thing-protocol-stack-from-sensors-to-business-value/ (accessed Jan. 16, 2019).

[22] W. Ayoub, A. E. Samhat, F. Nouvel, M. Mroue and J. Prévotet, "Internet of Mobile Things: Overview of LoRaWAN, DASH7, and NB-IoT in LPWANs Standards and Supported Mobility," in IEEE Communications Surveys & Tutorials, vol. 21, no. 2, pp. 1561-1581, Secondquarter 2019, doi: 10.1109/COMST.2018.2877382.

[23] A. Banks, E. Briggs, K. Borgendale, and R. Gupta, “MQTT.” 2018, [Online]. Available: http://docs.oasisopen.org/mqtt/mqtt/v5.0/mqtt-v5.0.html.

[24] C. Patsonakis et al., “Optimal, dynamic and reliable demand-response via OpenADR-compliant multi-agent virtual nodes: Design, implementation & evaluation,” J. Clean. Prod., p. 127844, 2021, doi: 10.1016/j.jclepro.2021.127844.

[25] Z. Jingxi, C. Min, W. Ling, Y. Lixia, P. Shixiong and L. Dong, "Research on Architecture of Automatic Demand Response System Based on OpenADR," 2018 China International Conference on Electricity Distribution (CICED), 2018, pp. 2984-2988, doi: 10.1109/CICED.2018.8592037.

[26] J. I. Guerrero Alonso et al., “Flexibility Services Based on OpenADR Protocol for DSO Level,” Sensors, vol. 20, no. 21, p. 6266, 2020, doi: 10.3390/s20216266.

[27] P. Aggarwal, B. Chen, and J. Harper, “Integration of OpenADR with node-RED for demand response load control using Internet of things approach,” SAE Technical Paper, 2017, doi: 10.4271/2017-01-1702.

[28] M. Pipattanasomporn, M. Kuzlu, W. Khamphanchai, A. Saha, K. Rathinavel and S. Rahman, "BEMOSS: An agent platform to facilitate grid-interactive building operation with IoT devices," 2015 IEEE Innovative Smart Grid Technologies - Asia (ISGT ASIA), 2015, pp. 1-

6, doi: 10.1109/ISGT-Asia.2015.7387018.

[29] M. Alonso-Rosa, A. Gil-de-Castro, R. Medina-Gracia, A. Moreno-Munoz, and E. Cañete-Carmona, “Novel Internet of Things Platform for In-Building Power Quality Submetering,” Appl. Sci., vol. 8, no. 8, p. 1320, Aug. 2018, doi: 10.3390/app8081320.

[30] M. Alonso-Rosa, A. Gil-de-Castro, A. Moreno-Munoz, J. Garrido-Zafra, E. Gutierrez-Ballesteros, and E. Cañete-Carmona, “An IoT Based Mobile Augmented Reality Application for Energy Visualization in Buildings Environments,” Appl. Sci., vol. 10, no. 2, p. 600, Jan. 2020, doi: 10.3390/app10020600.

[31] “async-mqtt-client/2.-API-reference.md at master · marvinroger/async-mqtt-client · GitHub.” https://github.com/marvinroger/async-mqtt-client/blob/master/docs/2.-API-reference.md (accessed Jun. 23, 2021).

[32] “FreeRTOS - Market leading RTOS (Real Time Operating System) for embedded systems with Internet of Things extensions.” https://www.freertos.org/ (accessed Jun. 23, 2021).

[33] “Welcome to OpenLEADR — OpenLEADR 0.5.24 documentation.” https://openleadr.org/docs/index.html (accessed Jun. 23, 2021).

[34] “FIWARE.” https://www.fiware.org/ (accessed Nov. 27, 2019).

[35] “Enterprise Container Platform | Docker.” https://www.docker.com/ (accessed Nov. 27, 2019).

[36] “GitHub - telefonicaid/iotagent-ul: IoT Agent for a UltraLight 2.0 based protocol (with HTTP, MQTT and AMQP transports).” https://github.com/telefonicaid/iotagent-ul (accessed Jul. 30, 2021).

[37] J. Garrido-Zafra, A. Moreno-Munoz, A. Gil-De-Castro, E. J. Palacios-Garcia, C. D. Moreno-Moreno, and T. Morales-Leal, “A novel direct load control testbed for smart appliances,” Energies, vol. 12, no. 17, 2019, doi: 10.3390/en12173336.

[38] J. Garrido-Zafra, A. Moreno-Munoz, A. R. Gil-de-Castro, F. J. Bellido-Outeirino, R. Medina-Gracia and E. Gutiérrez-Ballesteros, "Load Scheduling Strategy to Improve Power Quality in Electric-Boosted Glass Furnaces," in IEEE Transactions on Industry Applications, vol. 57, no. 1, pp. 953-963, Jan.-Feb. 2021, doi: 10.1109/TIA.2020.3029758.

[39] “UNE-EN 50160:2011/A2:2020 Voltage characteristics of electricity supplied by public electricity networks.” https://www.une.org/encuentra-tu-norma/busca-tu-norma/norma/?c=N0064209 (accessed Nov. 15, 2021).

[40] A. Moreno-Munoz, M. Gonzalez, M. Linan and J. J. Gonzalez, "Power quality in high-tech plants: a case study," IEEE Compatibility in Power Electronics, 2005., 2005, pp. 30-38, doi: 10.1109/CPE.2005.1547542.

[41] “IEC 61727:2004 Photovoltaic (PV) systems - Characteristics of the utility interface.” https://webstore.iec.ch/publication/5736 (accessed Nov. 16, 2021).

[42] “IEEE 929-2000 - IEEE Recommended Practice for Utility Interface of Photovoltaic (PV) Systems.” https://standards.ieee.org/standard/929-2000.html (accessed Nov. 16, 2021).

[43] “DIN VDE V 0126-1-1:2013-08 - Automatic disconnection device between a generator and the public low-voltage grid.” https://www.vde-verlag.de/standards/0100178/din-vde-v-0126-1-1-vde-v-0126-1-1-2013-08.html (accessed Nov. 16, 2021).

[44] A. Gil-De-Castro, S. K. Rönnberg, M. H. J. Bollen, and A. Moreno-Muñoz, “Study on harmonic emission of domestic equipment combined with different types of lighting,” Int. J. Electr. Power Energy Syst., vol. 55, 2014, doi: 10.1016/j.ijepes.2013.09.001.

[45] Ametek Programmable Power, “AC Power Sources i-iX Series II.” . Available: https://www.atecorp.com/products/california-instruments/3001ix (accessed Jun. 13, 2022).

[46] Ametek Programmable Power, “Electronic Loads.” . Available: https://www.programmablepower.com/products/electronic-loads (accessed Jun. 13, 2022).

[47] “DL850E/DL850EV ScopeCorder | Yokogawa Test & Measurement Corporation.” https://tmi.yokogawa.com/solutions/discontinued/dl850edl850ev-scopecorder/ (accessed Nov. 15, 2021).

[48] “Pearson Electronics Model 411 Clamp On Current Monitors.” https://www.pearsonelectronics.com/products/wideband-current-monitors (accessed Nov. 15, 2021).

[49] “E3631A 80W Triple Output Power Supply, 6V, 5A & ±25V, 1A | Keysight.” https://www.keysight.com/es/en/product/E3631A/80w-triple-output-power-supply-6v-5a--25v-1a.html (accessed Nov. 15, 2021).

[50] J. Nömm, S. Rönnberg, and M. Bollen, “An Analysis of Frequency Variations and its Implications on Connected Equipment for a Nanogrid during Islanded Operation,” Energies, vol. 11, no. 9, p. 2456, Sep. 2018, doi: 10.3390/en11092456.

[51] “The 5th CEER Benchmarking Report on the Quality of Electricity Supply (2011).” Available: https://www.ceer.eu/documents/104400/-/-/0f8a1aca-9139-9bd4-e1f5-cdbdf10c4609

Chapter 6

Conclusions

The Ph.D. thesis has presented several strategies to promote the flexibility of the power system in a context such as the current one where there is a high penetration of variable renewable energy sources. On the one hand, these strategies were aimed at making the power system more flexible through demand-side management, either by improving energy efficiency or implementing demand response techniques related to the direct control of the loads. Moreover, ensuring an acceptable power quality was another priority of these strategies as it is often compromised.

Firstly, the direct load control strategy developed for smart appliances has revealed that the participation of thermostatically controlled loads, with their associated thermal inertia, as well as the distributed energy resources combined with energy storage facilities are a key source of flexibility within the residential sector. Moreover, this strategy has shown to be particularly effective in the presence of peak and off-peak tariffs, although it can operate under various demand response schemes. On the other hand, the implemented spread spectrum techniques allowed the high energy efficiency achieved by LED lighting systems to be maintained as the same time as the high-frequency components emission of the power electronic converter was kept to a minimum.

Regarding the industrial sector, the load scheduling strategy developed for the glass melting process evidenced a better utilization of energy within this energy-intensive industry. From a financial viewpoint, economic penalties for exceeding the contracted power are much lower or even avoided which translates into considerable cost savings for these large end-users. In terms of power quality, this strategy not only brings a significant improvement over the conventional approaches but also ensures an optimal power quality to the extent that the waveform distortion due to subharmonics components is kept to a minimum. Furthermore, the ripple of the temperature waveform due to the AC cycles distribution is also minimized with the strategy, as it employs the accumulator-based method that has demonstrated to be optimal.

It should be pointed out this work has also provided the required technology to support the abovementioned demand-side management strategies and, therefore, some conclusions can be drawn. The use of GAMS provided the capability of including mathematical optimization rules for these strategies. The implementation of OpenADR and MQTT as standards protocols within the energy and the internet of things fields, respectively, facilitated all the developed strategies to be easily integrated within the Smart Grid from the interoperability and scalability point of view. Finally, the deployed advance metering infrastructure as a part of the grid-interactive appliance controller proposal enabled the monitoring of the microgrid energy resources according to several power quality standards.

Chapter 7

Future works

This section suggests the future lines of research that could be investigated to reinforce the achieved objectives and improve the obtained results:

- **Digital implementation of random pulse width modulation techniques:** By now, the digital implementation of the random pulse width modulation (RPWM) generator, as well as the converter control (inner current and outer voltage loop of the boost converter) shown in chapter 2, is performed by an industrial embedded controller with an architecture composed of a processor and a field-programmable gate array (FPGA) which cooperate to complete certain tasks. While this architecture is more than adequate and powerful enough to achieve the required flexibility of a research testbed that seeks to speed up the validation of the developed techniques, the construction of several converter prototypes using this controller does not seem to be the best solution from scalability and economic viewpoints. Rather, other alternatives such as the incorporation of small microcontrollers or even the use of certain integrated circuit that implement RPWM and already include the required logic to manage the control loops can be explored.

- **Incorporation of new loads into the model:** Until now, the thermostatically controlled loads (TCL) involved in the developed strategies to increase the demand flexibility are loads for heating applications such as the electric water heater (EWH) in chapter 3 or the electrodes mounted in electric-boosted glass melting furnaces in chapter 4. Nevertheless, loads used in cooling applications have not been considered. Therefore, a further step is needed toward the integration of these loads into the developed strategies, including the modeling stage.

- **Use of more complex optimization problems:** The mixed-integer programming problem (MILP) employed in the platform detailed in chapter 3 is an extremely straightforward optimization problem used to assess the mathematical optimization features of the proposed platform. Once the platform is functional, a more realistic problem can be formulated by including the inherent uncertainty in both sides of the power grid, i.e., variable renewable energy sources (VRES) and end-users consumption. Furthermore, ever-more relevant storage technologies such as hydrogen can also be considered besides conventional ones.

- **Solving algorithms for the optimization problem:** The number of variables used by the proposed mixed-binary quadratic programming (MBQP) problem stated in chapter 4 depends on the modulation period and the number of loads considered. The more loads and cycles considered within the modulation period, the more variables the problem will have. Although a period as short as possible is appropriate to avoid a large quantity of subharmonics components and space them within the frequency spectrum, the number of loads can grow as much as necessary. Therefore, conventional solving algorithms can take a long time to obtain the optimal choice of decision variables that yields the best value of the objective function. Sometimes, a reliable or approximate solution can be found in much less time than the optimal one by using other techniques such as genetic algorithms (GA) or particle swarm optimization (PSO) in which the maximum time dedicated to solving the problem and the threshold for the objective function can be fixed.

- **Demand uncertainty of the electric-boosting system:** The developed load scheduling strategy models the demand of the electric-boosted system employed within the glass melting furnaces as a resistor with a constant ohmic value. This ohmic value considers the resistance of the path composed of the electrodes, and the molten glass between two consecutive electrodes. While the resistance of the electrodes (typically made of molybdenum) can be considered constant, the resistance of the molten glass may vary depending on several parameters such as the temperature, the surface area in contact with the electrodes or the interaction with other electrodes among others. In this regard, deterministic optimization problems such as the one employed in chapter 4 (MBQP) are unable to deal with this uncertainty, instead, an interval optimization problem including the demand uncertainty would tackle this issue.

- **Coordination of energy and power quality management strategies:** Chapter 3 introduces a flexible platform to deploy several energy management strategies based on an optimization problem that considers the demand profile of the loads to minimize the day ahead cost of the energy. On the other hand, chapter 4 proposes a load scheduling strategy to minimize the energy of certain frequency components of the spectrum by modeling the harmonic emissions of the loads. Given this scenario, a combined strategy can be proposed to deal with both issues either through a multi-objective function in optimization problems or through a two-stage optimization considering the priorities of the microgrid.

- **More sophisticated protective functionalities:** Chapter 5 describes a battery of protective functionalities that the proposed grid-interactive appliance controller (GIAC) together with the deployed internet of things (IoT) platform offer under certain scenarios such as the presence of power quality (PQ) disturbances or load conditions (see the flowchart in section 5.5 for more details). The corrective actions and rules defined to trigger them with the occurrence of an event were simple enough to keep the research focused on the evaluation of the infrastructure performance. However, more sophisticated ones could be implemented once this architecture has been validated. An example of a more sophisticated rule can be noticed in the case of voltage sags and swells. It would be useful to consider other strategies that include the elapsed time since the last or since two consecutive disturbances besides the magnitude and duration of the PQ disturbance. Thus, a succession of connections

and disconnections can be avoided when multiple voltage sags or swells take place sequentially. Furthermore, the emissions of certain current harmonics can be considered to apply more sophisticated corrective actions. By now, the load is disconnected when the absolute value of a certain current harmonic is over the limits defined by the standard IEC 61000-3-2. Nevertheless, a scenario with smarter loads capable of modulating their current emissions can be investigated instead of being disconnected.

Curriculum Vitae

Joaquín Garrido Zafra

Joaquin Garrido-Zafra received the MSc degree in Distributed Renewable Energies (2018) and the degree in Industrial Electronics Engineering (2017) from the University of Cordoba (Spain). He is a Professor at the Department of Electronics and Computer Engineering of the same University, and a member of the research group of Industrial Electronics and Instrumentation (IEI). Since 2018, he has participated in several R&D projects obtained in national and international competitive public grants. His research interests are focused on power quality, the Internet of Things, electronic instrumentation, energy management, and the development of embedded systems to be used in the Smart Grid. He is also the author and co-author of numerous conferences and journal papers.